Fall 2009

Toward a better understanding of new particle formation

Alicia J Pettibone
University of Iowa

TOWARD A BETTER UNDERSTANDING OF NEW PARTICLE FORMATION

by

Alicia J. Pettibone

An Abstract

Of a thesis submitted in partial fulfillment of the
requirements for the Doctor of Philosophy degree
in Chemical and Biochemical Engineering in
the Graduate College of
The University of Iowa

December 2009

Thesis Supervisor: Assistant Professor Charles O. Stanier

ABSTRACT

The creation of new atmospheric particles via nucleation is an important source of particles, and may influence climate by altering the aerosol size distribution. The objectives of the dissertation research were to better understand the process by which new particles are created (homogeneous nucleation), and how these particles are modified throughout their lifetime in the atmosphere. The approach combined field-measurements and observations with advanced instrumentation development and extensive data analysis.

In the laboratory, a Dry-Ambient Aerosol Size Spectrometer (DAASS) was constructed. The DAASS is an automated combination of aerosol sizing instruments and supporting equipment that measures aerosol size distributions from 10.9 nm to 10 μm at both ambient and dry relative humidities and was deployed during the MILAGRO field campaign. The design and construction of a Differential Mobility Analyzer from parts was also completed in order to provide the capability to perform Tandem DMA (or TDMA) measurements.

New particle formation events, occurring in both rural (Midwest United States) and urban (Mexico City) locations were analyzed. In the Midwest, the temporal pattern, frequency, associated meteorology and contributing factors were quantified for the first time in Bondville, Illinois and West Branch, Iowa.

The urban observations were conducted in Mexico City, Mexico, as part of an international field campaign known as MILAGRO (Megacity Initiative: Local and Global Research Observations 2006). It was determined that new particle formation in Mexico City occurs following periods of decreased pre-existing aerosol surface area. These sharp decreases in pre-existing aerosol surface area are tied to the rapid ventilation of the Mexico City basin that occurs in the early afternoon as a result of its unique geographical setting in a mountain basin.

Number-based emission factors representative of Mexico City were determined using a method of signal peak identification in collocated SMPS and CO_2 measurements. The emission factor as a function of time of day, day of week, and wind direction were examined. The overall emission factor is size resolved, and comparisons to other size resolved emission factors determined in other locations (such as Los Angeles) were performed.

Abstract Approved: _____
Thesis Supervisor

_____
Title and Department

_____
Date

TOWARD A BETTER UNDERSTANDING OF NEW PARTICLE FORMATION

by

Alicia J. Pettibone

A thesis submitted in partial fulfillment of the
requirements for the Doctor of Philosophy degree
in Chemical and Biochemical Engineering in
the Graduate College of
The University of Iowa

December 2009

Thesis Supervisor: Assistant Professor Charles O. Stanier

Graduate College
The University of Iowa
Iowa City, Iowa

CERTIFICATE OF APPROVAL

PH.D. THESIS

This is to certify that the Ph.D. thesis of

Alicia J. Pettibone

has been approved by the Examining Committee
for the thesis requirement for the Doctor of Philosophy
degree in Chemical and Biochemical Engineering at the December 2009
graduation.

Thesis Committee: _____
Charles O. Stanier, Thesis Supervisor

_____
Gregory Carmichael

_____
Vicki Grassian

_____
William Eichinger

_____
Jennifer Fiegel

ACKNOWLEDGMENTS

I would like to thank my advisor, Charles Stanier, for introducing me to a career in atmospheric science. His hard work and dedication were exemplary and I gained valuable knowledge and experience as a member of his research group.

I was fortunate to be able to work alongside the members of the Carmichael and Stanier research groups. Not only are they talented scientists and engineers with valuable insight, but they are great friends who made the experience of graduate school so much more enjoyable.

I would like to thank Jian Wang of Brookhaven National Laboratories for providing Mexico City size distribution measurements for comparison. Thank you to Marcelo Mena, for providing the Mexico Emissions Inventory. Also, thanks to Allen Bradley for his help with the meteorological analysis.

I appreciate all of the help I received from Linda Wheatley and Jane Frank. Thank you to Greg Wagner who assisted with many of the electronic related issues in the lab. I would also like to thank the College of Engineering Design and Prototyping Center and Frank Turner in the Chemistry machine shop for working with us to design and machine the required equipment.

Words don't express my appreciation for all of the love and support I have received from my family and friends. My parents taught, by example, the importance of hard work and power of education and they have been a source of encouragement every step of the way. My deepest thanks go to my husband, John, who offered daily understanding, love, and support as a husband, friend, classmate and colleague which made the journey possible. Here's to the next step in our adventure.

TABLE OF CONTENTS

LIST OF TABLES

LIST OF FIGURES

CHAPTER 1: INTRODUCTION

1.1 Background

Atmospheric aerosol particles are ubiquitous throughout the atmosphere, and affect the quality of human life in many ways. Such particles are known to have negative effects on human health in polluted environments. They can also influence visibility and significantly change climate patterns. In order to gain a better understanding of the effects of these aerosols, we must better understand the processes by which they are created, and how they evolve throughout their lifetime in the atmosphere.

Atmospheric aerosols can directly affect climate by either scattering or absorbing solar radiation. The interaction of an aerosol with solar radiation is dependent on the aerosol particle's properties including size, shape, chemical composition, and optical thickness (Yu, Kaufman et al. 2006). Aerosols comprised of mostly scattering material, such as ammonium sulfate, tend to reflect solar radiation back to space and have a net cooling effect. Absorbing aerosols, like black carbon for example, absorb solar radiation, which decreases the amount reaching Earth's surface (cooling effect), while at the same time warming the atmosphere aloft (Randles and Ramaswamy 2008). This warming of the upper atmosphere with respect to the surface leads to greater stability, which can inhibit the deep convection that triggers rainfall (Ramanathan, Chung et al. 2005).

Aerosols can also affect the climate system indirectly by altering cloud properties in multiple ways (Lohmann and Feichter 2005). For example, an increase in the number of aerosols formed from biogenic and anthropogenic precursors may increase the number of particles that can seed cloud droplets, known as cloud condensation nuclei (CCN). Increasing the number of CCN in a cloud while keeping the liquid water content fixed results in (1) a decrease in droplet radius, (2) a decrease in precipitation efficiency in polluted clouds and (3) an increase in cloud lifetime (Ramanathan, Crutzen et al. 2001). Increasing the CCN in a cloud may also increase the cloud's reflectivity. Evidence of

this was observed off the coast of Peru, where consistent reflectivity enhancement of clouds was coincident with nearby aerosol emission sources (Kuang and Yung 2000). Conversely, it is thought that the addition of CCN larger than 5 μm, also known as giant cloud condensation nuclei (GCCN), to non-precipitating clouds may initiate precipitation and counteract the indirect effect of aerosols according to recent General Circulation Model simulations (Posselt and Lohmann 2008). The indirect effects of aerosols are likely to have a negative radiative climate forcing, but due to the complexity and number of interactions involved, the magnitudes of these effects are highly uncertain and are thought to be dependent on specific scenarios (Lohmann and Feichter 2005).

In order to accurately predict the indirect effect of aerosol, precise estimates of certain parameters are required. For example, the activation of aerosols to form CCN depends on water content in the atmosphere and particle size. Therefore, in order to accurately predict CCN, an estimate of the aerosol size distribution (including new particle formation) is required (Adams and Seinfeld 2002). In the polluted boundary layer, primary emissions of particles created during fossil fuel combustion are the largest contributor to condensation nuclei concentrations. These emissions must also be accurately estimated and included in global models that predict CCN concentrations if the indirect effect of aerosols is to be accurately described (Adams and Seinfeld 2002). Number-based emission factors (representative values that are used to relate, in this case, number of particles released with amount of fuel burned) are used to estimate emissions of various pollutants and can be a useful tool in estimating particulate emissions.

The Intergovernmental Panel on Climate Change was established to assess scientific and technical information regarding climate change (Alley 2007). In its 2007 report, a summary of anthropogenic agents, the corresponding radiative forcing (W/m^2), and the assessed level of scientific understanding was presented and is shown in Figure 1.1.

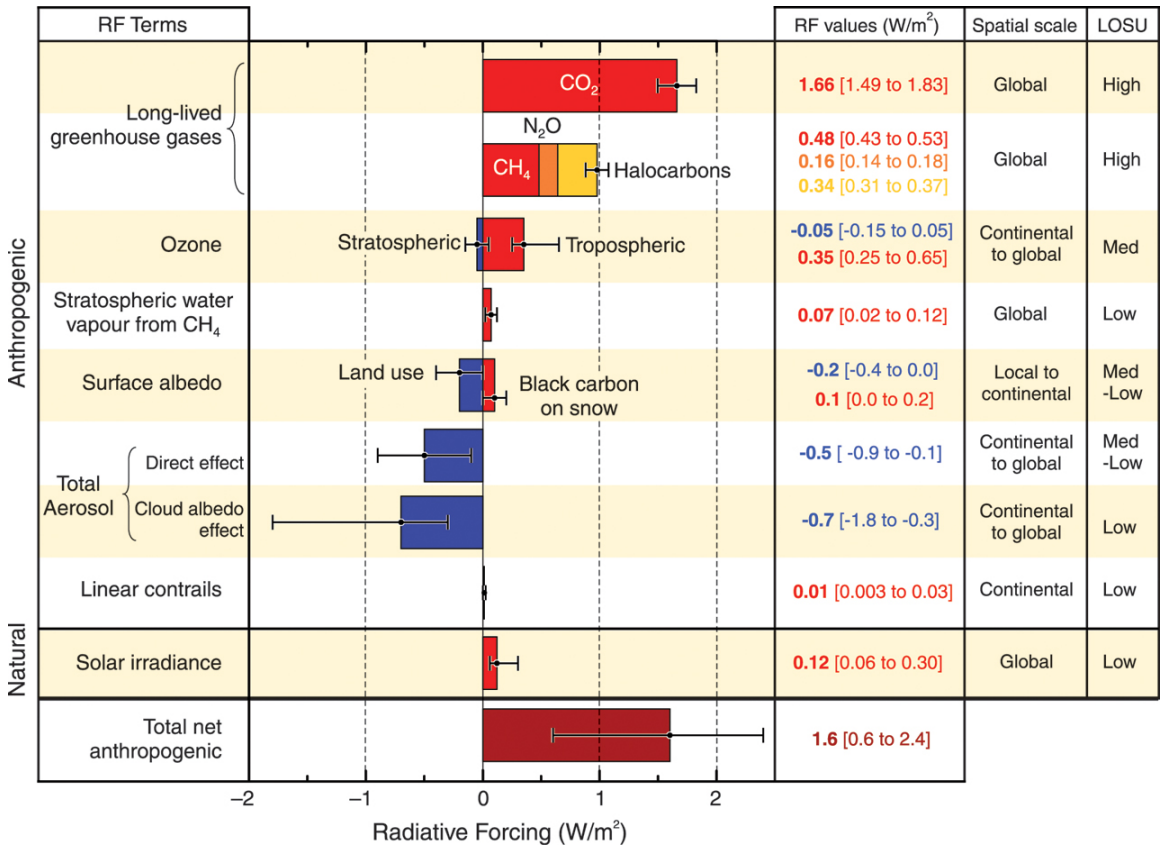

Source: Alley, R., 2007. Climate Change 2007: They physical science basis [Working Group I to the Fourth Assessment Report of the Intergovernmental Panel on Climate Change]. IPCC.

Figure 1.1. Global average radiative forcing (RF) estimates and ranges.

As shown in Figure 1.1, the level of scientific understanding of the direct and indirect effects of aerosols is relatively low. The objectives of this research are to study the physical and chemical processes that contribute to the direct and indirect effects, which have magnitudes of approximately -0.5 and -0.7 W/m^2 respectively. Reducing the uncertainty associated with aerosols and their effects is necessary in order to gain a better understanding of global climate change. Specifically, this research is motivated by the need to make a quantitative link between a specific atmospheric process, new particle formation, and aerosol climate effects.

New particle formation changes the size distribution of airborne particles, and therefore influences the indirect and direct effects of atmospheric particles, as well as the health effects they have on the human body. Particle size is one of the most important parameters when characterizing the behavior of aerosols (Hinds 1999) both from a fluid mechanical standpoint and from a cloud nucleating standpoint. In a study of air masses representing different chemical compositions, Dusek and colleagues determined that the size of a particle is even more important than the particle chemistry when estimating CCN concentrations (Dusek, Frank et al. 2006). Size is also an important parameter when determining the location that a particle may deposit in the respiratory system and the effect a particle may have on human health (Hinds 1999). Several epidemiologic studies have found associations between ambient ultrafine particles and adverse effects on respiratory and cardiovascular systems that result in morbidity and mortality for specific portions of the population that are most susceptible (Oberdorster, Oberdorster et al. 2005).

1.2 State of Knowledge of New Particle Formation

Particles are introduced into the atmosphere either by direct emissions or by homogeneous nucleation of low volatility species. The process of homogeneous nucleation is often called new particle formation to distinguish it from heterogeneous nucleation on existing aerosol particles and also from homogeneous nucleation activity that does not lead to stable particles. Nucleation of new particles has been observed in a multitude of different environments around the world including coastal regions (Weber, McMurry et al. 1998), urban environments (Stanier, Khlystov et al. 2004), rural environments, forests (Tunved, Hansson et al. 2006), mountainous regions (Weber, Marti et al. 1997), and the Arctic region (Pirjola, Laaksonen et al. 1998). Although it has yet to be resolved which mechanisms govern new particle formation, it is generally accepted that new particle formation occurs via homogeneous nucleation of two or more vapor

species that form new stable particles (Kulmala, Korhonen et al. 2002). The process is dependent on several steps, including the initial formation of a stable cluster, particle formation, and subsequent growth through condensation; and it is possible that the nucleation and growth processes are decoupled (Kulmala, Laakso et al. 2004). In general, new particle formation events usually occur during the day, suggesting that they are driven by solar radiation, or more specifically the OH-oxidation of aerosol precursors through photochemistry. Favorable conditions also include low pre-existing aerosol concentrations, which may serve as a sink for condensable vapors, and high vapor source rates (Kulmala and Kerminen 2008).

Various mechanisms have been proposed to explain new particle formation, and it is likely that different mechanisms dominate in different locations. Although it has not yet been resolved as to which mechanisms are the most important, the most likely candidates are 1) binary homogeneous nucleation of sulfuric acid and water; 2) ternary nucleation of sulfuric acid, water and ammonia; 3) ion-induced nucleation; and 4) barrier-less homogeneous nucleation (Kulmala and Kerminen 2008). Barrier-less nucleation differs from the other proposed mechanisms in that all clusters of molecules are considered stable; where as the other mechanisms are governed by the probability of critical cluster formation versus cluster decay (Clement and Ford 1999). This particular thesis is concerned with new particle formation occurring in the continental troposphere and boundary layer and is therefore focused on the binary and ternary mechanisms, rather than on the ion-induced or barrier-less mechanisms that are thought to be more important in the upper troposphere and coastal environments, respectively.

In addition to the uncertainty associated with the mechanisms and growth processes, there is much to be discovered concerning the geographic extent and the vertical profile of new particle formation. For example, particle formation events can be classified as regional when the growth is observed over a period of several hours as different air masses pass over the monitoring site. Regional nucleation events are

common in the continental boundary layer, and have been observed in many different environments such as forested areas (Dal Maso, Kulmala et al. 2005), urban areas (Stanier, Khlystov et al. 2004), and remote areas (Weber, Marti et al. 1997). . Conversely, when the growing mode disappears quickly, it is often assumed that the event was short lived or local (Stanier, Khlystov et al. 2004). This is more common in larger industrial plumes (Brock, Washenfelder et al. 2002) or localized traffic plumes (Kittelson, Watts et al. 2004).

It appears the new particle formation may be tied to meteorological parameters such as boundary layer evolution and mixing processes. On initially cloud-free days, solar heating at the ground creates an unstable situation where buoyant thermals rise and are replaced by subsiding colder air from above. The mixed layer grows by entraining the clean, dry, air from aloft and mixes heat, moisture, and momentum vertically (Stull 1988). The vertical motion of an air parcel leads to an effective temperature decrease by adiabatic expansion and thereby increases the saturation ratio of potentially nucleating vapors in the parcel (ratio of ambient vapor pressure to saturation vapor pressure) by decreasing the saturation vapor pressure, creating favorable conditions for nucleation.

Because the majority of nucleation studies have been conducted at the ground level, there are many questions regarding the vertical profile of new particle formation. In 1994, Easter and Peters performed a theoretical study that predicted enhanced formation rates due to small-scale fluctuations in temperature, relative humidity, and vapor concentrations, which are likely to occur higher in the atmosphere near the inversion layer (Easter and Peters 1994). Field observations have also been performed in order to examine the role of micrometeorology in new particle formation. Siebert and colleagues conducted observations of ultrafine particles from tethered balloons and found increased particle concentrations (in the 5 to 10 nm range) consistent with fluctuations of temperature and humidity at the inversion layer, supporting the hypothesis that new particles are formed near the inversion (Siebert, Stratmann et al. 2004).

Turbulence kinetic energy (TKE) is used to measure the intensity of turbulence in the atmosphere, and is therefore a very important parameter in micrometeorology. TKE is related to the transport of momentum, heat and moisture throughout the boundary layer. Nilsson et al. performed measurements in the boreal forest in springtime, and found that nucleation days, on average, had twice the turbulence kinetic energy as non-event days and that this was correlated with the passage of Arctic air masses. They noted that nucleation days had half the cloud cover of non-nucleation days, and while this increase in solar radiation is often considered to enhance new particle formation by enhancing photochemistry (and hence H_2SO_4 levels) it also is an important factor in boundary layer evolution, turbulence and mixing (Nilsson, Rannik et al. 2001). Lauros et al. combined surface measurements with sodar observations in order to determine how boundary layer meteorology affects particle formation. They determined that the strength of mixing (calculated from turbulence kinetic energy) was greater on event days, although perhaps the most important factors in predicting new particle formation are the ones that inhibit it.

Because new particle formation is a global phenomenon with climate implications, it is important to increase our understanding of the processes that govern the creation of new particles and their growth. Future research requires field observations including vertical resolution, as conditions at the ground are not always capable of predicting particle formation aloft. Continuous field observations obtained at various locations will provide insight into the features of particle formation such as strength, frequency and associated meteorology. Gas phase measurement of compounds that are likely to be participating in particle formation and growth are also necessary. Other recommendations include the advancement of instrumentation to allow for measurement of clusters below 3 nm as well as the chemical composition (Kulmala and Kerminen 2008). This information will be vital in creating suitable predictive models that will be able to adapt to changing future scenarios.

1.3 Overview of Thesis

The objectives of this work were to better understand the process by which new particles are created, and how these particles are modified throughout their lifetime in the atmosphere. The approach combined field-measurements and observations, with advanced instrumentation and extensive data analysis in order to parameterize the process of new particle formation in the continental boundary layer, thereby increasing the predictive capability of atmospheric models. In addition, a platform for studying ultrafine aerosols, both in laboratory and field settings, has been developed through the construction of various instruments. A mobile laboratory, ideal for field observations, was also constructed.

The specific objectives of the thesis are further discussed and outlined in Chapter 2. The experimental methods and instrumentation are detailed in Chapter 3. This includes information about completed projects and ongoing instrumentation development, namely the Dry-Ambient Aerosol Size Spectrometer (DAASS), a Differential Mobility Analyzer (DMA) to be used for tandem differential mobility analysis studies, and inlets for the conditioning of aerosols. The designs for an automated SO_2 calibration system and a flow tube for thermal denuding experiments are also included in Appendix D.

Chapter 4 discusses the measurements and results obtained during the Midwestern field campaigns. The first half of the chapter includes the results from observations collected at the BEARS research site in Bondville, Illinois and the second half of the chapter focuses on measurements from West Branch, Iowa. The final portion of the chapter draws comparisons between the two measurement locations and conclusions about new particle formation in the Midwest.

Chapter 5 describes the measurements and results obtained during the MILAGRO (Megacity Initiative: Local and Global Research Observations) campaign, in Mexico City in March of 2006. The analysis includes observations of new particle formation events

recorded with the DAASS, and the coupling of these events to the local meteorology. Size resolved, number-based emission factors were also calculated for Mexico City and the methods and results are also included in this chapter.

Chapter 6 provides an overall summary of the dissertation research, and the major conclusions that can be drawn as a result. The significance of the results and their contribution to the understanding of particle formation processes is also discussed. The prescribed future work and recommendations are also included in the final chapter.

CHAPTER 2: OBJECTIVES

Atmospheric aerosols have the ability to affect Earth's climate system in multiple ways, as discussed in Chapter 1. Aerosols may indirectly affect climate by altering cloud properties. For example, anthropogenic activity may increase the number of aerosol particles that serve as the nuclei upon which cloud droplets form. The resulting clouds, made up of an increased number of cloud droplets, will be more reflective and will have longer lifetimes in the atmosphere. The uncertainty associated with the indirect effects of aerosols largely contributes to the uncertainty in our understanding of climate sensitivity to anthropogenic perturbations (see Figure 1.1)

In order to accurately predict cloud condensation nuclei concentrations, an accurate prediction of the atmospheric aerosol size distribution is required. Modeling sensitivity studies have shown that the addition of atmospheric particles, via both new particle formation and primary emissions, has significant effects on predictions of cloud condensation nuclei concentrations (Adams and Seinfeld 2002). Therefore, in order to quantify the indirect effect of aerosols, an increased understanding of the processes affecting ambient aerosol size distributions, namely new particle formation and primary emissions, is required and provides the motivation for this work.

The overarching goal of the thesis is to decrease the uncertainty associated with the aerosol climate effects through an advanced understanding of new particle formation occurring in the continental boundary layer. The approach combined advanced aerosol sampling techniques and instrumentation, with lab and field observations of ultrafine aerosols. The specific objectives of the research are outlined in detail below.

- Construct and optimize a Dry-Ambient Aerosol Size Spectrometer (DAASS) which will be used for measurements of aerosol water content, new particle formation events, and will serve as a detector for nearby ultrafine particle sources (Chapter 3).

- Design and build a DMA system and a thermal denuder flow tube to provide the necessary instrumentation for future TDMA measurements (Chapters 3 and Appendices).
- Construct a mobile laboratory to be used by the Stanier research group during field observations. The design for the mobile lab will include inlets that are specific for aerosol measurements; however, adaptations can be easily made to accommodate future campaigns with differing objectives. The mobile laboratory was deployed in Bondville, Illinois in 2005 and is discussed in Chapter 4.
- Parameterize new particle formation in the Midwest according to the ternary mechanism (H_2SO_4-NH_3-H_2O). Determine the frequency, intensity, and dependence of nucleation events on precursor gas concentrations, associated meteorology, etc. This will be achieved through measurements of aerosol size distribution and SO_2 concentrations, obtained at the Bondville Environmental Atmospheric Research Site in Bondville, Illinois. The measurements will be performed in collaboration with other groups at the BEARS research site (which will provide meteorological measurements and NH_3 concentrations) (Chapter 4).
- Identify the vertical profile of new particle formation in the Midwest (i.e. Do new particles form homogeneously throughout the atmosphere? Do they form preferentially aloft and mix down to the ground?) This will be completed during a small-scale field campaign in West Branch, Iowa at the base of the NOAA tall tower. The vertical resolution of new particle formation will be explored by combining ground-based size distribution measurements with lidar and vertically resolved meteorological and SO_2 measurements obtained from the tower. (Chapter 4)
- Perform observations of new particle formation and determine the aerosol water content of Mexico City aerosols. This will be completed through deployment of the DAASS in Mexico City as part of the MILAGRO field campaign. The

characterization of new particle formation events according to local meteorology, gas phase concentrations, etc. will be completed utilizing measurements gathered by collaborators. (Chapter 5).

- Determine size resolved number-based emission factors representative of Mexico City. Observe the effects that wind direction, time of day, day of week, and other parameters have on this emission factor. Compare the Mexico City emission factors to those previously determined in other locations (Chapter 5).

CHAPTER 3: INSTRUMENTATION AND EXPERIMENTAL SET-UP

3.1 Dry-Ambient Aerosol Size Spectrometer (DAASS II)

3.1.1 DAASS II Introduction

Atmospheric aerosols can affect radiation and climate in multiple ways, as discussed in previous chapters. Atmospheric aerosols have the ability to absorb water, increasing in size with increasing relative humidity. Consequently, this affects many properties of the aerosol including light scattering ability, partitioning, reactivity, and lifetime in the atmosphere. Understanding the hygroscopic behavior of aerosols is necessary in order to understand how they will react to different atmospheric concentrations of water, and hence how they will affect the climate both directly and indirectly (Swietlicki, Hansson et al. 2008).

One of the most commonly used techniques to measure aerosol water uptake is the hygroscopic tandem differential mobility analyzer (H-TDMA). The H-TDMA has been used since Rader and McMurry in 1986, and allows for the collection of real time hygroscopicity data for submicron particles (Rader and McMurry 1986). H-TDMA systems have been used in field and laboratory settings to observe the hygroscopic behavior of urban, rural, marine, and household aerosols as well as aerosols of specific chemical composition (Cocker, Whitlock et al. 2001). In an H-TDMA system, a narrow size range of aerosols is selected using the first DMA. Then, the particles are humidified at the desired relative humidity, and the resulting aerosol size distribution is then measured using a second DMA.

While the H-TDMA is a very useful instrument for observing the water uptake properties of aerosols, it does not measure in-situ aerosol water content. Stanier, Khlystov, et al. addressed this need for in-situ measurements of aerosol water by designing and deploying the Dry-Ambient Aerosol Size Spectrometer (Stanier, Khlystov et al. 2004). The DAASS was designed to measure aerosol water content and aerosol

volume growth factor in 15 minute intervals at atmospheric conditions using an automated system of sizing instruments. It was deployed at an urban location downwind of Pittsburgh during the Pittsburgh Air Quality Study (PAQS) and the results are described in the 2005 paper by Khlystov et al. (Khlystov, Stanier et al. 2005).

In 2006, a second generation version of the DAASS (referred to here as DAASS II) was built at the University of Iowa for deployment in the MILAGRO field campaign in Mexico City, Mexico. The goal for the campaign was to measure the aerosol size distribution from 15 nm to 10 μm multiple times per hour at both ambient and dry relative humidities, allowing the aerosol water to be calculated. The DAASS II also serves to detect new particle formation and provides a sensitive monitor for nearby ultrafine particle sources.

3.1.2 DAASS II Experimental

The DAASS II is an automated combination of aerosol sizing instruments and supporting equipment that measures aerosol size distributions from 10.9 nm to 10 μm at both ambient and dry relative humidities. The spectrometer includes two aerosol sizing instruments, a Scanning Mobility Particle Sizer (SMPS) and an Aerodynamic Particle Sizer (APS). The SMPS (TSI 3085) sizes particles from 10.9 nm to 478 nm at 5 minute intervals, while the APS (TSI 3321) measures the size distribution from .542 μm to 19.8 μm at 20 second intervals. The ambient sample enters a common inlet (shown in Figure 3.1) which splits the sample to the APS and SMPS and ensures that a representative sample of the aerosols enter the instruments. Modifications were made in order to approach isokinetic sampling. The inlet was insulated from solar heating using foam pipe insulation and foil.

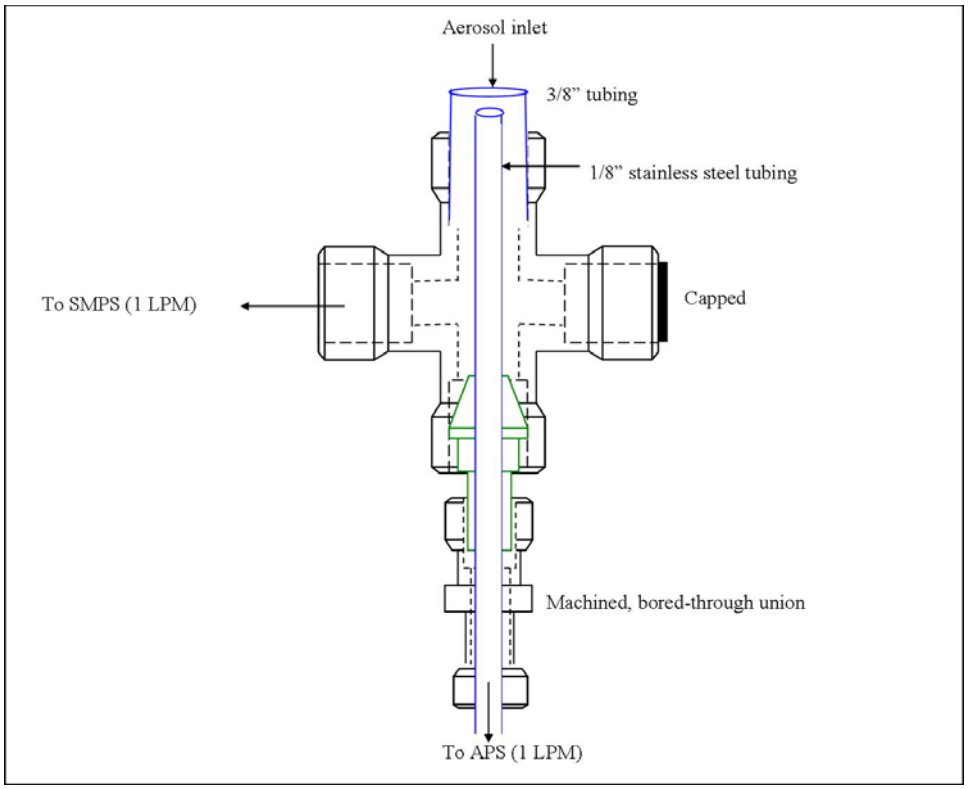

Figure 3.1. Diagram of the DAASS II inlet.

After passing through the DAASS II inlet, the sample stream is split to the APS and SMPS. Here, each instrument has its own relative humidity controlling inlet. Pneumatic and solenoid valves are switched in order to determine if the sample will pass through the ambient or the conditioned side of the inlet before being sent to the sizing instruments (Figure 3.2). When sampling in dry mode, aerosols are passed through Permapure Nafion dryers (MD-110-24S) and a TSI diffusion dryer. Stainless steel, copper, and conductive tubing are used throughout the sample lines to avoid particle losses. Flow splitters with gradual bends were machined by the College of Engineering Design and Prototyping Center and were used instead of 'T' connectors. Modifications were made to the TSI 3062 diffusion dryer in order to minimize particle losses in the sample lines (shown in Figure 3.3). A dry air generation system is also used in support of

the DAASS II to provide relative humidity controlled air for the sheath flows. A mass flow controller (MFC) was used to control the sheath flow into the DMA column (MKS 0-20 LPM model 1479A, SN 001701317) which controlled the flow to within 0.2 LPM of the desired 5.0 LPM.

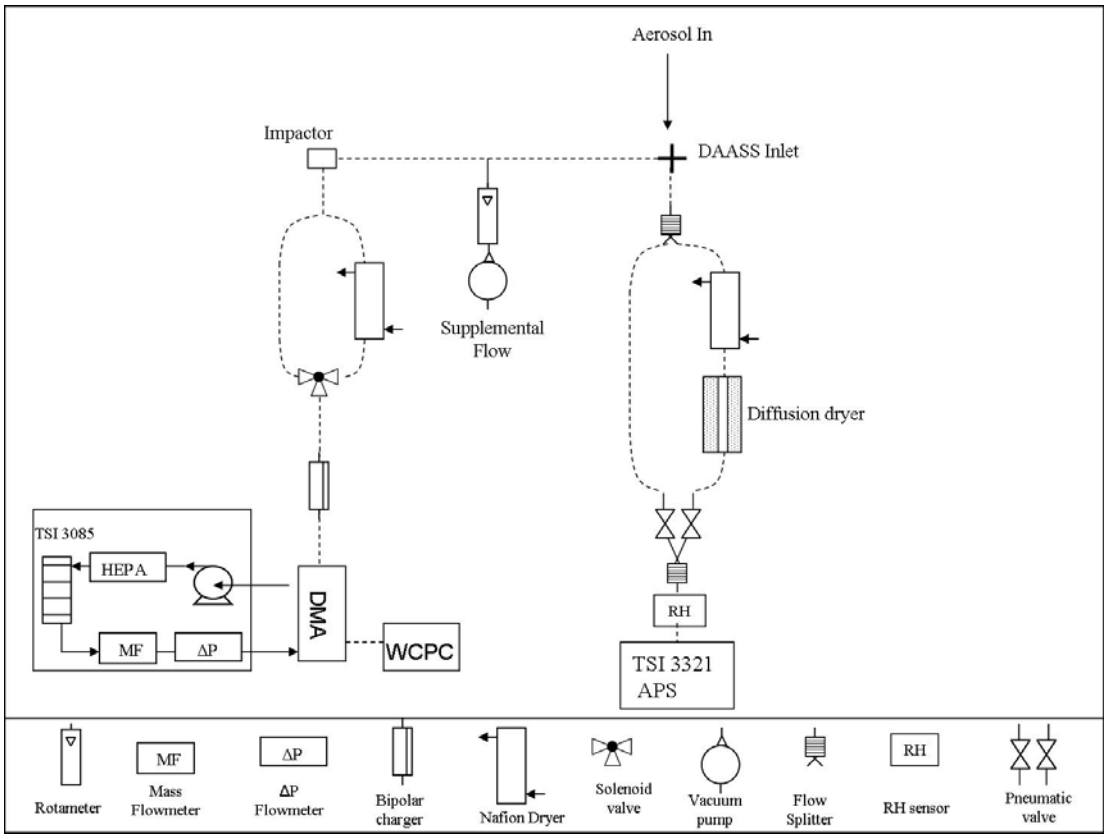

Figure 3.2. Flow diagram of the Dry-Ambient Aerosol Size Spectrometer (DAASS II). The aerosol flow paths are denoted by the dashed lines. All other flows denoted by solid lines.

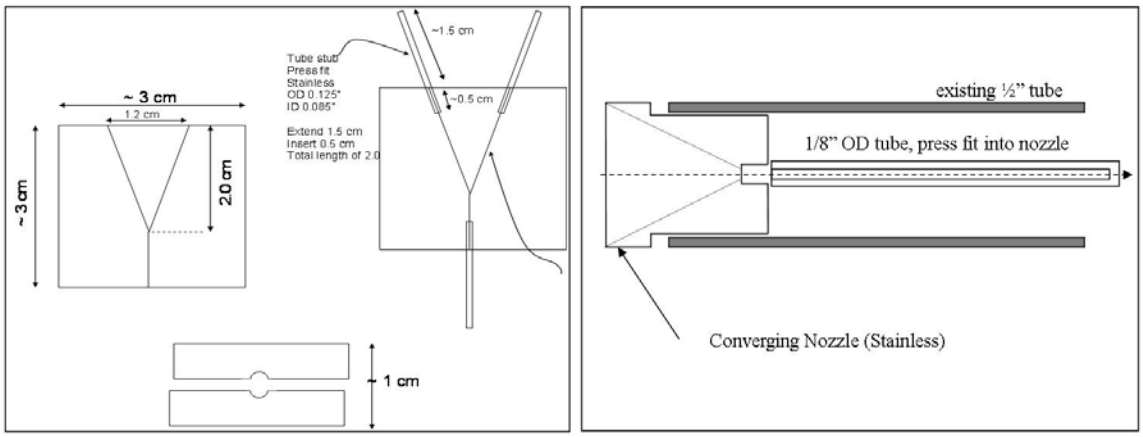

Figure 3.3. Schematic drawing for flow machined flow splitters used to direct flow in the APS inlet of the DAASS II (left). Schematic drawing for the machined conical insert and tubing modifications made to the TSI diffusion dryer (right).

The DAASS II was deployed in Mexico City during March of 2006 for the MILAGRO field campaign. After deployment in the field, the instrument was reconstructed in the lab in order to determine the particle losses in both the APS and SMPS inlets. Having a quantitative measure of the efficiency of the instrument inlet is important. It allows for a correction to be applied to the measured distributions during data processing so that they more accurately reflect the ambient distributions and total concentrations. To characterize the losses in the APS inlet, ammonium sulfate aerosols were created by bubbling clean dry air into Holmes HM485 ultrasonic humidifier filled with ammonium sulfate solution. Then the particle size distributions were measured in both ambient and dry modes. Next, the DAASS inlet and downstream plumbing were removed and the aerosol generation system was placed just before the pneumatic valve and the size distribution was measured again. Transmission was calculated as:

$$n°(Dp)\,with\ inlet \Big/ n°(Dp)\,without\ inlet$$

For the SMPS inlet, a TSI 3076 atomizer with 1g/L solution of ammonium sulfate was used to generate aerosols and the losses before the DMA column were characterized in a similar manner.

Figures 3.4 and 3.5 show the experimental configurations that were used to characterize the inlet losses in both the APS and SMPS respectively. For the APS, losses were only measured for the tubing sections before the pneumatic valve. This is a reasonable approach since the pneumatic valve has no change in internal diameter and the major losses would be expected to occur in the flow splitters and dryers.

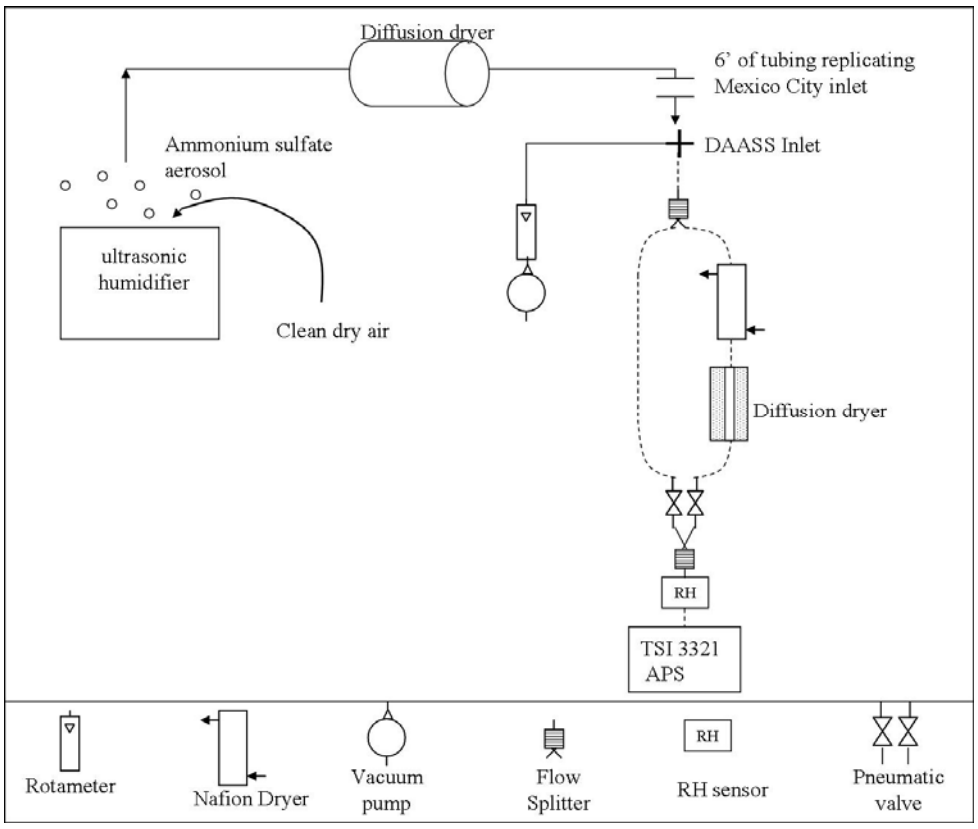

Figure 3.4. Experimental set-up used to characterize the particle losses in the APS inlet of the DAASS II.

The TSI 3321 APS is a time-of-flight instrument that operates by overlapping two laser beams. As a particle passes through the detection area, a continuous double crested signal is produced. Under high particle concentrations, a second particle may enter the measurement area, before the previous particle has left (coincidence counting) and is documented in the data output as an "event 3" ("event 1" occurs when signal is produced

by single low scattering particle, "event 2" is valid particle event). Coincidence counting can be a problem in loss testing if the concentration of particles is high enough that in the "without inlet" mode (low losses) some particles are missed due to event 3, but in "with inlet" mode (high losses) all particles are counted.

Initially the aerosol concentrations from the generator were high enough that coincidence counting was a problem. By diluting the aerosol concentration with clean air, the coincidence rate was reduced to approximately 20% where it was no longer a problem and did not interfere with the test results.

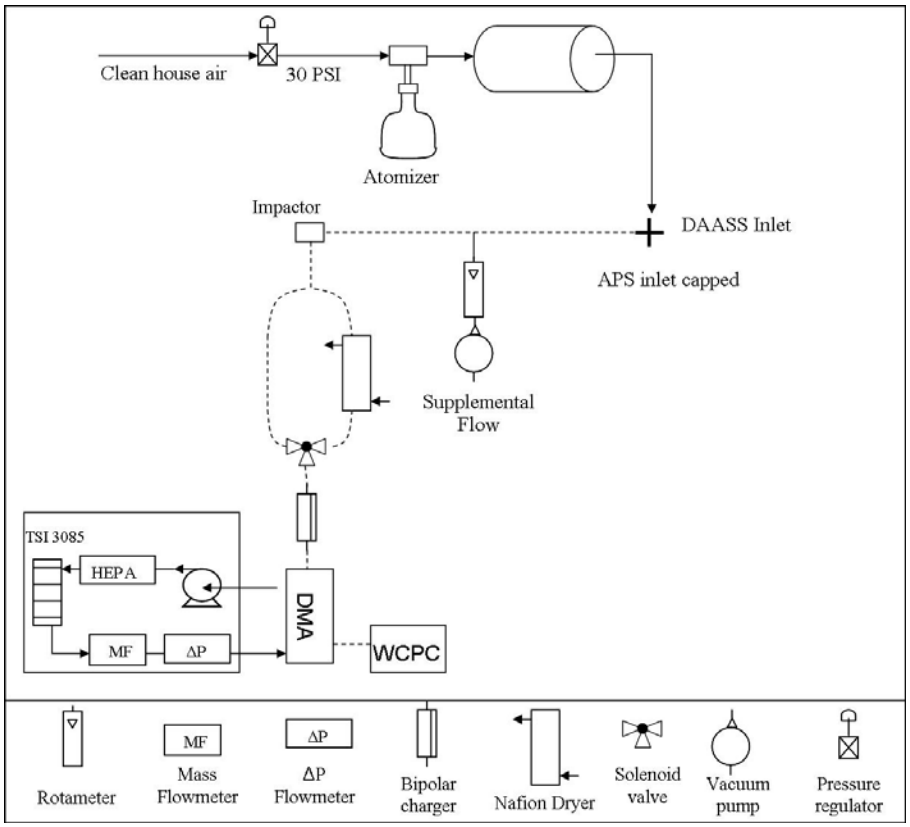

Figure 3.5. Experimental set-up used to characterize losses in the SMPS inlet of the DAASS II.

The results from the transmission efficiency testing are shown in Figures 3.6 and 3.7. Figure 3.6 shows the percentage of particles that were transmitted in the APS inlet at

each particle size in both ambient (blue) and dry (red) mode, while Figure 3.7 shows the SMPS results.

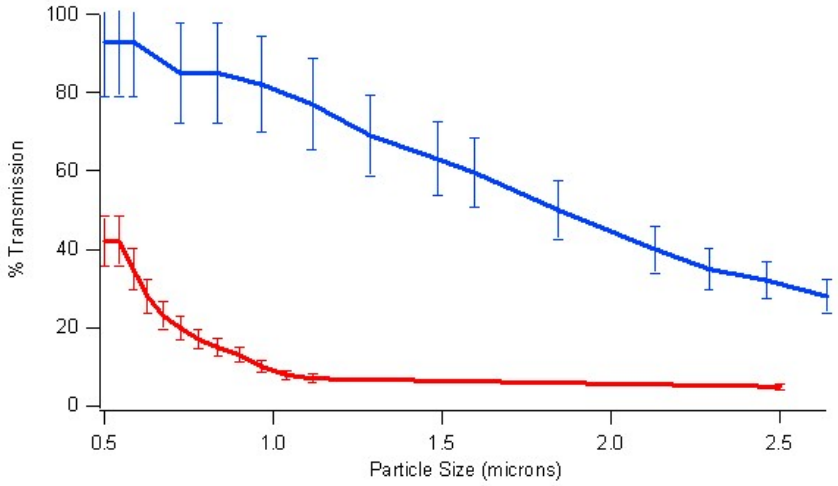

Figure 3.6. Transmission efficiency in the APS inlet of the Dry-Ambient Aerosol Size Spectrometer II. The blue line represents the efficiency of the inlet when the instrument is sampling in ambient mode, and the red line represents the efficiency when sampling in dry mode. Error bars represent $\pm$ 15 %.

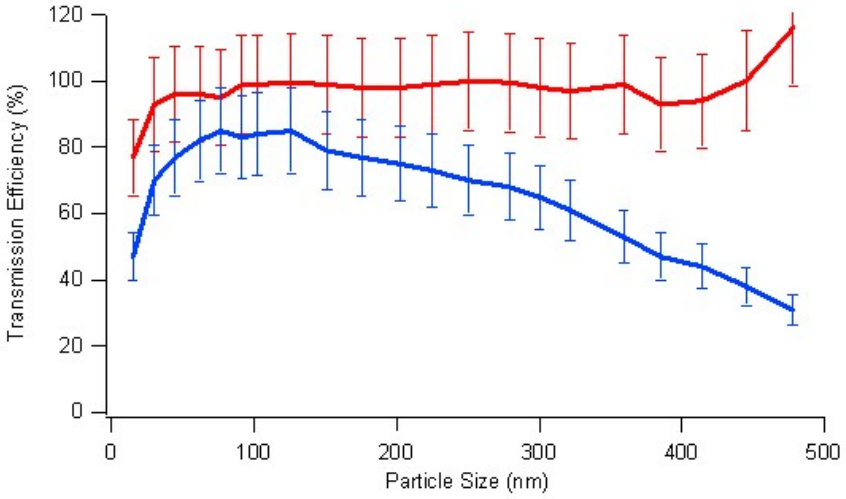

Figure 3.7. Transmission efficiency in the SMPS inlet of the Dry-Ambient Aerosol Size Spectrometer II. The blue line represents the transmission efficiency in ambient mode and the red line in dry mode. The error bars represent $\pm$15%.

The transmission efficiency for particles in the APS inlet when operating in dry mode is notably less than the efficiency when operating in ambient mode (see Figure 3.6). The losses in dry mode are most likely occurring in the Nafion and diffusion dryers, which provide the major difference between the two modes. The losses in each specific portion of the dryers and adjacent fittings could be easily quantified by comparing the size distributions measured directly from the aerosol generator to the size distributions measured by adding each piece of the inlet sequentially, until each component has been added. After the components significantly contributing to the losses have been identified, specific measures can be taken to correct them.

The aerosol concentrations and distributions measured during the losses testing were consistent considering the nominal variability in the generated aerosols, and were considered reproducible. However, as the instrument is disassembled and reconfigured in the field, it would be expected that these losses would change due to minor adjustments in the instrument set-up such as tubing bends and pipe fittings. Therefore, for the most accurate estimates of size resolved particle losses in the inlet configuration leading up to the sizing instruments, it is recommended that the losses be characterized in the field with the instrument in the same configuration as it would be during the experimental data collection.

The DAASS was deployed in Mexico City as part of the MILAGRO campaign in March, 2006 at the T0 research location. At T0, adjacent to the DAASS, Jian Wang of Brookhaven National Lab (BNL) was also sampling with an SMPS system. His SMPS system was designed to measure the size distribution and concentration of aerosols at T0, without any additional processing. Therefore, the BNL SMPS had a short inlet, and did not have any upstream valves or fittings. For this reason, the BNL SMPS system can be assumed to have minimal aerosol losses. In order to characterize the losses occurring in the SMPS portion of the DAASS, a comparison to the BNL SMPS size distributions was made. The DAASS SMPS size distributions were then corrected according to the BNL

SMPS and provide the finalized data set for the Mexico City campaign. Figure 3.8 represents the transmission efficiency of the DAASS SMPS system when compared to the BNL SMPS system. Hourly average size distributions for each SMPS system were compared for twenty-four hours to determine the efficiency shown below.

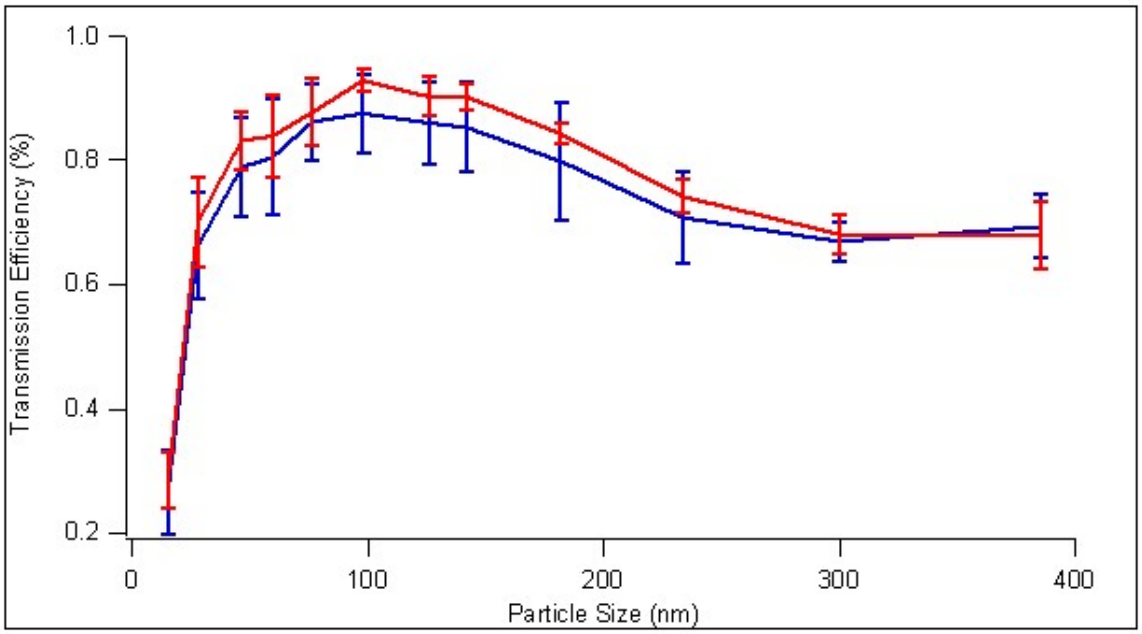

Figure 3.8. Transmission efficiency of the DAASS SMPS system when compared to the BNL SMPS system. The blue line represents the efficiency of the DAASS SMPS when operating in ambient mode, and the red line represents the efficiency in dry mode. The error bars represent ± one standard deviation.

The goals of the initial deployment of the DAASS II were to focus on the hydration state of aerosols and the incidence of new particle formation. The system was successful in detecting new particle formation events, however, the measurement of aerosol water content proved to be more challenging. In order for the aerosol water measurements to be made successfully, better temperature control between the indoor sampling location and the ambient conditions would be necessary. During the first

deployment of the DAASS II, the temperature of the enclosure housing the instruments was elevated compared to ambient conditions, and therefore the samples were drying before they reached the sizing instruments. Incidentally, the instrument sampled in dry mode for the majority of the campaign. For future deployments of the DAASS II, extra precautions should be taken in order to insure that the instruments and inlets are kept at ambient temperatures. This can be done by using a series of fans to draw ambient air into the enclosure or by keeping the instruments and inlets out-of-doors in a protected environment.

3.2 Design and Construction of a Differential Mobility Analyzer

The use of multiple instruments in tandem often provides more complete information about the physical properties of particles than can be obtained with a single instrument. Tandem differential mobility analysis (TDMA) is often used to study particle size changes associated with humidity, evaporation, chemical reactions, and the uptake of organic vapors (Park, Dutcher et al. 2008). In TDMA studies, a DMA system is used to select particles of a narrow size range that are then processed (heated, humidified, etc.) before being sent through a second DMA system to observe the resulting change in particle size.

A DMA system consists of two main parts; the column, which is commonly referred to as the DMA, and the classifier which serves to control the voltage and flow rates. A classifier has been designed and constructed to provide the Stanier research group the capability to perform TDMA measurements of various kinds and is described in the following appendix. The groundwork for the construction of a classifier has been laid, however this remains a work in progress and further steps must be taken in order to optimize the DMA system.

3.2.1 Principle of operation of DMA system

The input aerosol is first passed through a neutralizer which produces both positive and negative ions. Particles carrying a charge are discharged by capturing ions of opposite polarity until equilibrium is reached. Then the particles enter the Differential Mobility Analyzer (DMA) column which separates particles based on their electrical mobility. The column is made up of two concentric cylinders; a center rod where voltages from 20-10,000V are applied, and a coaxial tube which is grounded. Aerosols enter the tube and join a laminar flow of particle free sheath air which flows through the column. Near the bottom of the column is a gap that allows air flow to exit through a central tube. Particles with a specific mobility will exit through the gap where they can be counted or further processed, while particles with a greater mobility will be collected on the center rod before reaching the gap and particles with a lower mobility travel beyond the gap and are filtered out. By adjusting the voltage on the central rod, particles with a specific mobility, therefore size, can be selected (Hinds 1999). The voltage can be scanned from 20 to 10,000 V in order to obtain a measurement of the size distribution. When used in this manner the DMA is often referred to as a Scanning Mobility Particle Sizer (SMPS).

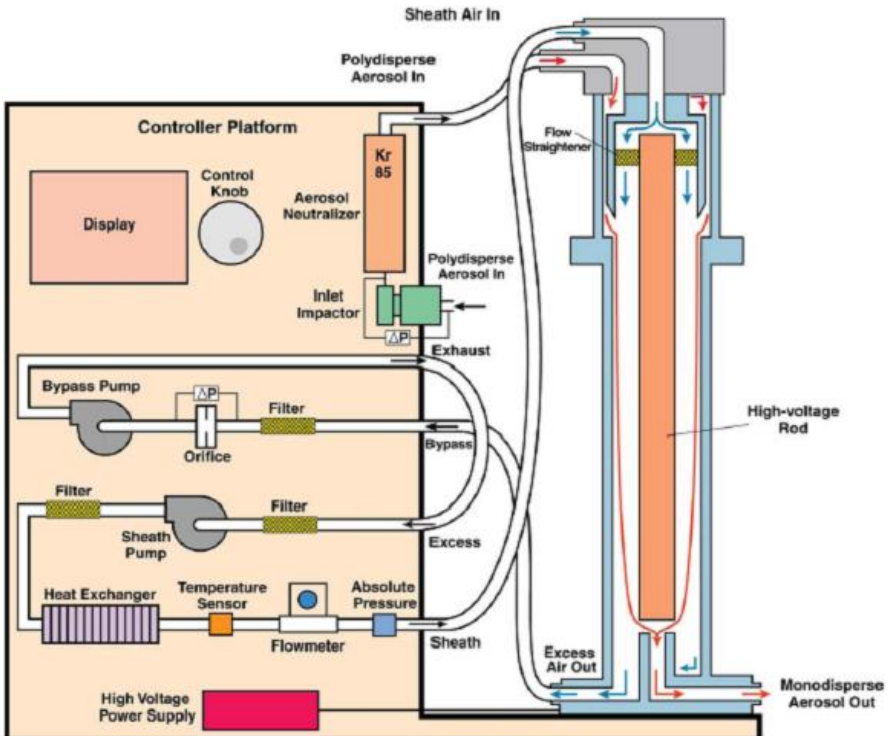

Source: TSI Inc. 3080 Electrostatic Classifier Manual.

Figure 3.9. Diagram of the Differential Mobility Analyzer with the column on the right and the classifier on the left which serves to control the flowrates and the voltage of the system.

3.2.2 Design and Construction of the DMA

A list of required parts for the construction of the DMA classifier is listed below. While there are multiple vendors and components that would be sufficient for the construction of a classifier, the list below represents the parts that were purchased for this specific instrument. Data acquisition for the system was performed using a data acquisition board, connector block, and NI-DAQmx driver manufactured by National Instruments. Programming was done in LabVIEW.

Table 3.1. List of parts required for construction of the DMA system.

Item Number	Description	Vendor/Part Number
1	Po-210 Inline Ionizer	NRD Model 2031
2	Pressure Gauge	Dwyer Magnehelic, Model 2330 with zero center
3	Nano DMA Column	TSI Inc. 3085
4	Specialty high voltage cable	TSI Inc.
5	High Efficiency Particle Filter	Pall Life Science
6	Blower	Rotron Ametek Minispiral HDC Blower, SE12RE21SA
7	Heat Exchanger	
8	TSI Flowmeter	Model 4140 w/RS232 and analog interface cables
9	High Voltage Module	Spellman High Vol. Electronics, Bertan 605C-100N
10	Power Supply to HV module	Power-One 28V @ 1 amp, HB28-1-AG
11	Power Supply to Blower	Omron switching power supply, 25 W 12 V, S82J-02512D
12	Transistor	
13	Capacitor	
14	Fuse	
15	Connector Block to National Instruments	National Instruments SCB-68 Shielded Noise Rejecting I/O Connector Block
16	NI Specialty Cable	NI SHC68-68-EPM Shielded Cable
17	NI Data Acquisition Card	NIPCI-6229, M Series DAQ (32 analog inputs, 48 digital I/O, 4 analog out)

Figure 3.10 is a wiring diagram showing the overall configuration of the parts listed in Table 3.1. These parts are then packaged in an aluminum x-frame box so that each of the components are accessible for maintenance and performance checks while at the same time functioning as a compact, mobile unit.

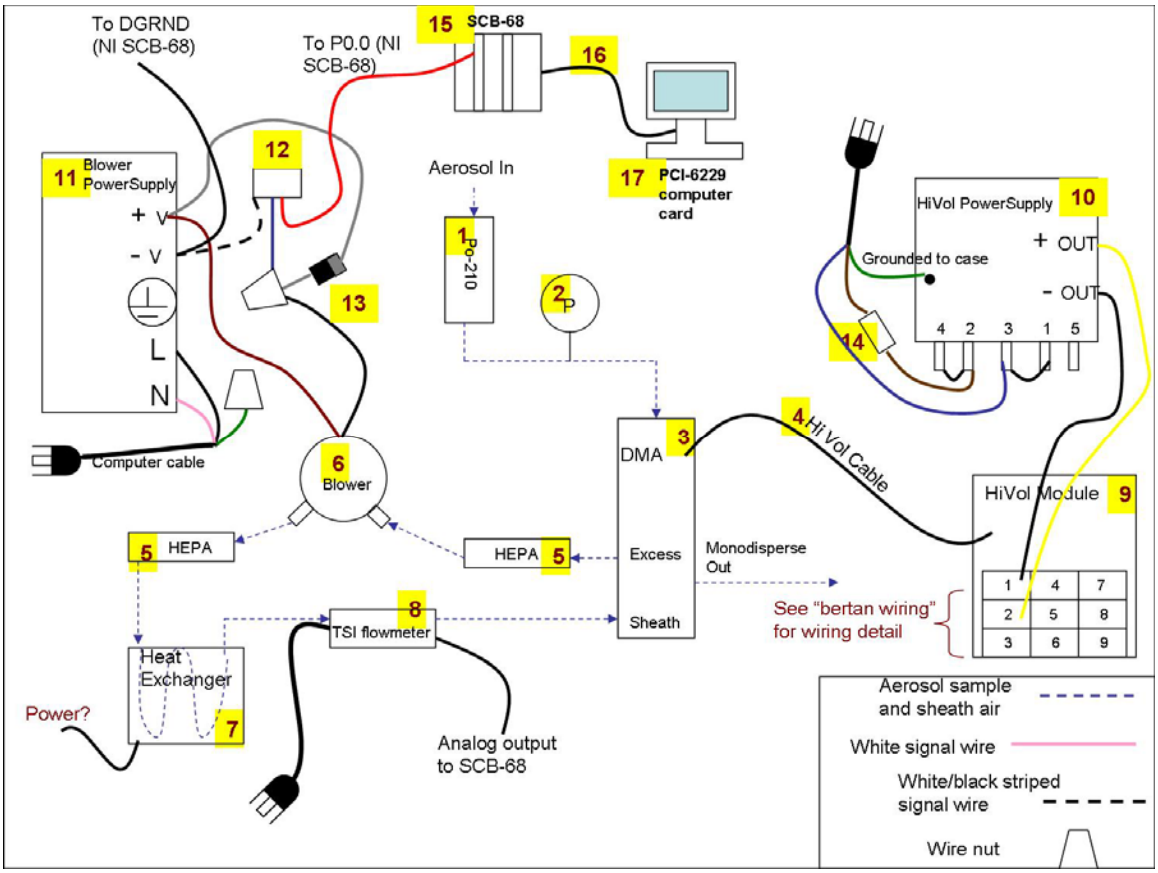

Figure 3.10. Overall wiring diagram of components used in classifier construction. The numbers in yellow correspond to the item numbers listed in Table 1.

The sheath air flow control is done using a variable flow blower powered by a switching power supply. The power supply accepts AC power and supplies DC power to the blower. Higher voltages from the power supply to the blower result in faster fan speed and more air flow. LabVIEW graphical interface is used to communicate with the power supply and by varying the frequency, duty cycle and voltage, the desired sheath flow rate is obtained. Downstream of the blower are a heat exchanger and particle filters to ensure dry, particle free sheath air. The performance of the blower and controlling power supply was tested and the results are shown in Figure 3.11.

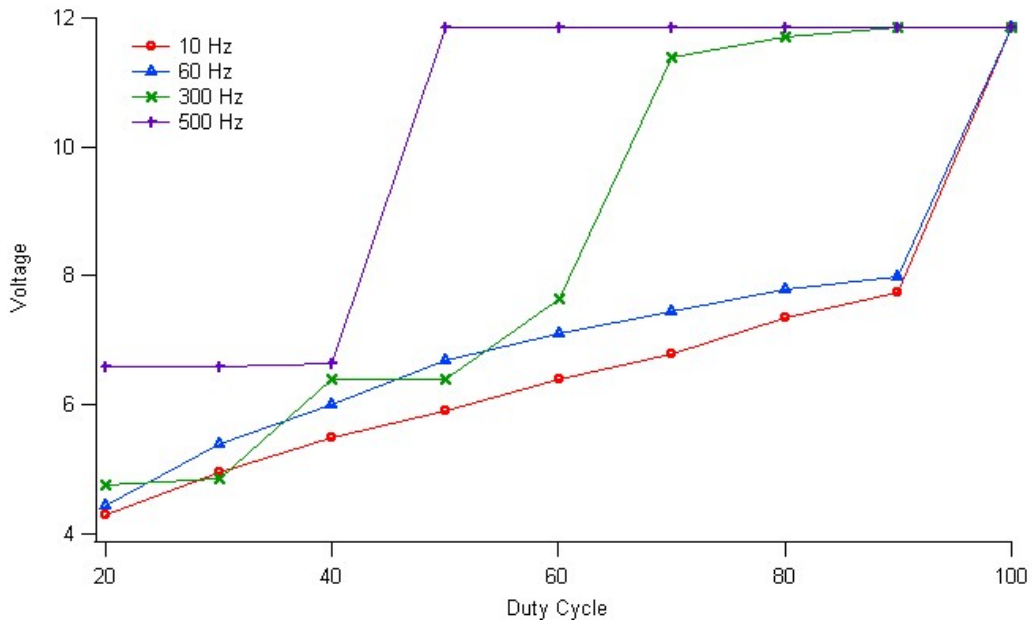

Figure 3.11. Results from sheath flow blower performance testing. The voltage (plotted on the y-axis) was measured across the wires extending from the blower. Using LabView, the duty cycle for the power supplied to the blower was increased and the corresponding voltage (indicative of blower flow rate) was observed for 4 different frequencies (10, 60, 300, and 500 Hz).

The duty cycle was steadily increased from 20 to 100%, and the resultant voltage was measured across the blower wires (refer to Figure 3.10). This was repeated for 4 different frequencies. This voltage corresponds to air flow rate generated by the blower, where 4 V is approximately 3.3 LPM and 12 V is approximately 10.7 LPM. As shown in Figure 3.11., maintaining a steady increase in the flowrate (voltage) output from the blower is difficult using the current programming and components. For fine tuned sheath flow control, further work focusing on LabVIEW programming is necessary.

The voltage that is applied to the DMA column is supplied by a negative polarity high voltage power module. A Power-One power supply provides the high voltage module with a 0-5 VDC analog signal. The 0-5V input signal is proportional to the 0-10,000V output voltage and is controlled using the National Instruments data acquisition system.

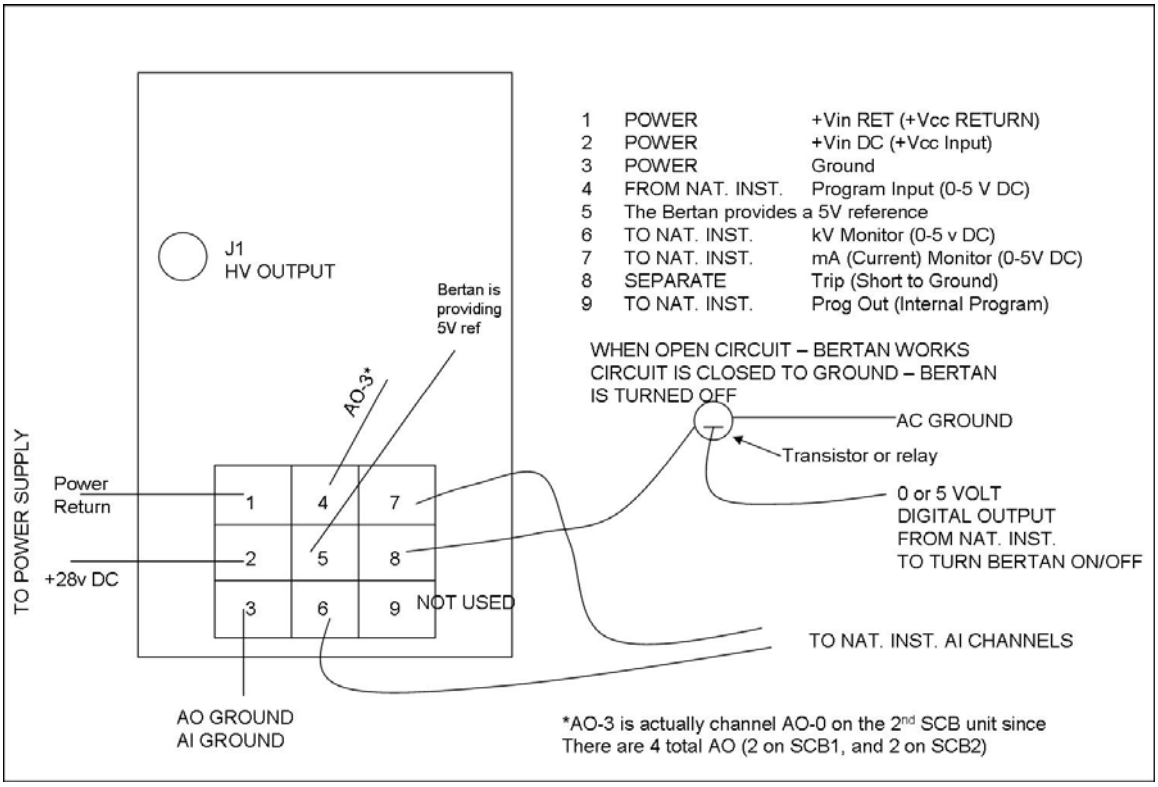

Figure 3.12. Wiring diagram for the Bertan high voltage module.

The accuracy of the high voltage module output is $\pm$ (0.1% of the setting + 0.1% of the maximum). Because the maximum output voltage of this particular unit is 10,000 V the accuracy of the output is at least $\pm$ 10 V. In order to accurately size particles below 20nm, fine control over the voltage is necessary. For example, the required voltage on the DMA column to size a 3nm particle is 16.5 V and is 22.8 V for a 5nm particle. Therefore the uncertainty of at least 10V on the column is not ideal for classifying particles below 20nm in size.

In order for the DMA system to be operational in a field setting, further optimization is necessary. A high voltage meter/probe is required to verify the voltage output from the module as it is applied to the DMA column. More precise control over the sheath flow rates may also be required. Then, characterization of the instrument

using manufactured particles of a known size (polystyrene latex spheres) should be performed to verify that the particle sizing is accurate.

CHAPTER 4: NEW PARTICLE FORMATION OBSERVATIONS IN THE MIDWESTERN UNITED STATES

4.1 Introduction

The creation of new atmospheric particles via nucleation is an important source of atmospheric particles and may influence climate by altering the aerosol size distribution. While there are many theories to describe the process of nucleation, there are still significant gaps in the knowledge of new particle formation. Due to this lack of knowledge, current models used to predict this phenomenon are inaccurate. The goals of the measurements obtained in the Midwest (Iowa and Illinois) were to parameterize the new particle formation events that occur in this region according to the ternary (ammonia-sulfuric acid-water) mechanism and to observe the nucleation response to changing atmospheric conditions and boundary layer dynamics.

The binary nucleation mechanism (sulfuric acid and water) was previously regarded as the primary mechanism for new particle formation (Nilsson and Kulmala 1998). Field measurements have since shown that there are situations that are inconsistent with this theory, indicating that although sulfuric acid appears to play a role, observed particle formation rates can not always be explained by the binary nucleation theory (Weber, McMurry et al. 1999). It was hypothesized that a third molecule may be participating, and ammonia (NH_3) was considered the most likely candidate. In 1999, Korhonen et al. developed a ternary nucleation model of sulfuric acid-ammonia-water that produced higher nucleation rates that those associated with the binary mechanism (Korhonen, Kulmala et al. 1999). Then, in 2005, Gaydos et al. combined their extensive field measurements in Pittsburgh, Pennsylvania, with an aerosol dynamics and chemistry model assuming ternary nucleation of sulfuric acid-water-ammonia. Using the ternary model, they were able to obtain more accurate model-measurement agreement than with a binary model (Gaydos, Stanier et al. 2005).

Results from two Midwestern sites, Bondville, Illinois and West Branch, Iowa are discussed in this chapter. The two locations were chosen based on their proximity to supplemental measurements concurrently taken by various groups and agencies. The Midwestern portion of the United States serves as an interesting place for studying new particle formation due to the high ammonia and moderate sulfate concentrations. The goals of these two campaigns were to quantify the features of nucleation such as strength, frequency, and associated meteorology, as well as to understand whether the observed nucleation events are occurring broadly or if they are confined to specific air masses. Additionally, we are interested in exploring the vertical profile of new particle formation. For example, are the formation events occurring in the atmosphere aloft and only seen at the ground when vertical mixing occurs? The general assumptions were made that Midwestern new particle formation follows the ternary mechanism, and ammonia concentrations are adequately high and therefore not limiting. The specific hypotheses that were to be tested during the Bondville and West Branch campaigns include:

- There are sufficient concentrations of SO_2 throughout the atmosphere for nucleation to occur. The condensational sink at the ground inhibits nucleation and growth at the ground level; therefore nucleation occurs aloft and mixes down to the ground.
- SO_2 limited scenario where plumes rich in SO_2 are emitted in the nocturnal boundary layer aloft and travel to the rural sites. After sunrise, the mixed layer grows and eventually reaches the height of the elevated plume, at which time the SO_2 is mixed to the ground where conditions favorable for nucleation occur.
- The features in the meteorology and the nucleation are driven by the same factor (e.g. solar radiation) and appear to be linked although they are independent.

4.2 Bondville, Illinois

4.2.1 Background

The Bondville Environmental and Atmospheric Research Site (BEARS), is located 8 miles southwest of Champaign-Urbana in rural Champaign County, Illinois and is managed by the Illinois State Water Survey (see Figure 4.1). The BEARS site serves as a monitoring location for multiple research groups and agencies with interest in researching air quality, atmospheric chemistry, meteorology, and climate variability in the Midwestern United States. Due to its location, this site is often used as a representative measure of regional background pollution with minimal local influence (Buzcu-Guven, Brown et al. 2007). The sharing of information is required at the site and the availability of supplemental data makes it an ideal location for deployment.

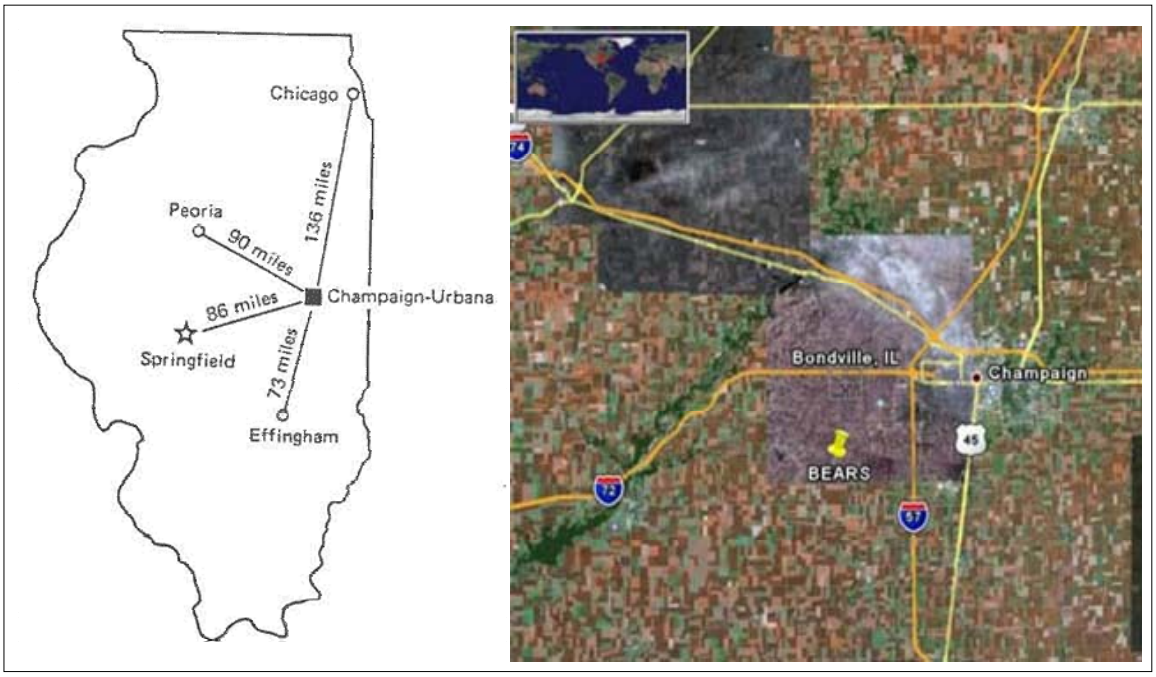

Source: http://www.isws.illinois.edu/atmos/bears/map.asp

Figure 4.1. Location of Bondville Environmental Atmospheric Research Site (BEARS).

The sources that contribute to the particulate matter at Bondville were examined by Buzcu-Guven et al. using Positive Matrix Factorization (PMF) after multiple urban areas in the Midwest were found to be in non-attainment for fine particulate matter (PM) according to the National Ambient Air Quality Standards in 2004 (Buzcu-Guven, Brown et al. 2007). The study was performed in an effort to support more effective control strategies by better understanding the sources that contribute to carbonaceous PM. The analysis was performed on $PM_{2.5}$ data collected at 5 different monitor locations (near Detroit, Cincinnati, Indianapolis, Chicago, and Bondville) from 2002-2005 throughout the Midwest as part of the Speciation Trends Network and the IMPROVE program. Their results suggested that Bondville is greatly affected by aged, transported emissions. Differences in weekday versus weekend emissions were obscured for this reason. At Bondville, the average $PM_{2.5}$ level from 2002 to 2004 was 10.9 $\mu g/m^3$. They determined that the major source contribution to $PM_{2.5}$ was secondary sulfate (27%) followed by secondary nitrate (24%), mobile sources (17%), biomass burning (12%), soil (6%), and steel and mixed industrial sources (each less than 5%).

In 2008, Lewandowski et al. used a chemical mass balance and a secondary organic tracer technique in order to estimate primary and secondary contributions to ambient organic carbon. Similarly to Buzcu-Guven et al., they used ambient $PM_{2.5}$ samples from East St. Louis, Detroit, Cincinnati, Northbrook, IL and Bondville. Their results from Bondville showed that the primary contribution was relatively low (less than 1 $\mu g\ C\ m^{-3}$) and that there is a strong secondary contribution (1.2-2.5 $\mu g\ C\ m^{-3}$) from May to August (Lewandowski, Jaoui et al. 2008).

The Illinois State Water Survey measured atmospheric gases and fine particles at the BEARS site from 1999 to 2003 in order to characterize $PM_{2.5}$. Using a denuder in front of Teflon filters, gas phase ammonia, nitric acid, and sulfur dioxide were measured (Lear 2003). An ion chromatography sampler and a commercial gas analyzer were also deployed for spring and summer of 2003. They determined that ambient ammonia

concentrations are typically around 1 ppb, but values as high as 10 ppb were seen in the fall. Sulfur dioxide averages 1.5 ppb, with maximum concentrations up to 9 ppb during the winter. They determined that the average $PM_{2.5}$ concentration was approximately 13 $\mu g/m^3$, slightly higher than suggested by Buzcu-Guven et al. (10.9 $\mu g/m^3$) although within measurement uncertainty for these processes (Lear 2003).

4.2.2 Experimental

The preparation for the Bondville field deployment began with the design, construction and testing of a mobile laboratory in 2005. The mobile laboratory was constructed inside a Pace American Cargo Sport trailer. The trailer is fully enclosed and equipped with air conditioning, which provides temperature control of the instrument housing environment. Masts were fixed to the exterior of the trailer to support the aerosol inlets. Shelving was built on the inside of the trailer so that the aerosol sampling equipment could sit nearest the aerosol inlets, which allows the inlets to remain as short as possible for increased particle transmission efficiencies. Photographs of the mobile laboratory are shown in Figure 4.2.

Figure 4.2. Photograph of mobile laboratory (left) and inside of mobile laboratory, housing the Scanning Mobility Particle Sizer, Condensation Particle Counter and SO_2 monitor (right).

The goal of this study was to gauge the frequency, intensity and dependence of nucleation events on precursor gas concentrations and local meteorological parameters. The instruments in operation included a nano-Scanning Mobility Particle Sizer (SMPS) (TSI 3080) which measured the size distribution from 3.8 nm to 140 nm, an Ultrafine Condensation Particle Counter (CPC) which measured concentrations of particles from 5 nm to 3μm, and an SO_2 monitor.

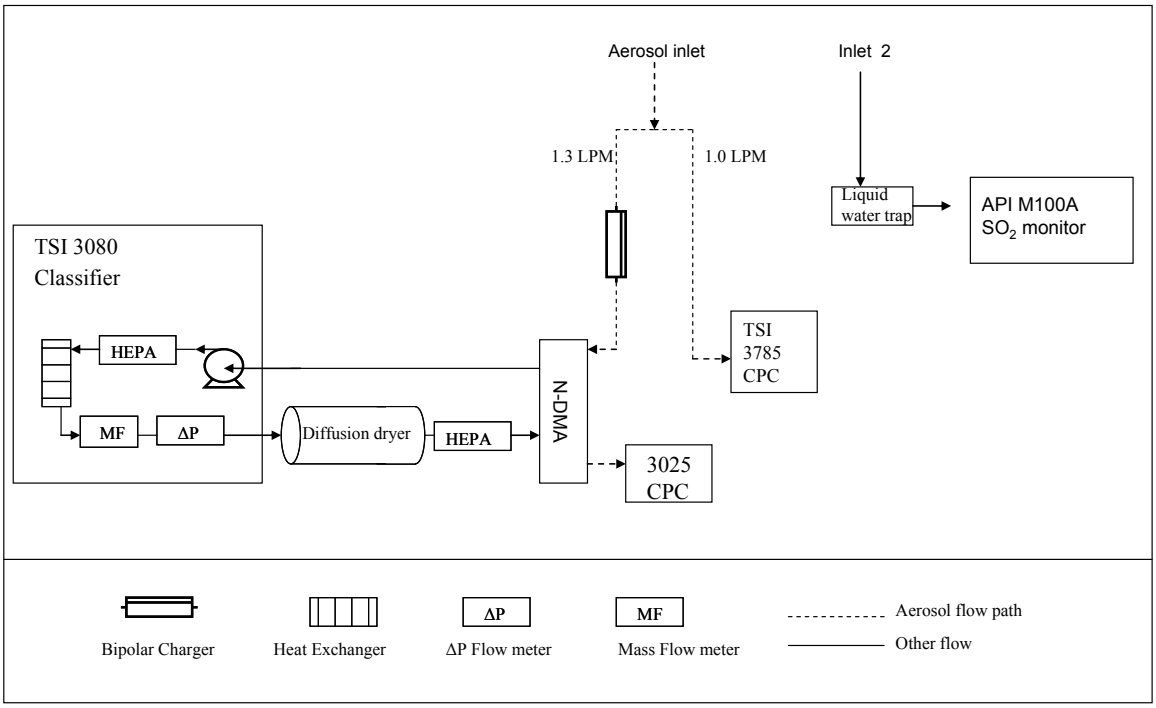

Figure 4.3. Experimental set-up for the Bondville field campaign, August 2005.

For the analysis presented here, 25 days from August 10 to October 5 are analyzed. A list of the additional data sets used in this analysis, including the organization that collected the data, the instrumentation used, the frequency of the measurement and the location of the publicly available data is found in Table 4.1. There

is access to various other measurements that are recorded at the site, but because they are not used specifically for this work they will not be discussed.

Table 4.1. Measurements and data used in the Bondville data analysis.

Organization	Measurement	Method/ Instrumentation	Frequency	Location of Data
Ameriflux Network	Water vapor measurements, carbon dioxide, soil measurements, meteorological data	Vaisala temp/humidity probe, Li-Cor infrared gas analyzers (CO_2 and H_2O), Kipp and Zonen radiometer, Gill sonic anemometer, etc.	Long-term, continuous measurements	http://public.ornl.gov/ameriflux/index.html
Surface Radiation Budget Network (SURFRAD)	Surface radiation measurements, UVB, pressure, net radiation, metrology	Yankee UVB Broadband Radiometer, LI-COR Quantum (PAR) sensor, pryheliometer, pyranometer	Daily files of 3-minute averages	http://www.srrb.noaa.gov/surfrad/index.html
Interagency Monitoring of Protected Visual Environments (IMPROVE)	Particulate chemistry, optical adsorption, PM, etc.	Filter based measurements	Bi-weekly	http://vista.cira.colostate.edu/improve
State of Illinois Environmental Protection Agency (EPA)	PM2.5, SO_2	Federal Reference Method,	6 day monitoring	

UVB irradiance from 280-320nm was measured by the SURFRAD Network using a Yankee UVB Broadband Radiometer. Wind speed and direction were measured by the AmeriFlux Network using a wind monitor and 3-D Sonic Anemometer (R.M. Young 05103 and 81000V). Temperature and relative humidity were also measured by AmeriFlux using a Vaisala temperature/humidity probe (HMP50Y, HMP35D-A). Although an SO_2 monitor was deployed at the site, the monitor did not operate without

internal drift, resulting in negative values for portions of the campaign. Gas phase SO_2 is monitored by the EPA in multiple locations throughout Illinois, and measurements obtained from a representative rural background location in Nilwood, Illinois, (approximately 85 miles southwest of Bondville) are used throughout this chapter as an indication SO_2 levels due to a lack of continuous on-site SO_2 measurements at Bondville.

4.2.3 Bondville Results

Nucleation events occurred on approximately 25% (6 out of 25) of the days studied. Table 4.2 provides a summary of conditions during nucleation events, and includes information about non-event days for comparison as well. All of the events began between 9:00 am and 11:00 am local time. Although the average SO_2 concentration from 9:00am to noon on non-event days is 2.4 ppb, the 24-hour average SO_2 concentration for non-nucleation days during the measurement period at was approximately 1.5 ppb, and it appears that all but one event (on August 11) occurred at elevated SO_2 concentrations. However, the SO_2 concentrations shown in Table 4.2 were measured at a separate location and it is possible that gas phase SO_2 concentrations differed between the monitor location and Bondville. The events beginning on August 30 and October 1 occurred at significantly decreased relative humidities, while the other four occurred at near average values. A longer observation period would be required in order to more accurately determine the effect that each of the listed parameters has on the appearance or absence of an event.

Figure 4.4 is a colorplot of the size distributions recorded on two different days when new particle formation occurred. The plots are for 24-hour time periods and are labeled in local time (Central Daylight Time). September 17 is an example of a day when new particles were observed beginning at 10 nm, whereas on September 30 new particles were detected as low as 5 nm. During two of the six observed new particle

formation events, new particles were detected at 5 nm. During the other 4 events, new particles appeared at 10 nm.

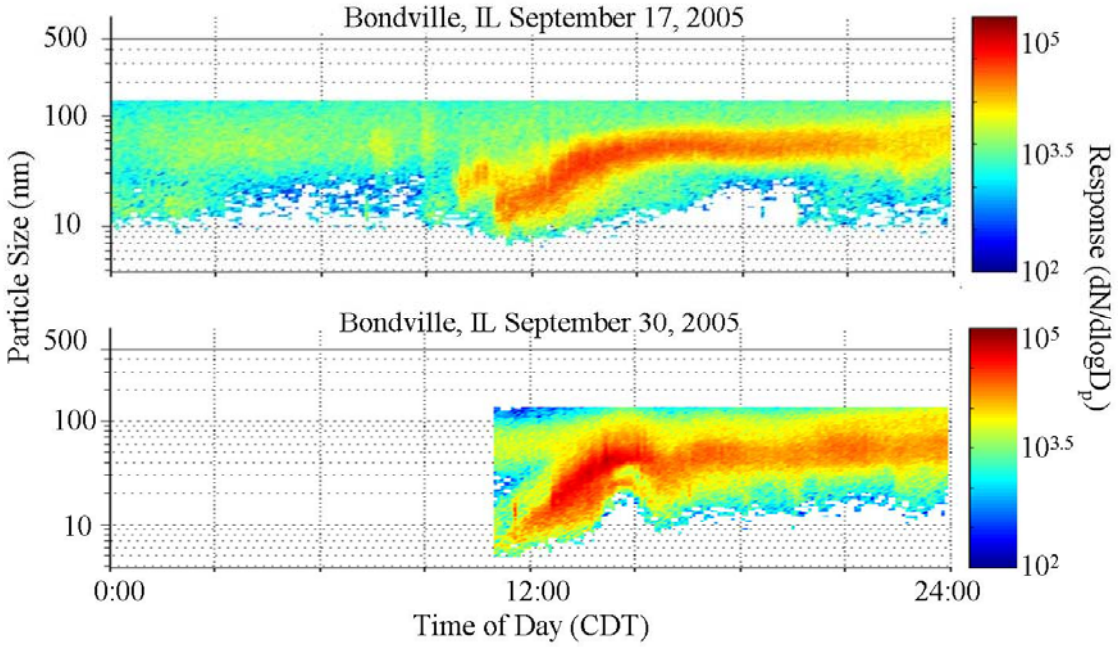

Figure 4.4. Particle size distributions measured on a day where new particles were seen at 10 nm (Sept. 17) and a day where new particles were seen at 5nm (Sept. 30).

Wind roses are shown in Figure 4.5 and are useful in examining how wind speed and direction are distributed. Each bar of the wind rose represents the frequency of time that the wind blew from the corresponding direction (0 to 359 degrees), and the color scale indicates the wind speeds. Panel (a) of Figure 4.5 shows the distribution of wind speed and direction for 24-hour periods on the 19 non-nucleation days during the observation period. The wind on non-event days blew from the southeast quadrant nearly 40% of the time.

Table 4.2. Summary of conditions during Bondville nucleation events.

Date	Time	RH %	Temp °C	Wind Dir. Degree	Wind Speed m/s	UV mW/m^2	SO_2 ppb	CS (3-57nm) cm^{-2}	Number Concentration (#/cc)		
									Before	During	% Change
8/11/05	9:15	79	25.5	167	0.75	59.4	1	7.3E-4	3.4E+3	1.1E+4	235
9/9/05	10:25	63	26.3	300	1.2	89.3	6	NA	NA	NA	NA
9/17/05	10:20	69	19.1	56	2.0	92.3	2	5.2E-4	3.0E+3	8.1E+3	170
9/18/05	10:00	67	20.5	172	3.8	68.4	2	3.7E-4	2.5E+3	6.5E+3	160
9/30/05	11:00	35.7	17.5	174	4.1	104.4	6	4.3E-4	NA	1.0E+4	NA
10/1/05	10:10	51.4	20.2	179	3.1	69.1	13	7.2E-4	3.0E+3	7.6E+3	153
Non-NPF days	9-12	70	26.5	175	3.7	95.6	2.4	4.5E-4		2.8 E+3	

Panel (b) includes the 24-hour periods on event days, where winds from the southeast quadrant dominated. The bottom panel (c) of Figure 4.5 shows the wind distributions from 9:00 am to noon on the non event days, and panel (d) is the hours during new particle formation events. Four of the six nucleation events occurred under conditions of southerly (or SSE) winds, although this may not necessarily be significant due to the fact that winds from this direction occurred at Bondville on the majority of non-event days before noon as well.

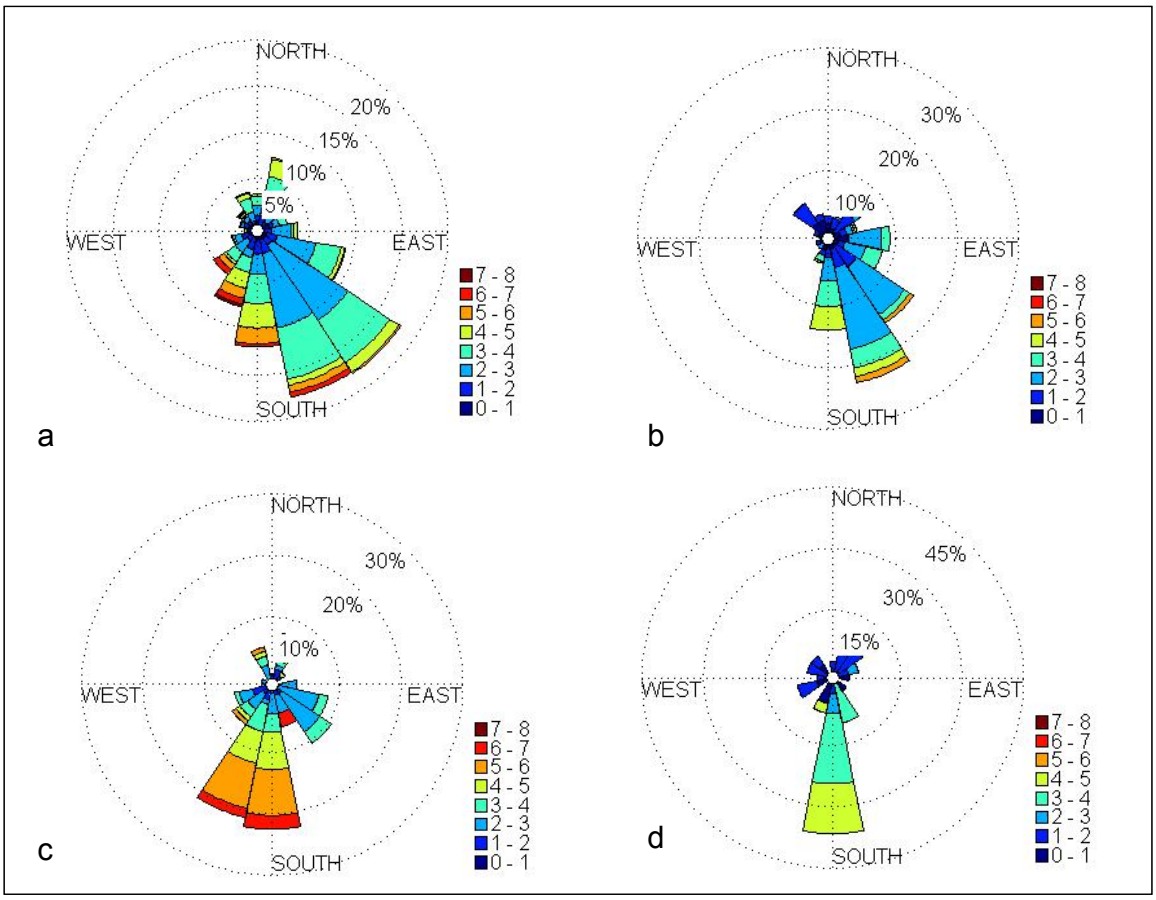

Figure 4.5. Bondville wind roses for a) non nucleation days (24 hour periods from midnight to midnight) b) nucleation days (24-hour periods) c) hours 9-12 for all non nucleation days d) hours during nucleation. Wind speed is indicated in m/s by the color scale.

The HYSPLIT (Hybrid Single Particle Lagrangian Integrated Trajectory) model was used to aid in identifying the correlation between transport of air masses and nucleation. Twenty-four hour backward trajectories leading up to Bondville at the start of each nucleation event were computed. These trajectories show an aerial view of the path an air parcel traveled for the twenty four hours leading to its arrival in Bondville. The trajectories for the six events were all different, and it is therefore concluded that new particle formation is not correlated with a region of longer range transport (see Appendix A).

Figure 4.6 was created in order to test the assumption that new particle formation in the Midwest occurs under increased sulfuric acid concentrations and decreased pre-existing aerosol surface area. Condensational sink (y-axis) is used as a measure of how fast molecules will condense onto pre-existing surface aerosols and is dependent on the shape of the aerosol size distribution (Kulmala, Dal Maso et al. 2001). Because sulfuric acid was not measured directly, the product of SO_2 and ultraviolet light intensity are used as an indication of periods of increased sulfuric acid and is plotted on the x-axis (Boy, Kulmala et al. 2005). The condensational sink calculations presented in Figure 4.6 were integrated from 3 nm to 57 nm. The red dots represent values for time periods when new particle formation was not observed. The black dots represent time periods during new particle formation. One would expect to see the dots representative of new particle formation in the lower right quadrant of the plot (conditions of low condensational sink and high sulfuric acid production). According to Figure 4.6, new particle formation occurs during periods of expected increased sulfuric acid production (UV x SO_2 values ranging between 100 and 1000 Wm^{-2} ppb). The average condensational sink value during new particle formation events is approximately .00054 cm^{-2}, which is only a 10% decrease from the average CS value during the campaign of .00060 cm^{-2}. Although the SO_2 data used to make this plot was collected in Nilwood, the idea that new particle formation occurs during periods of increased SO_2 can be supported using Figure 4.7.

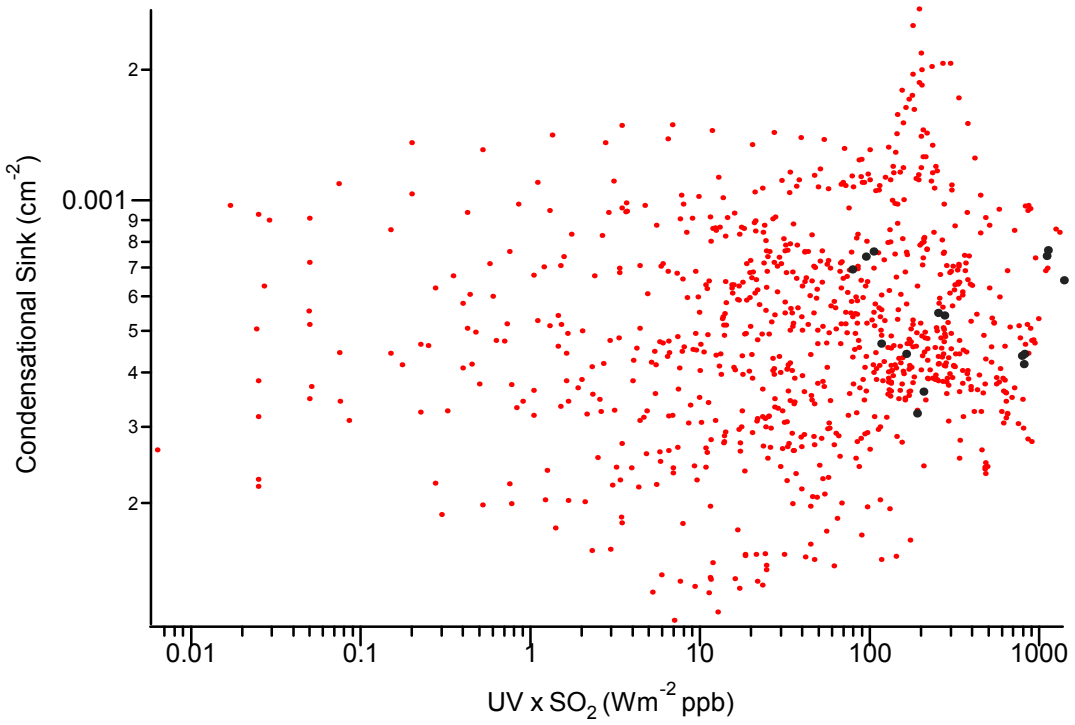

Figure 4.6. Correlation between condensational sink, the product of ultraviolet light and SO_2 (precursors for H_2SO_4), and new particle formation events. The red dots correspond to time periods from August 10 to October 5 when no nucleation occurred. The black dots correspond to the times during the on-set of the nucleation event.

Figure 4.7 represents ambient size distributions and SO_2 measured simultaneously for a day when new particle formation occurred. The SO_2 measurements shown here were gathered using a Teledyne M100A monitor, collocated with the SMPS instrument in Bondville. Although this SO_2 data is not used in the formal data analysis for Bondville due to the drift and variation in internal parameters over time (evident from the negative values), three distinct increases in particle concentration can be correlated with simultaneous increases in SO_2.

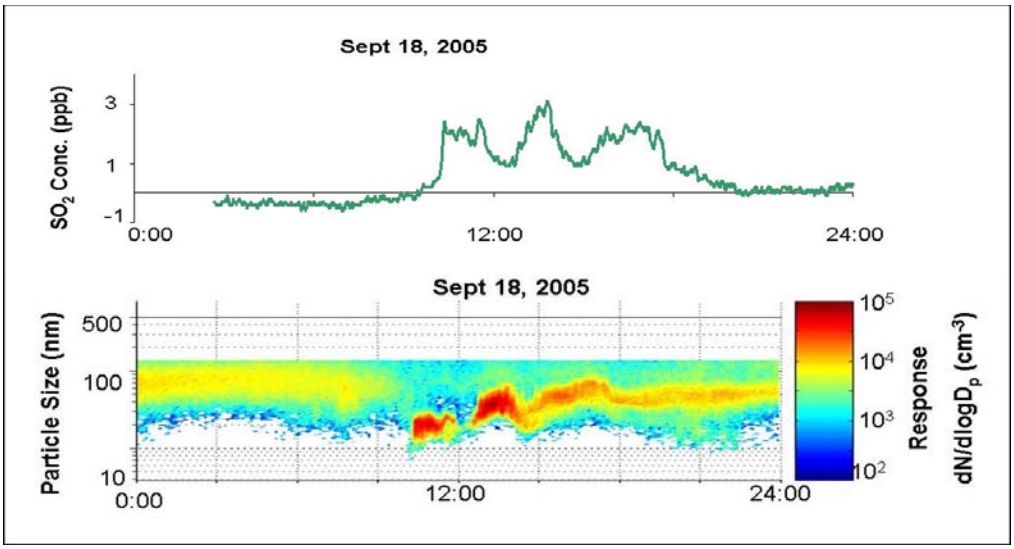

Figure 4.7. Twenty four hours of SO_2 (top) and size distribution (bottom) measurements collected at the Bondville site on September 18, 2005. Increases in SO_2 concentration can be correlated with simultaneous increase in particle concentration.

4.2.4 Bondville Discussion and Conclusions

Nucleation in Bondville occurs under conditions of relatively elevated sulfuric acid and average condensational sink values (see Figure 4.6). This is perhaps an expected result for a location like Bondville, where the average condensational sink values are relatively low when compared to less remote areas. Upon examination of Figure 4.8, it appears that Bondville is situated in a central location with multiple category 5 (10,000-50,000 tons/year) SO_2 emitting facilities in all directions. This may provide an explanation of why nucleation was observed during periods of winds from multiple directions. As mentioned previously, two different types of nucleation events were seen at the Bondville location, one where new particles were seen at 5 nm and another where new particles were not detected until 10nm. Although there is nothing in the data to fully explain this, one possibility is that there exists a link to atmospheric mixing in the vertical direction. For example, if new particle formation occurs aloft and is detected at the ground only when the boundary layer reaches the correct height and

mixes the new particles down, the size of the 'new' particles seen at the ground would depend on the amount of time they have had to grow aloft before they were transported downward. Unfortunately, during this time period for 2005, there are not any measurements that provide a clear picture of the vertical profile of the atmosphere. This plausible link between vertical mixing and onset of nucleation will be further explored in the West Branch, Iowa section of this chapter, where lidar data, provided by Bill Eichinger, is available and provides the necessary information about the vertical profile.

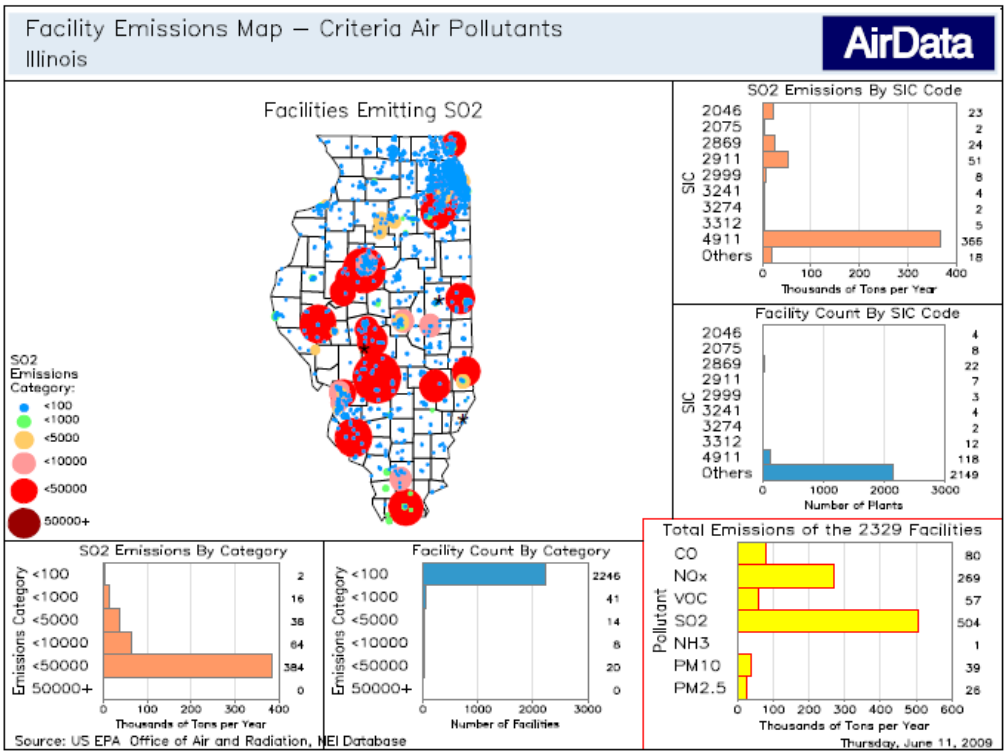

Figure 4.8. Map of SO_2 emitting facilities in Illinois. Emissions come from the EPA's Office of Air and Radiation, National Emission Inventory (NEI) database.

4.3 West Branch, Iowa

4.3.1 Background

During the summer of 2008, a small-scale field campaign was launched in West Branch, Iowa. The goal of the campaign was to observe new particle formation events while simultaneously obtaining information about the vertical profile of gas and aerosol concentrations, and boundary layer dynamics using lidar and tall tower measurements. The West Branch, Iowa site (WBI), located approximately 10 miles east of Iowa City, was chosen for this deployment because it is currently an active site for the National Oceanic and Atmospheric Administration (NOAA) CO_2 monitoring program that uses television tall towers as a platform. Since 2007, monitors installed at the KWKB tall tower in West Branch have been continuously providing measurements of carbon monoxide and carbon dioxide at the surface level, 31 meters, 100 meters, and 379 meters above ground level (see Figure 4.9).

Figure 4.9. West Branch, Iowa Tall Tower (41.72 lat, -91.35 lon). Upward looking view of the KWKB transmitter tower with three met stations extending out to left (left). A temperature controlled shipping container at the base of the tower is used to house the NOAA CO, CO_2 and Stanier group measurements (right).

This tower is the fifth one in the United States to operate as part of the 'NOAA tall tower network' which serves to better understand the carbon balance by quantifying greenhouse gas fluxes (http://www.esrl.noaa.gov/gmd/ccgg/towers/).

Measurements of $PM_{2.5}$, ammonia (NH_3) and sulfur dioxide (SO_2) are monitored at a number of different locations throughout the state of Iowa by the DNR and EPA. Although these measurements are not obtained in West Branch, there are several monitoring locations within a 50 mile radius (Cedar Rapids and Davenport will be presented here). Figure 4.10 shows the hourly data obtained by the Iowa DNR at a non-industrial site approximately 40 miles southeast in Davenport (Jefferson Elementary School) for $PM_{2.5}$, SO_2, and NH_3 and provides and overall background picture of the pollutant levels in the vicinity for the examined time period. In Davenport, the average $PM_{2.5}$ level during June and July was 12.9 $\mu g/m^3$, and was measured using a TEOM-FDMS. The average SO_2 concentrations in Davenport were 0.46 ppb, and the average NH_3 level was 4.7 ppb.

The overall goal for the West Branch deployment was to observe new particle formation and its connection to boundary layer dynamics. The working hypothesis was that new particle formation occurs in the boundary layer aloft (either due to increased SO_2 or decreased condensational sink aloft), and that the new particles are not detected at the ground level until the mixed layer height reaches the air masses where the formation is occurring. Performing the observations at the base of the NOAA tall tower is advantageous, as the tall tower provides vertically resolved pollutant and meteorological information, allowing inference about boundary layer growth and the presence of pollutant plumes. Obtaining gas-phase SO_2 measurements at the three different levels of the tower was attempted. The NOAA system that is used for tower measurements of CO and CO_2 operates by pumping air down to the instruments at ground level through lengths of tubing that run up the tower to the 3 levels. More air than required by the CO and CO_2 monitoring instruments is pumped down, and the SO_2 monitor was to sample this excess

air. However, due to a flaw in the SO_2 monitor calibration system, the quantitative values are suspect and will not be used in the subsequent data analysis. The lidar data and radiosonde measurements, collected twice daily, are used to obtain information about the boundary layer and atmosphere aloft.

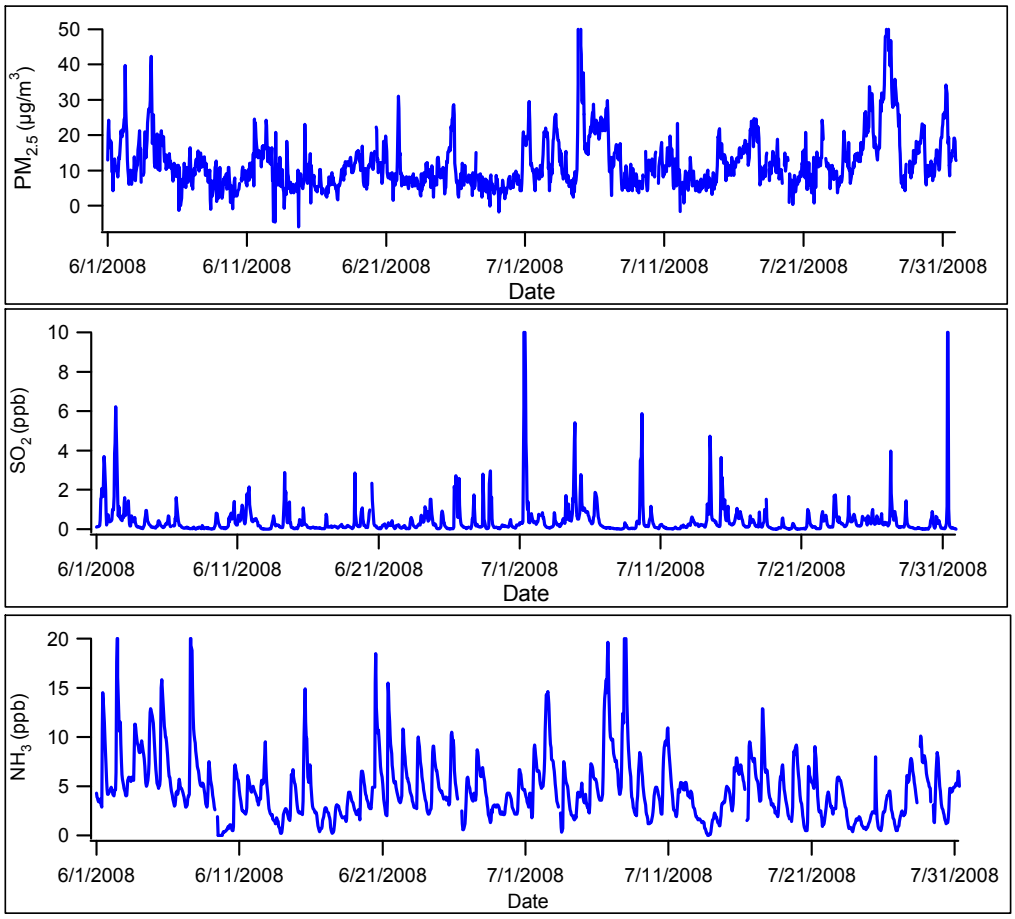

Figure 4.10. Hourly measurements of $PM_{2.5}$, SO_2 and NH_3 taken in Davenport by the Iowa DNR in June and July of 2008.

4.3.2 Experimental

The Stanier group instrumentation was located inside the temperature controlled shipping container, also used to house the NOAA equipment. The shipping container

was modified to allow the inlets for the instruments to extend outside and beyond the influence of the nearby buildings. The size distribution of particles from 3-100 nm was measured on 25 days from June 23 to July 20, 2008 using a nano-SMPS (TSI 3080N and 3025A). The size distributions were measured at ambient relative humidity except during periods of high dew point, when a known volume of dry dilution air was added to the sample stream from the dry air generation system to avoid condensation in the sample lines (see Figure 4.11). An Aerodynamic Particle Sizer (TSI 3321 APS), fitted with a Graseby Anderson PM_{10} inlet, was deployed to measure the size distribution of particles from 0.5-10 μm. The PM_{10} inlet was equipped with a relative humidity sensor and a heated section of the inlet was set to turn on when the relative humidity in the sheath line reached 80%. The SMPS and the APS were housed inside the NOAA shipping container which was equipped with knock-out panels allowing the inlets to extend outside and above the influence of the nearby buildings. Although the APS inlet was equipped with a liquid water trap and a heated inlet, a large rainstorm occurred on the night of July 7 and liquid water was introduced into the APS at which time an electrical short occurred. The APS was not operational for the remainder of the campaign. An API SO_2 monitor was deployed in order to sample the SO_2 concentrations at the 3 different tower levels by sampling the excess air that was pumped down by the NOAA system for CO and CO_2 measurements. All controls for the automated valve switching (dilution air and calibration gas), data logging, and time averaging were custom controls created in Labview. The 'virtual instrument' names and stored location are listed in Appendix B.

There were additional measurements provided by various groups during the campaign, which are detailed in Table 4.3. Forecasting for the campaign was provided by the Carmichael research group. A vertical staring lidar was deployed by the Eichinger research group. Rawinsondes were launched twice daily by the Davis group from Penn State in order to measure the vertical profiles of meteorological parameters. The balloons

were launched from an open field 1.75 miles away from the tower (41.70 lat, -91.34 lon). Also deployed during the campaign was a CO_2 DIAL L IDAR, operated by NASA.

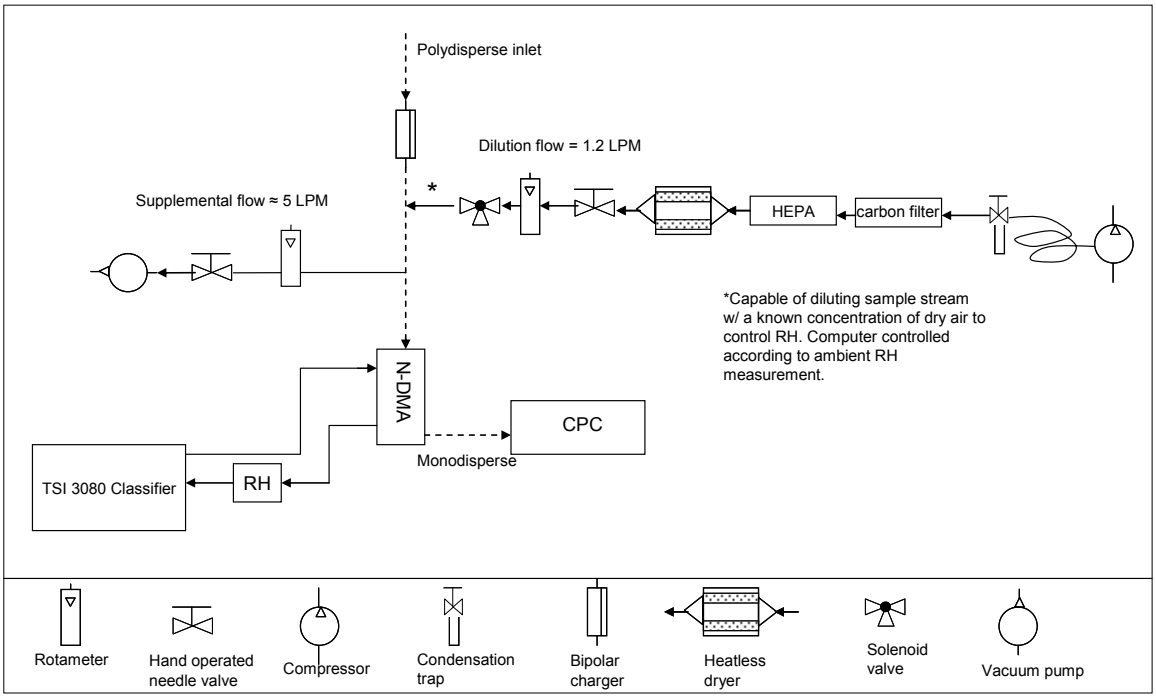

Figure 4.11. Experimental setup of the SMPS during the WBI, summer 2008 campaign. The SMPS was equipped with a dry air generation system, which was computer-controlled to automatically dilute the ambient sample with a known concentration of dry air during periods of high dew point.

Table 4.3. Measurements performed during the West Branch summer 2008 campaign.

Group/Organization	Measurement	Method/Instrumentation	Frequency
Carmichael Research Group, University of Iowa	CO, meteorology (temp, wind speed, dir, etc.)	STEM Air Quality and Transport model	Data output every 6 hours
Eichinger Research Group, University of Iowa	Aerosol backscatter	Vertical Staring lidar 1.064 microns	Continuous, weather permitting
Davis Research Group, Penn State University	Vertical profiles of temp, pressure, RH, wind	Balloon born, rawinsonde	Morning and afternoon launches
NOAA (Aarlyn Andrews and Pieter Tans)	CO and CO_2 at 31, 100, and 379 meters	Licor CO_2 Analyzer, TECO CO Analyzer	Continuous
NASA (Syed Ismail, and Grady Koch)		CO_2 Differntial Absorption Lidar (DIAL)	

4.3.3 West Branch Results

Tall Tower Data used as an indicator of BLH

It appears that new particle formation events are, at times, coupled to rapid boundary layer growth and vertical mixing. Tall tower measurements, such as the ones recorded by the NOAA tall tower monitoring network, can be useful in providing information about the boundary layer.

The tall tower is equipped with three meteorological sampling stations (31 meters, 100 meters, and 379 meters above ground) which provide measurements of temperature, relative humidity, wind speed, and wind direction every 30 seconds (see Figure 4.12). The comparison between the meteorological values at the different levels can be used as an indicator of the boundary layer height. After sunrise, solar heating of the ground causes a turbulent mixed layer to form. This mixed layer grows through entrainment of the air above and as a result of this turbulent mixing, heat, moisture, and momentum become uniform. At the tall tower, the mixed layer grows in this manner from the ground

until it reaches the second level of the tower (100m) and convergence of water content and pollutant concentrations occurs between levels 1 and 2. As the mixed layer continues to grow above the second level and on to the third level, the well-mixed atmosphere extends beyond the height of the tower and the water/pollutant concentrations are the same regardless of what level they are obtained. Figure 4.13 represents the carbon dioxide and dewpoint temperatures measured at the three levels of the tower on July 4, 2008. The CO_2 concentrations measured at level 1 and level 2 converge at approximately 8:15 am as the mixed layer reaches 100 meters. The mixed layer continues to extend until it reaches 379 meters at approximately 10:15 am when the CO_2 concentrations at the first and second levels now converge with the third level. The same trends are seen in the dewpoint temperature measurements which were taken simultaneously.

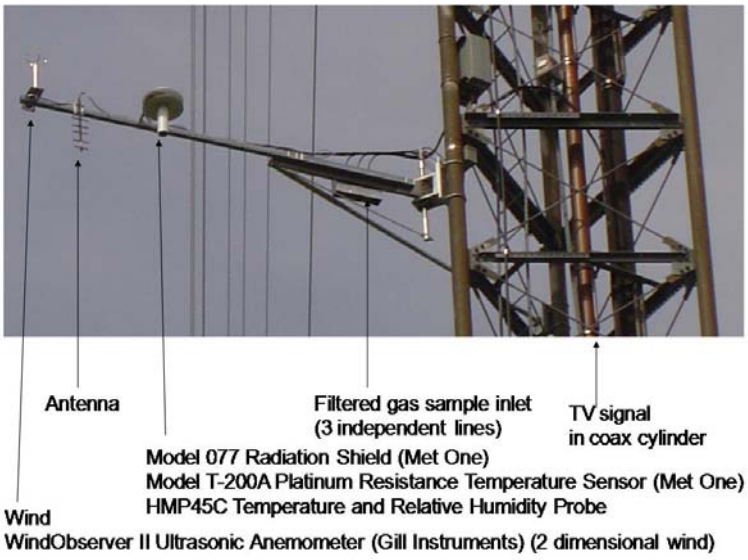

Figure 4.12. A photograph of one of the three tall tower meteorological sampling stations, which are located at 31m, 100m and 379m above ground level. Instrument names and manufacturer listed below.

The method of using the tall tower measurements as an indicator of boundary layer height can be confirmed by comparison with the rawinsonde data. In the lower atmosphere, the water vapor mixing ratio decreases with increasing height, due to the evaporation of moisture from the ground and entrainment of dryer air from above. The moisture decrease across the top of the mixed layer is often relatively sharp and can be used to determine the top of the mixed layer (Stull 1988). Figure 4.14 shows the data from a rawinsonde launch for the same day described in Figure 4.13 (July 4, 2008). The y-axis represents the height of the balloon in meters above sea level (ASL). West Branch, Iowa is located at 240 meters above sea level, and therefore the data here represents the lowest 560 meters above ground. The mixed layer height is approximately 190 meters above ground just after 9:00 am, which is reasonable assuming the height was 100 m at 8:15 am and 379m at 10:15 am.

The planetary boundary layer is the region of the atmosphere near the surface that is directly affected by conditions or events on the earth's surface. There are multiple definitions for boundary layer height and therefore many parameters can be used to estimate it (i.e. height at which moisture sharply increases, or height of zone with significant wind shear). Useful resources on boundary layer height monitoring and boundary layer height determination can be found in the textbook by Kovalev and Eichinger (Kovalev and Eichinger 2004).

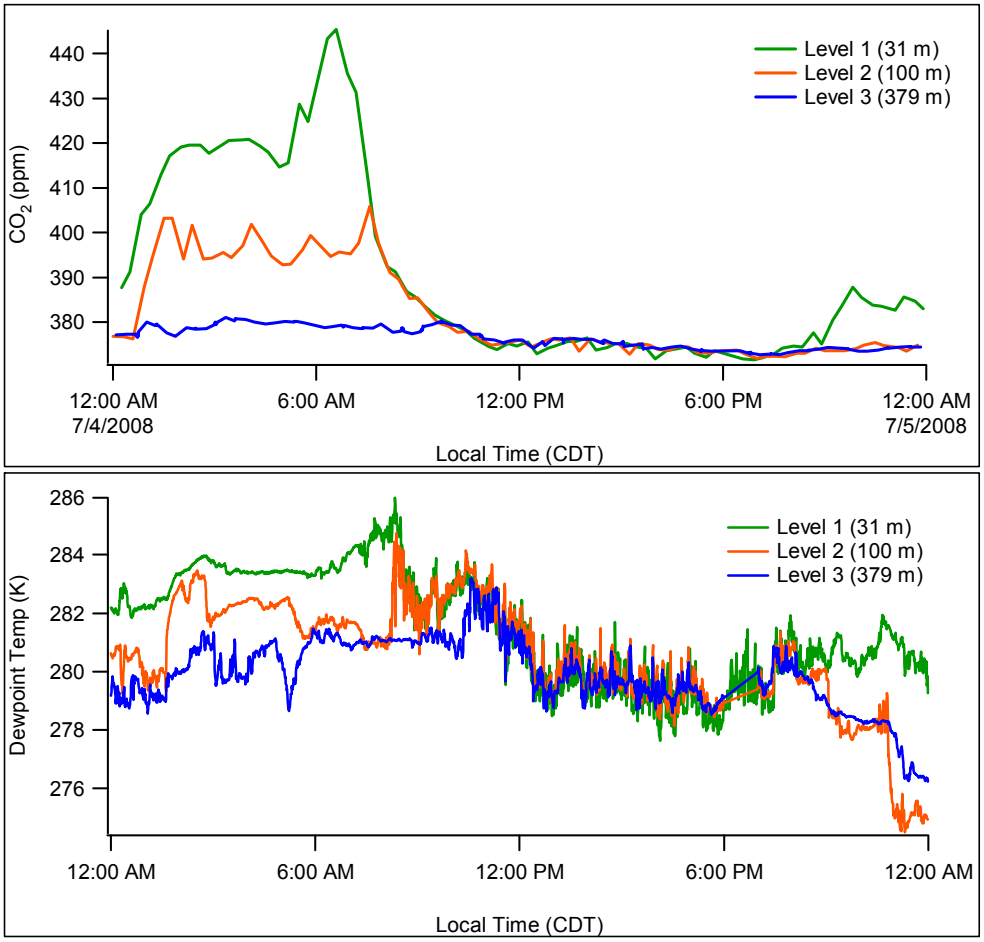

Figure 4.13. Carbon dioxide concentrations (top) and dewpoint temperatures (bottom) as measured at the three sampling levels of the tall tower located in West Branch, Iowa for July 4, 2008. The boundary layer appears to reach 100 meters at approximately 8:15 am and 379 meters at 9:30 am.

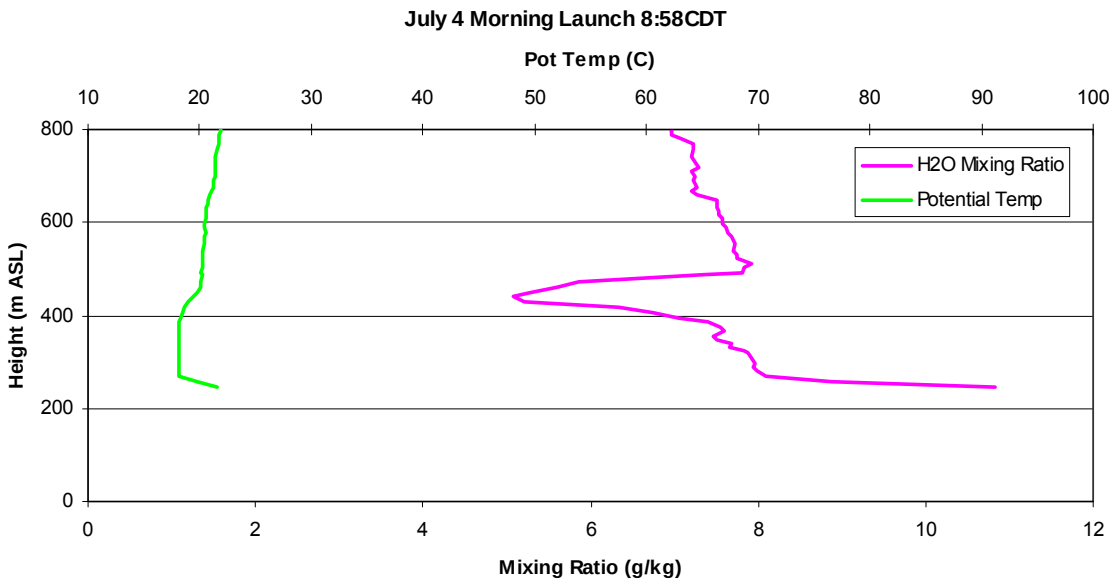

Figure 4.14. Rawinsonde data collected beginning when the balloon was launched at 8:58 am on July 4. The height (y-axis) is measured in meters above sea level. The sharp decrease in water mixing ratio at 430 m ASL suggests the top of the mixed layer.

New Particle Formation in West Branch, Iowa

New particle formation events were observed on 10 of the 25 days (40%) sampled. Table 4.4 provides a summary of the conditions during the events, as well as the average conditions for non-event days. Nucleation events in West Branch occurred as early as 6:30 am and as late as 3:00 pm. The events were classified into three different types; 1) strong morning formation events, 2) afternoon formation events, and 3) intermittent new particle formation. Half of the events (5 of 10) were classified as type 1, and are examples of commonly observed events which occur shortly after sunrise. Two of the events occurred in the afternoon and are classified as type 2, and the remaining three events were characterized by bursts of new particles, followed by significant decreases in particle concentrations (type 3). An example of each type of event as recorded by the SMPS is shown in Figure 4.15.

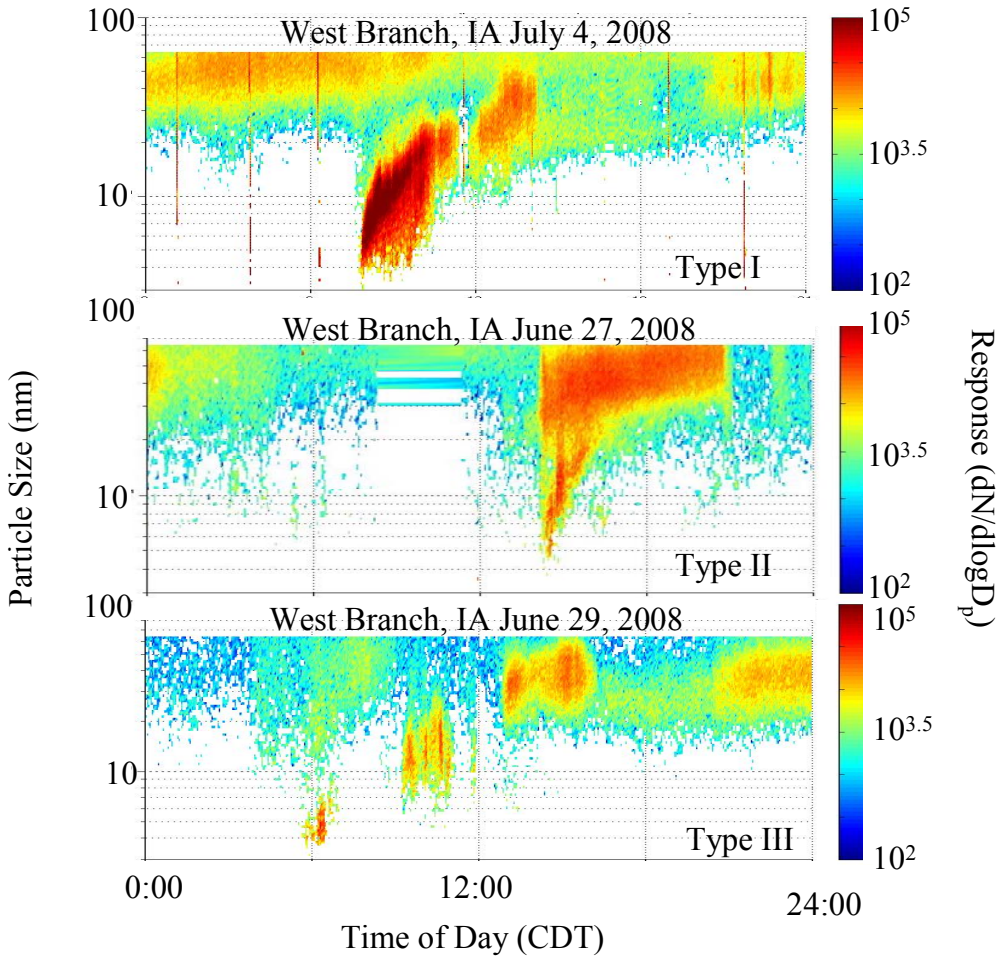

Figure 4.15. Three days of recorded size distributions, representing the three different types of new particle formation events observed in West Branch, Iowa. July 4 provides an example of a type I event, described as a strong event occurring in the morning (top). June 27 is representative of a type II (afternoon) event (middle) and June 29 is an example of an intermittent new particle formation event (bottom), or type III.

Meteorological data from the tower regarding wind direction and speed, as well as back trajectory analyses were used to determine whether or not air masses of different origins could be used to distinguish between non-event and event days, or between the different types of events seen in West Branch. Figure 4.16 shows the wind rose plots for West Branch. The wind direction and wind speed data used to make these plots was taken from the lowest level of the NOAA tall tower, at approximately 31 meters above

ground level. The top left panel of Figure 4.16 is the plot of wind speed and direction for twenty-four hour periods on the days where no new particle formation event occurred. The top right panel shows twenty-four hour periods on days when an event occurred. The lower left panel is an average of the wind speeds and directions from 9am-noon for all non-event days and the lower right panel includes the wind data obtained during a formation event.

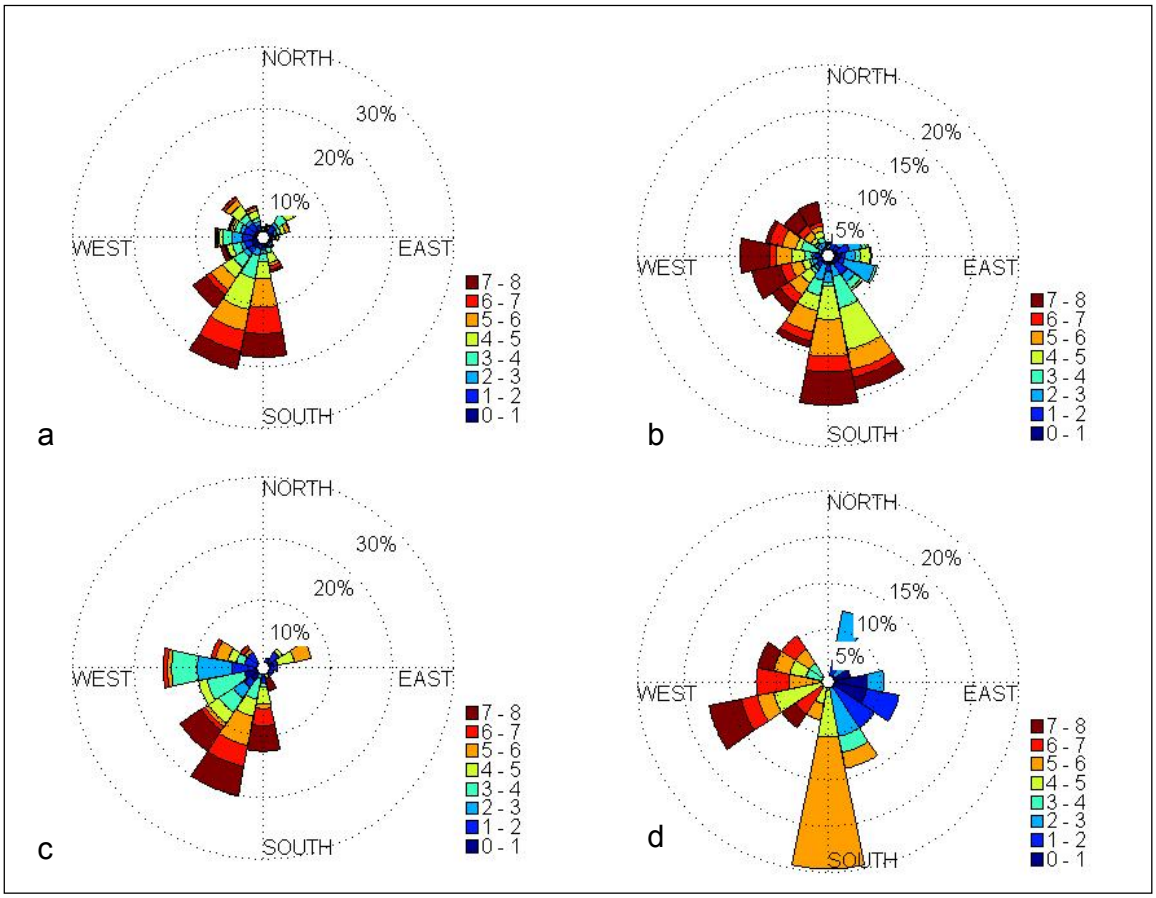

Figure 4.16. West Branch wind roses for a) non nucleation days (24 hour periods from midnight to midnight) b) nucleation days (24-hour periods) c) hours 9-12 for all non nucleation days d) hours during nucleation. Wind speed is indicated in m/s by the color scale.

Table 4.4. Summary of conditions during West Branch nucleation events.

Date	Time	RH %	Temp °C	Wind Dir. Degree	Wind Speed m/s	Type I, II, III	SO_2 ppb	Transport from nearby SO_2 sources likely?	Time for BL to grow from 99 to 379m (min)
6/23/08	NA	73	17.5	40	2.2	I	2	Y	95
6/24/08	8:44	57	22.4	183	5.3	I	23.3	Y	95
6/27/08	15:03	70	23.9	246	7.2	II	3	Y	125
6/28/08	9:00	62	20.2	246	4.8	III	1.1	N	110
6/29/08	6:37	88	15.7	299	5.2	III	1.3	N	110
7/4/08	8:34	62	18	102	0.8	I	2.8	N	115
7/5/08	8:32	57	20.3	145	2.1	I	2.8	Y	100
7/7/08	9:40	76	25.9	179	5.1	I	11.5	Y	90
7/10/08	11:10	75	25.6	212	5.4	III	1.6	Y	60
7/12/08	13:26	61	20.5	284	5.7	II	1.6	Y	inconclusive
Non-NPF days	9-12	67	23.5	210	4.4		6		112

It appears from Figure 4.16 that the hours during new particle formation events were more heavily influenced by winds from the south than non-event time periods, suggestive of a local influence. Therefore, SO_2 emissions data were acquired for eastern Iowa from the EPA National Emissions Inventory database. Although the inventory is for the year 2002, it reflects facilities that were still operational as of 2008 and provides an accurate estimate. Figure 4.17 is a map of Iowa that marks the location of facilities emitting SO_2 and the relative amount of pollutant released per year in tons. West Branch, Iowa lies just over the Johnson County boarder in Cedar County. As shown on the map, significant SO_2 emitting facilities lie just south of West Branch. The major point sources contributing to the emissions are concerned with electric power generation (15,901 tons/year) and grain processing (10,900 tons/year).

Back trajectories for West Branch were created using the NOAA HYSPLIT model in order to determine, along with the meteorological data, on which days transport from the nearby SO_2 emitting facilities was likely. The results from this part of the analysis were then summarized in Table 4.4. Transport to West Branch from a significant nearby SO_2 emitting facility was likely on seven of the ten event days.

Further estimation of the impact of SO_2 concentrations on new particle formation events was attempted using data recorded by an Iowa DNR monitor located 23 miles southeast of West Branch in Muscatine County. This monitor lies in between the West Branch measurement site and the major SO_2 facilities in Muscatine and Louisa counties, and would therefore be expected to capture likely increases in SO_2 at the WBI measurement site on days when transport from facility to WBI is likely. The time series of SO_2 concentration from this monitor for the duration of the campaign is shown in Figure 4.18 and the hourly averages are represented in Table 4.4. The blue 'x' symbols on the x-axis represent the times when new particle formation began. It is interesting to note that for the seven events where transport from the SO_2 emission areas to WBI was likely, new particle formation in West Branch usually occurred during a peak in SO_2

concentration above 2 ppb. The two events (June 28 and June 29) that do not follow this trend occurred when transport from the SO_2 emitting facilities to the monitor and on to West Branch, Iowa was not likely.

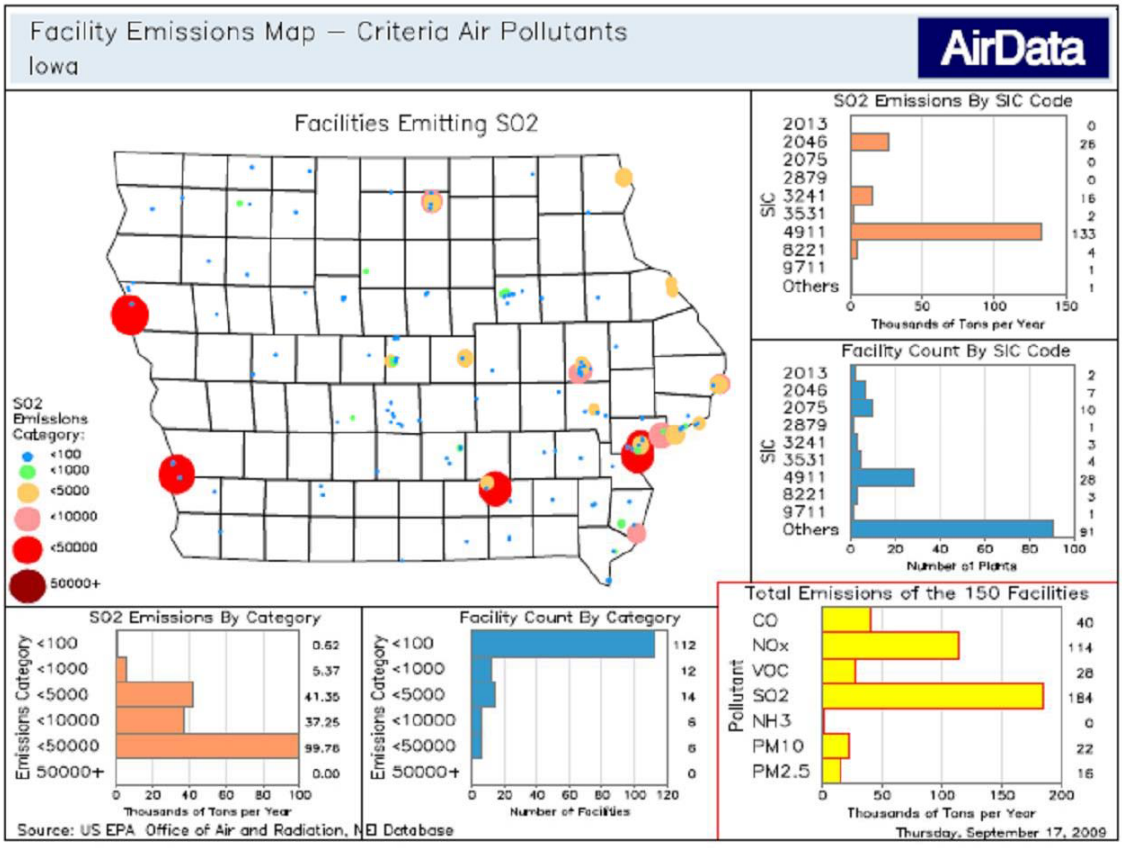

Figure 4.17. Map of SO_2 emitting facilities in the state of Iowa. Emissions come from the EPA's Office of Air and Radiation, National Emission Inventory (NEI) 2002 database.

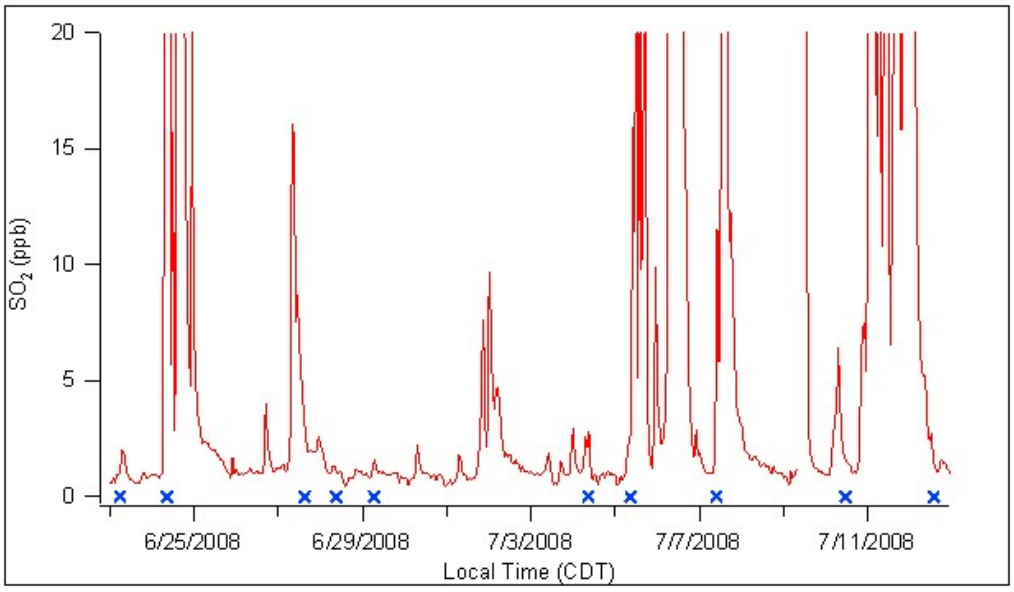

Figure 4.18. SO_2 concentrations measured in Muscatine, Iowa during the campaign. The x-symbol represents the times that new particle formation events began.

Of the seven events that occurred during time periods when transport from the emission facilities was likely, two occurred in the afternoon and 5 occurred in the morning. The time series of SO_2 concentrations for each of the seven days was compared in order to determine if the timing of peaked SO_2 concentrations could account for the difference between morning and afternoon events (types I and II). However, increases in SO_2 in the morning were seen on both the days with morning and afternoon events alike.

The link between boundary layer growth and new particle formation was explored using the tall tower and rawinsonde data as an indicator of boundary layer growth up to 379 meters. The tall tower provides an estimate of the time that the boundary layer reaches 99 and 379 meters. The elapsed time required for boundary layer height to increase from 99 to 379 meters was calculated for all event and non-event days during the campaign. These values are listed in Table 4.4. The average time required for the boundary layer to elapse the 280 meters between the tower levels was relatively similar between event days (100 minutes) and non event days (112 minutes). The time required

on non-event days ranged from 75 minutes to 140 minutes. The mixed layer height versus time for new particle formation days is plotted in Figure 4.19. The mixed layer height was determined using CO_2 tall tower data and rawinsonde data when available. The triangles on the x-axis represent the time that new particle formation began and are color coded corresponding to the date. The on-set of the formation events occurring on June 27 and June 29 do not fall within the generally expected timeframe for a typical event, however a major difference in the boundary layer growth between these events and the other eight is not noted.

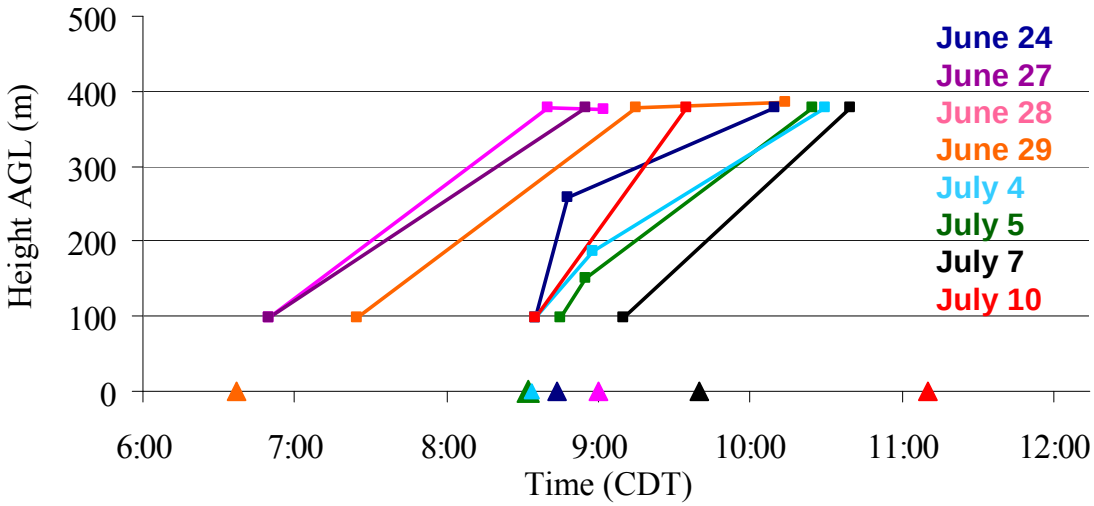

Figure 4.19. Mixed layer height versus time for days with nucleation events during the West Branch 2008 campaign. Mixed layer height was determined using both CO_2 concentrations from the tall tower, and rawinsonde data when available. The triangles at the bottom indicate the time that nucleation started on the specific day.

Potential of Future Measurements

Lidar (light detection and ranging) is a useful tool in quantifying the amount, existence, and reflective properties of atmospheric aerosols. Lidar systems are remote

sensing instruments transmit laser light, which is scattered off of molecules, cloud droplets and aerosols in the boundary layer. The returned light is collected and focused on a photomultiplier detector, then amplified, digitized and recorded (Stull 1988). The data collected can be used to obtain a relationship between the backscattered light and the altitude at which the scattering occurred and therefore, the lidar was deployed at West Branch in order to provide information about the vertical profile of aerosols in the atmosphere. Simultaneous measurements of SMPS size distributions, lidar backscatter, and gas phase SO_2 would be valuable in understanding the conditions leading to new particle formation. Unfortunately, the overlap of existing lidar data and SMPS data during a new particle formation event is low during the West Branch campaign. However, a few periods of coincident lidar data and interesting ultrafine particle observations are shown here as an illustration of the potential for future campaigns. Figure 4.20 shows side-by-side lidar and SMPS data for June 23. The lidar data shows rapid, consistent boundary layer growth with relatively clean afternoon conditions on a day where strong morning new particle formation occurred. The measurements shown in Figure 4.21 were recorded on June 28. The blue lines overlaying the figure are used to denote equivalent time periods in the data. The lidar was not operational for the first burst of ultrafine particles, but shows a break in the clouds at 1500 m and evidence of increased radiation at the beginning of the second burst. As clouds reappear around 13:30, the ultrafine particle concentrations decrease, only to increase again around 15:00 as the clouds pass. It is known that solar radiation is a factor contributing to new particle formation, and perhaps this is evidence of the relationship. Further analysis would be required for definitive conclusions; however this provides an example of the type of information that can be gained through lidar techniques.

Future new particle formation observations in the Midwest would greatly benefit from consistent lidar data, which could be used to gain insight into vertically resolved aerosol concentrations, pollutant plumes, and clouds.

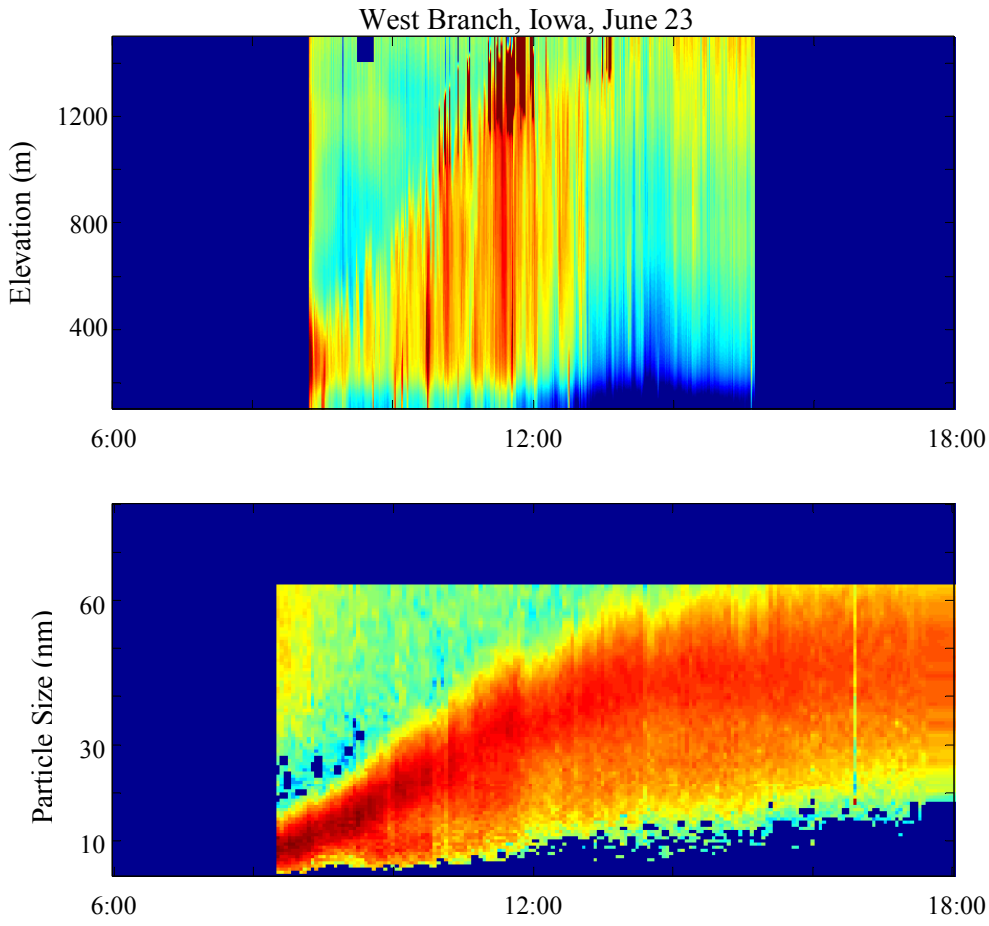

Figure 4.20. Lidar data (top) and the SMPS aerosol size distribution (bottom) recorded at West Branch, Iowa on June 23.

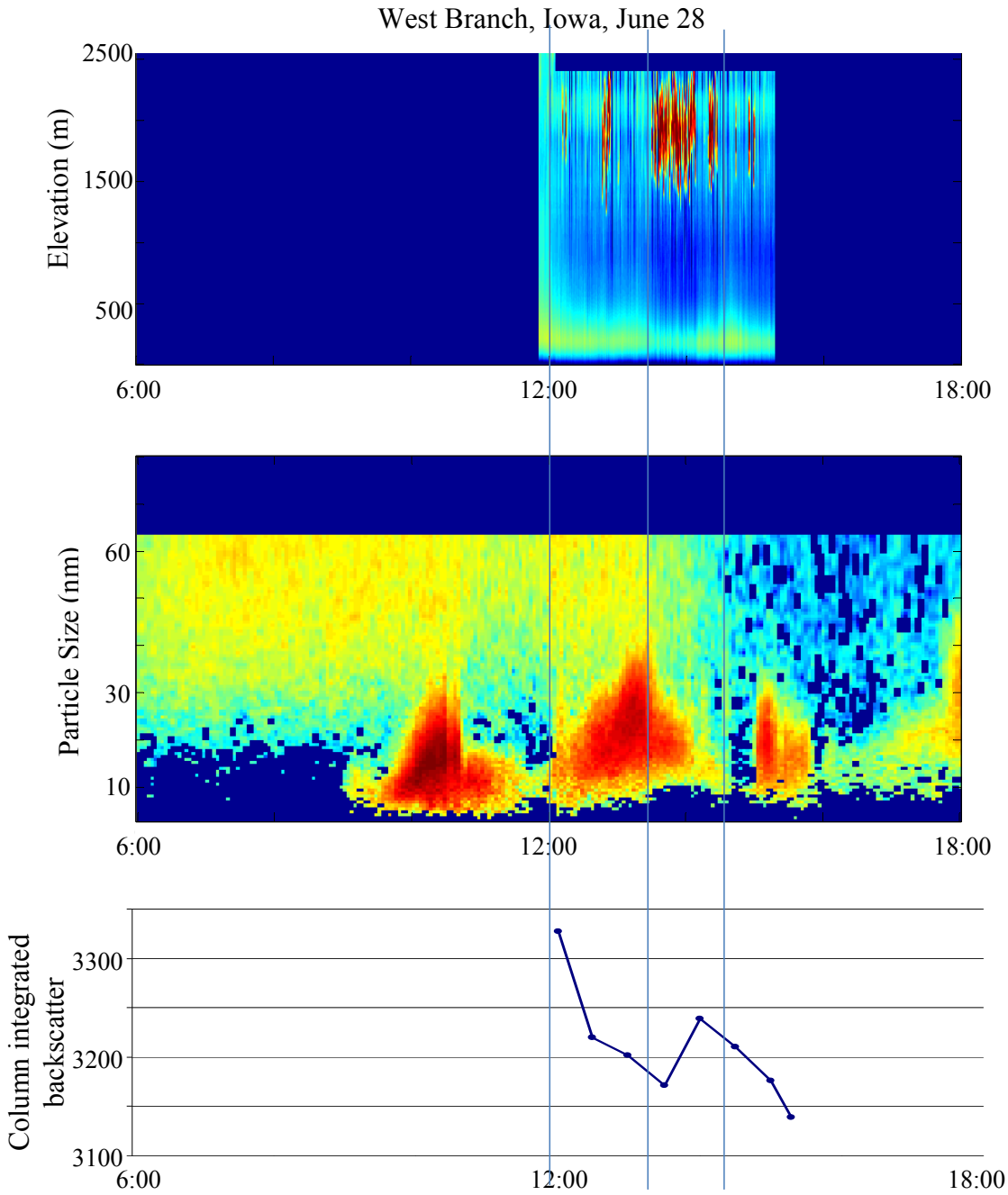

Figure 4.21. Lidar data (top) and the SMPS aerosol size distribution (bottom) recorded at West Branch, Iowa on June 28, 2008.

4.3.4 West Branch Discussion and Conclusions

It appears that West Branch, Iowa is frequently affected by air masses transported from the south, an area of relatively increased SO_2 emissions. Seventy percent of the new particle formation events occurred during periods of time when transport from this area was likely. Sharp increases in SO_2 concentration were detected at a monitor in between West Branch and the emitting facilities, located approximately 23 miles away. However, the timing of increased SO_2 periods and events are not always coordinated, and there are periods of transport from the south that do not result in formation events. For example, afternoon nucleation events occurred on June 27 and July 12. Both days exhibited high SO_2 concentrations in the early morning at the nearest monitor, and transport from the monitor to the site was likely. However, the formation events did not occur until later in the afternoon suggesting a different parameter either inhibiting or enabling new particle formation is playing a factor. While it is likely that SO_2 emissions released on a consistent basis south of WBI play a role in the formation of new particles, an on site vertically resolved measurement of SO_2 is required to verify concentration increases and make a quantitative link between concentrations and the appearance of new particles.

The boundary layer growth between 99 and 379 meters was not substantially faster on NPF days than on non-event days. It was previously hypothesized that particles often nucleate in the residual layer above and are only detected at the ground when they are transported to the ground under conditions of rapid boundary layer growth. Although this may be the case for certain formation events, the data suggests that there are other scenarios that result in new particle formation at work in West Branch. Events were seen on days where boundary layer growth was relatively slow when compared to the growth occurring on non-event days. Regardless, without consistent vertically resolved SO_2 concentrations and lidar data, a discernment of the presence or absence of plumes aloft is inconclusive.

4.4 Summary and Conclusions

Twenty five days of measurements were analyzed from Bondville, Illinois and West Branch, Iowa. In West Branch, new particle formation events occurred on 10 of the 25 days (40%) measured, while in Bondville events occurred on 6 of 25 days (25%). The Bondville campaign spanned from late summer to early fall of 2005 (August to October). The West Branch campaign occurred earlier in the season from early to mid summer (June to July). Although measurements of gas phase SO_2 were not made on location at either of the two sites, nearby monitors were used as a proxy for average SO_2 concentrations seen at the respective sites. From the proxy data, it appears that SO_2 concentrations are greater on average in West Branch than in Bondville which may contribute to the more frequent formation events. However, in order to make accurate comparisons of the frequency of events between the two sites, similar time periods must be compared in order to reduce the influence of other variables correlated to the time of year (i.e. temperature, UV radiation intensity, etc.).

In Bondville, wind speeds and direction were measured at the ground level. On average, over 24 hour time periods, winds from the southeast dominated on formation and non-formation days alike. From 9-noon specifically, the winds were most commonly from the south (170-200 degrees) and therefore it is not surprising that two-thirds of the formation events occurred between 9:00 and 11:00 am during southerly winds.

Condensational sink (CS) calculations were performed in order to test the assumption that new particle formation occurs under conditions of decreased condensational sink and increased H_2SO_4. The results showed that while events occurred under likely periods of increased H_2SO_4 production, the CS values during formation events was similar to the CS on non-formation event days. Perhaps the average condensational sink in Bondville is relatively low, and below the threshold required for new particle formation. Because these sink values were generated by integrating from 3-57 nm, intensive calculations and assumptions about the rest of the size distribution

would be required in order to create a time series of condensational sink that is comparable to those previously reported in the literature (and calculated over a different size distribution).

In Bondville, all new particle formation events began between 9am and 11am. The events occurred under conditions of elevated SO_2 as suggested from an off-site monitor. Two different types of new particle formation were seen; one where new particles were detected as low as 5nm and another where particles were not detected until 10nm. There was no indication in the meteorological parameters that a simple relationship exists to explain the difference in the two types. It is possible that the new particles were nucleated aloft and were mixed down to the surface as the boundary layer height increased, and particles that mixed down more slowly had more time to grow before being detected. Due to the lack of measurements regarding the vertical profile in Bondville, it is difficult to draw conclusions about new particle formation events and the correlation with boundary layer mixing. Unfortunately, the measurement period discussed here did not overlap with the time period that aircraft measurements were obtained. Beginning in June of 2006, NOAA launched an Airborne Aerosol Observatory (AAO) that flew over Bondville recording measurements of aerosol optical and chemical properties. A collocated measure of particle concentrations with vertical resolution would be very beneficial in determining whether or not new particle formation events originate aloft. Initial testing of a condensation particle counter has been completed in the Stanier lab in order to determine its performance in a reduced pressure environment, such as a light aircraft. Future plans include deployment on a light aircraft in order to observe the vertical profile of particles. This will provide the information required to support or negate the working hypotheses regarding the vertical profile of parameters such as condensational sink and new particle formation.

In West Branch, wind speed and direction were measured at 31 meters above ground. Southwesterly winds dominated on both event and non-event days. When

comparing the 24 hour wind roses for event and non-event days, the event days have a larger westerly component than the non-event days. Regardless, the hours during new particle formation events were dominated by winds from the south and southwest which correspond to the direction of the SO_2 emitting facilities in Eastern Iowa. Events at the West Branch site were less consistent in their starting times than the events in Bondville. Events in West Branch started as early as 6:30am and as late as 3:00pm. The nearest monitors suggest that SO_2 concentrations near West Branch are higher than those at Bondville, and if nucleation is indeed H_2SO_4 limited in this area, perhaps the arrival of a plume in the afternoon is enough to explain the afternoon events.

In West Branch, measurements taken from the tall tower served as an indication of boundary layer growth in the lower atmosphere. Although these measurements provide insight into the speed of boundary layer height growth in between 99 and 379 meters, it does not provide a clear picture of the vertical profile of either gas or particle pollutant concentrations. The speed of the boundary layer height increase alone was not enough to explain the timing of the events or to distinguish between the different types of events.

The first hypothesis for Midwestern new particle formation was that there are sufficient SO_2 concentrations throughout the atmosphere for nucleation to occur, and the process is limited by condensational sink at the ground level. Therefore nucleation occurs aloft and mixes down to the ground. If this were the case, events would most likely look like they did in Bondville, where new particles were first detected at different sizes on different days (see Figure 4.4), depending on the elapsed time from nucleation until turbulent mixing brought the particles to the surface. While the conditions surrounding some event days support this hypothesis, it remains inconclusive until a clearer picture of the vertical profile of condensational sink is acquired.

The second hypothesis for the study was that nucleation is SO_2 limited, and that SO_2 is emitted aloft, travels downwind to the measurement site and as the mixed layer

height reaches the plume height, SO_2 is mixed down to the surface where conditions are favorable. Attempts were made in order to measure SO_2 with vertical resolution from the tall tower; however the first generation instrumentation did not operate properly and modifications have been made in preparation for a subsequent deployment.

The third hypothesis was that although new particle formation and boundary layer evolution appear to be linked, they are actually independent and are merely driven by the same factor. If this were the case, new particle formation would be seen during periods of cloud free, intense solar radiation, which may or may not occur in the morning (as seen in West Branch data set). In this scenario, the presence of SO_2 would be a critical factor in the appearance of new particles and on-site collocated measures of SO_2 and size distribution would be critical.

From the data at hand, it is quite likely that more than one of the proposed hypotheses is valid for new particle formation in the Midwest. For example, if new particle formation in this area is H_2SO_4 limited, it is possible that SO_2 is emitted in the atmosphere aloft at night and travels downwind to the site. The next day, as the boundary layer grows and the SO_2 is mixed to the ground where favorable conditions for new particle formation occur. In this H_2SO_4 limited scenario it would also then be possible that new particle formation would be triggered by a H_2SO_4 plume that is horizontally advected to the site and on this day would be linked to horizontal advection rather than vertical mixing. Further measurements that include gas and particle concentrations with vertical resolution and increased operational time would be valuable in further exploration of the coupling between vertical motions, pollutant concentrations, and new particle formation.

CHAPTER 5: MEASUREMENTS AND FINDINGS FROM THE MILAGRO FIELD CAMPAIGN, MEXICO CITY

5.1 Introduction

Mexico City is one of the world's largest mega-cities, with nearly 20 million inhabitants. The city is located in the basin of the central Mexican plateau (19.5°N) at an altitude of approximately 2200m above sea level, with mountains to the south, west and east allowing for limited ventilation and intense solar radiation. Air pollution is a persistent problem in this area, with levels exceeding the limits set by the World Health Organization on a regular basis.

A large scale field campaign brought hundreds of scientists from around the world to Mexico City in March of 2006. The campaign, known as the "Megacity Initiative: Local and Global Research Observations" (MILAGRO) was designed to study the transformation of pollutants originating in the Mexico City urban area and to better understand the impact that these pollutants have on regional air quality and climate. Three main surface sampling sites were constructed in and around Mexico City. The locations of these sites were chosen in order to sample the polluted air over the city and then twice more downwind, and are hence called T0, T1, and T2 (see Figure 5.1, left). The measurements discussed in this chapter were conducted at the urban background site (T0), which was located at the Mexican Petroleum Institute (IMP) in the northwestern part of the basin of Mexico City. An aerial view of the T0 location is shown on the right side in Figure 5.1.

A regional scale overview of the meteorological conditions during the campaign is provided by Fast et al. (Fast, de Foy et al. 2007). Using the meteorology, the campaign was split into three main regimes. The first main regime occurred prior to March 14, and was characterized by dry, sunny conditions. The second regime began with strong, northerly near-surface winds (known as a 'cold surge') and increased humidity on March

14 with a gradual drying of the atmosphere over the next few days. The third regime occurred after March 23 and began with the strongest cold surge and led to humidity, afternoon convection, and precipitation over the central plateau that was greater than during the second regime (Fast, de Foy et al. 2007).

Source: Google Earth version 5.1

Figure 5.1. The placement of the three ground-based sampling locations (T0, T1, and T2) in the Mexico City metropolitan area (left) and an aerial view of the T0 sampling location and surrounding land use (right). Particle size distribution and CO_2 were both measured at T0 (marked SMPS and CO_2 respectively), although the instruments were separated by approximately 150 meters.

In his 1988 publication, Jaruegui explained in detail the diurnal wind regime in the Mexico City basin which includes drainage flow into the basin, followed by erosion of the stable layer and start of turbulent mixing after sunrise, until the coupling with the gradient regional wind occurs (Jauregui 1988). It was concluded that the diurnal pattern of the surface winds in the basin during the campaign were representative of the typical patterns that occur during the warm dry season in Mexico City (deFoy, Fast et al. 2008).

The air quality in the basin during the 2006 campaign was compared to 10 years of data collected by the Ambient Air Monitoring Network (RAMA) and it was concluded that $PM_{2.5}$ and PM_{10} levels were mostly within their usual range, with PM_{10} maximum loadings occurring in either the end of the morning or the end of the afternoon while $PM_{2.5}$ peaks around noon. $PM_{2.5}$ and PM_{10} levels measured at T0 and other urban locations varied between 24-46 $\mu g\ m^{-3}$ and 50-56 $\mu g\ m^{-3}$ and were markedly impacted by traffic emissions during rush hours (Querol, Pey et al. 2008). At urban monitoring locations, the PM_{10} speciation study showed that 25-27% is comprised of mineral matter, 32-46% is carbonaceous, and secondary inorganic aerosols represent 10-20%. The $PM_{2.5}$ speciation shows that 15% is mineral matter, 50-55% is carbonaceous compounds, and 15-20% is secondary inorganics (Querol, Pey et al. 2008).

Stone et al. defined significant sources of organic carbon during the campaign which included gasoline and motor vehicles (49%). Contributions from biomass burning were variable from 5-26% and the remaining organic carbon was considered to be secondary in nature (Maynard, Aitken et al. 2006).

The main point sources of SO_2 and NO_2 emissions near the Mexico City Metropolitan Area (MCMA) are the Miguel Hidalgo Refinery and the Francisco Perez Rios Power Plant, which are located in the Tula industrial complex, northwest of city (Rivera, Sosa et al. 2009). In order to determine the impact that these emissions have on the MCMA, Rivera and colleagues recorded measurements of SO_2, NO_2 and meteorological parameters near Tula during the 2006 campaign using a mini-DOAS. They estimated that the average emissions of SO_2 during the campaign were 384 ± 103 tons per day, which were in good agreement with emission inventories and simulations. They concluded that although local sources are a dominant cause of SO_2 baseline levels, the Tula area provides a potential source of SO_2 for the metropolitan area.

5.2 Experimental

The DAASS II (Dry-Ambient Aerosol Size Spectrometer II) was deployed in Mexico City as part of the MILAGRO field campaign. The instrument was in operation from March 7 to March 29, 2006, at the T0 research location, on the roof of building 32 at the Mexican Petroleum Institute (IMP). The DAASS II is an automated combination of aerosol-sizing instruments and supporting equipment that measures aerosol size distributions from 10.9nm to 10μm at both ambient and dry relative humidities. Aerosol water content can then be calculated based on the differences between the ambient and the dried distributions. The purpose of the DAASS II was to measure the aerosol size distribution from 15 nm to 10 μm multiple times per hour, at both ambient and dry relative humidities. From these measurements the aerosol water content can be calculated. The DAASS II also serves to detect new particle formation and is a sensitive monitor for nearby ultrafine particle sources.

The DAASS II includes two aerosol sizing instruments, a Scanning Mobility Particle Sizer (SMPS), and an Aerodynamic Particle Sizer (APS). The SMPS measures the size distribution from 10.9 to 478 nm, while the APS measures the distribution from .5 to 19.8 μm. The SMPS recorded a sample every 5 minutes, and the APS sampled every 20 seconds. Ambient air is continuously sampled into the DAASS II inlet where it is then split and enters the SMPS and the APS inlets simultaneously. Aerosol relative humidity was controlled inside the separate inlets. The aerosols were sampled in either 'ambient' or dry mode depending on the position of the automated 3-way valve. When sampling in dry mode, the aerosols were passed through Nafion or diffusion dryers. The system was checked daily to ensure that the instrument was operating at the proper flow rates and that there were no leaks in the inlet.

Under the existing circumstances in our sampling location, it was challenging to measure the aerosol at ambient relative humidity. The building where the DAASS II was housed was warmer than ambient conditions due to the amounts of power used, and the

large number of people and instruments inside. As the ambient aerosols entered the inlet and were brought inside to the instrument, the relative humidity dropped to below ambient levels. Therefore, the aerosols were measured in dry mode for a large portion of the study. Further detail regarding the DAASS II instrumentation, construction, and performance can be found in Chapter 3.

5.3 Ultrafine Particle Observations

5.3.1. Background

New particle formation events have previously been observed in Mexico City. In the spring of 2003, Dunn et al. conducted measurements of the aerosol size distribution from 3-48 nm in two locations in the Mexico City area; a rural site in the mountain pass in the southeast corner and another site in the city's center. Formation events were observed on 3 of 10 days sampled. They determined that the events observed in the mountain pass were correlated with northerly winds, elevated SO_2 concentrations, and low PM concentrations. At the urban site, in the morning, high concentrations of 15-25 nm particles correlated with high levels of NO_x and CO. They also noted that sudden decreases in condensational surface area allowed for new particle formation to occur, although they provided no explanation for the sudden decrease in PM (Dunn, Jimenez et al. 2004).

Iida and colleagues also made observations of new particle formation during the 2006 MILAGRO campaign at a site in Tecamac, Mexico, approximately 35 km northwest of the city. They observed nucleation on 13 of 17 days and found that the events occurred between 7:00am and noon and were accompanied by elevated H_2SO_4 concentrations and sub 5nm particles. Thermal Desorption Chemical Ionization Mass Spectrometry (TDCIMS) was used to determine the composition of the 10-33nm particle for one of these events. They observed that during this specific event, the nucleated

particles contained far more organics than sulfates, and therefore organic compounds play a dominant role in the growth of the particles.

5.3.2. Results

New particle formation events were observed on 4 of 15 (27%) days sampled at the T0 sampling location. Table 5.1 characterizes the new particle formation events, and includes data from a day without a nucleation event for reference.

Table 5.1. Summary of new particle formation events occurring during the MILAGRO field campaign.

Date	Description	Hours	Number conc. 10-50nm (cm^{-3})	Number conc. 10-100nm (cm^{-3})	Growth Rate (nm/hr)	Wind Dir (degree)
March 16	before	10:30-11:30	--	--		72
	during	11:30-13:30	10,500	15,100	5.4	71
March 17	before	11:30-12:30	5,800	9,580		85
	during	13:00-15:00	15,200	17,600	5.7	99
March 21	before	9:45-11:45	6,300	9,230		12
	during	11:30-13:30	15,600	21,300	9.6	22
March 25	before	10:00-12:00	4,440	6,300		57
	during	13:30-15:30	8,430	9,340	7.8	15
March 11	no event	12:00-14:00	11,400	16,000		76

The new particle formation events in Mexico City began in between 10:30 and 13:00, which is later than typically and observed in the Midwestern United States. The observed growth rates during the events varied from 5.4 to 9.6 nm/hr, which fall within the reported range for other urban areas (0.5-9 nm/hr) (Kulmala, Vehkamaki et al. 2004). The commonality among all the new particle formation and growth events was lower than average number concentrations just prior to the event. The hypothesis that is explored in the subsequent analysis is that new particle formation in urban Mexico City is

limited by high pre-existing condensational sink. The decrease in number concentration prior to the event triggers nucleation, and is caused by a rapid increase in boundary layer height. This rapid ventilation of the boundary layer consistently occurs in the late morning/afternoon due to a sudden increase in turbulent kinetic energy that has been documented in mountain basin areas (Banta 1985) and this diurnal pattern will be explained in greater detail.

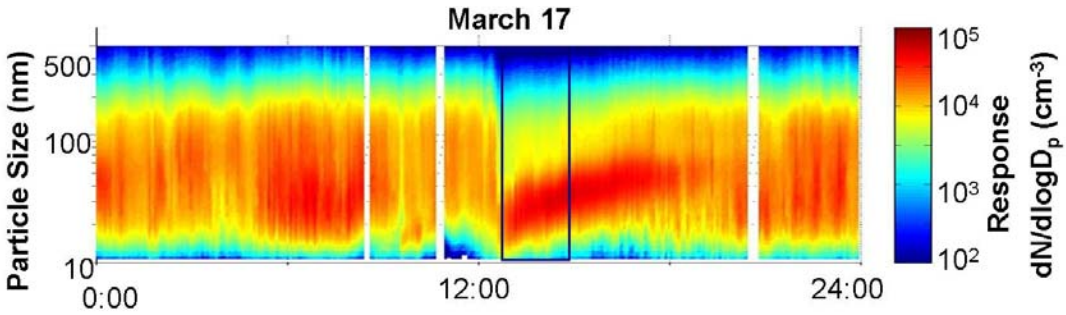

Figure 5.2. Size distribution measured by the DAASS II on March 17, 2006 at T0. The new particle formation event, which is defined by the emergence of a clear and growing mode at 10-15 nm, begins just before 1:00 pm.

Figure 5.2 is a twenty-four hour time series for March 17, 2006. An increase in particle concentrations during rush hour traffic can be detected (and is noted by the increased response, shown on color scale at the right of the figure). Just after noon, there is a sharp decrease in particles of all size, at which point new particle formation occurs. The same sharp decrease in particle concentrations is detected by two different nephelometers, which were deployed at T0 by Jeff Gaffney at University of Arkansas-Little Rock. Scattering coefficients were measured at 450, 550, and 700 nm by TSI Model 3563 integrating nepheolometer and at 530nm by an MRI model 1560 nephelometer. The sharp decrease in extinction at all 5 wavelengths just after noon on March 17 can be seen in Figure 5.3. Particle number is plotted over the extinction and

shows a similar decrease at the same time. However, particle number rapidly increases again due to the new particle formation event triggered by the low condensational surface area, while the scattering coefficients build gradually.

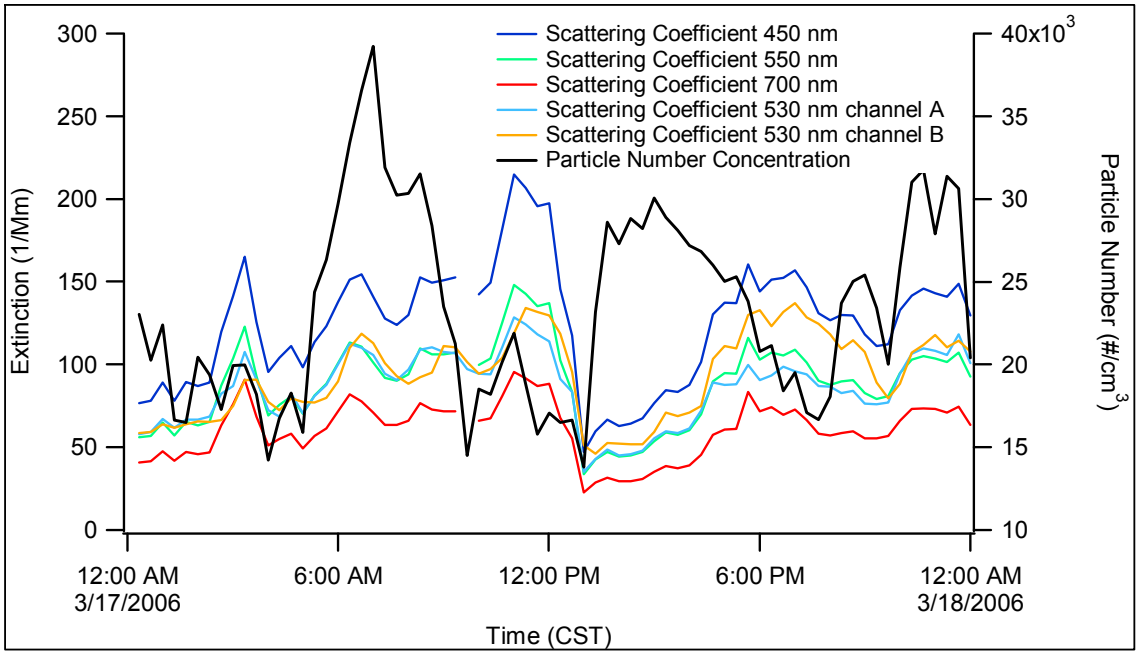

Figure 5.3. Extinction coefficient time series for March 17, 2006 as measured by integrating nephelometers (U Alabama, Little Rock) at the T0 research site (left axis). Total particle number concentration measurement (black trace) is shown for the same time period (right axis).

Wind speed and direction, measured at the T0 site using a Vaisala WXT510 weather transmitter, are plotted in Figure 5.4 in order to observe the diurnal variation in the wind pattern, and to detect any directional correlation with new particle formation events. There is a general diurnal wind pattern observed in Mexico City as a result of its geographical setting which can be observed in the wind roses representing different time periods of the day in Figure 5.4. After sunset, the mountain surface to the west of the city cools and the cold dense air sinks down the mountain side toward the basin, resulting in

westerly winds at T0 (which can be observed in the night time wind rose, Figure 5.4, panel (e)). These drainage flows (commonly called katabatic winds) are reinforced by the urban heat island. In other words, in the city where much of the land surfaces are concrete, heat is stored more efficiently than in the surrounding terrain, and as the surface-layer air is warmed, it rises, and is replaced by the downslope winds. After sunrise, the solar heating warms the air adjacent to the mountain walls, causing upslope (or anabatic) winds (easterlies at T0). As the sun warms the basin floor, a shallow mixed layer begins to form. Because the upslope winds are continuously draining the mixed layer, it may grow slower than one would expect over flat terrain. Then, in the late morning/early afternoon when the cold pool is eliminated, the turbulent kinetic energy greatly increases and is accompanied by a rapid growth in boundary layer height. An afternoon phase follows, where prevailing synoptic winds eliminate the local flow pattern until the sun sets again (Banta 1985; Jauregui 1988; deFoy, Fast et al. 2008). Panel (d) shows the wind speeds and direction occurring during the hours of new particle formation. It appears that winds from the northwest at relatively increased speeds dominate during periods of new particle formation.

The correlation between wind direction and new particle formation was examined using Figure 5.5. The Mexico National Emissions Inventory from 1999 was used to plot the locations of major SO_2 point sources relative to the T0 site. The figure shows a map of the T0 research location (denoted by the yellow push pin icon in the center) with the major SO_2 point sources marked by the blue dots. The yellow square represents 5 x 5 miles surrounding the site. The area to the northwest of T0 contains many sources which may support the idea that formation events occur more frequently under periods of northwesterly winds. However, a limited number of hours (during 4 events) were used in the analysis and while it appears that northwesterly winds dominate during new particle formation events (over 20% of the time) all wind directions are represented (Figure 5.4,

panel (d)). In order to make a definitive conclusion on the effect that wind direction has on the appearance of new particles, a longer time period must be observed.

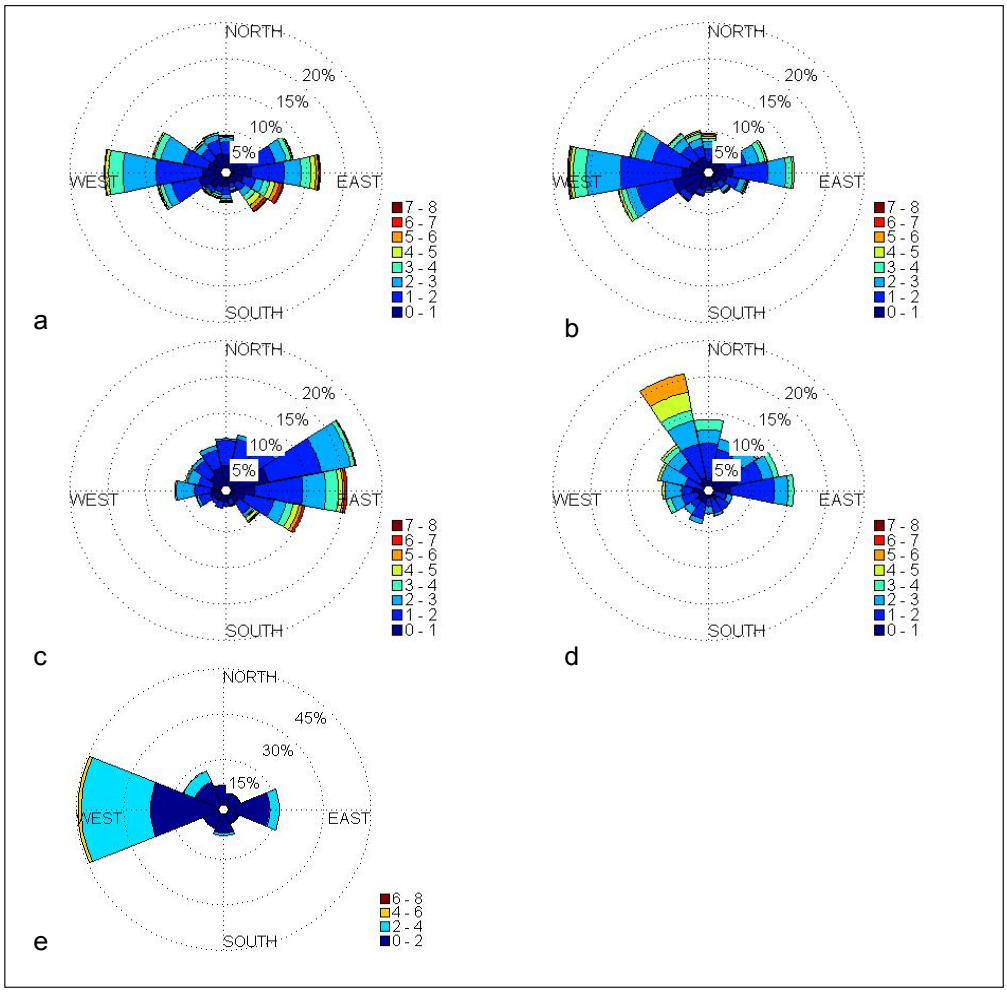

Figure 5.4. Windroses of wind speed (indicated by the colorscale in meters per second) and direction during the MILAGRO campaign for a) midnight to midnight on non-event days b)midnight to midnight on new particle formation event days c) 9 am to noon on all non-event days, d) the hours during new particle formation, and e) hours 10 pm to 4am.

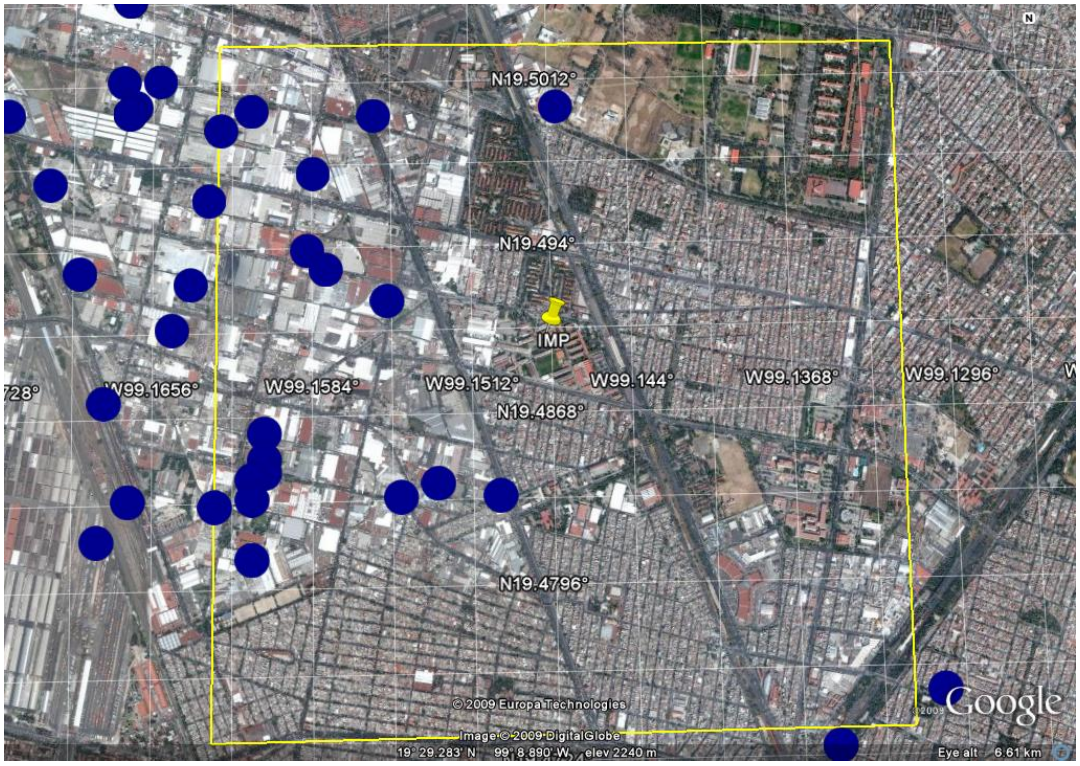

Figure 5.5. Map showing the locations of SO_2 point sources in the vicinity of the T0 research location (denoted by yellow push pin icon in the center). The yellow box outlines a 5 mile x 5 mile square around T0. The point sources and their locations come from the Mexico National Emissions Inventory (1999).

Our hypothesis regarding new particle formation in Mexico City was that boundary layer ventilation in the afternoon leads to a decrease in pre-existing condensational surface area, allowing nucleation to occur. Therefore, boundary layer height for formation days was plotted in Figure 5.6. The boundary layer heights were determined subjectively using the backscatter profiles from the 915MHz wind profiler, operated by University of Alabama, Huntsville. All four of the new particle formation events began in between 11:30 and 13:30 CST. Boundary layer growth on March 17 appears slower than on March 16 and 21, but cannot necessarily be correlated to the later onset of the event due to the discrepancy caused by the rapid boundary layer growth on March 25 that results in the latest event onset. In this analysis, boundary layer height is

used as an indicator of the amount of vertical mixing that has occurred between ground level air (with higher surface area acting as a sink) and cleaner air aloft, however no precise boundary layer height exists for new particle formation to occur. This is most likely due to the fact that the vertical profile of pollutant concentrations is varying from day to day, and therefore the boundary layer height may need to reach a different height before the air is sufficiently clean to reduce the condensational sink to the required level. This could be further explored using lidar data, aircraft data (when available) and ground level pollutant concentrations.

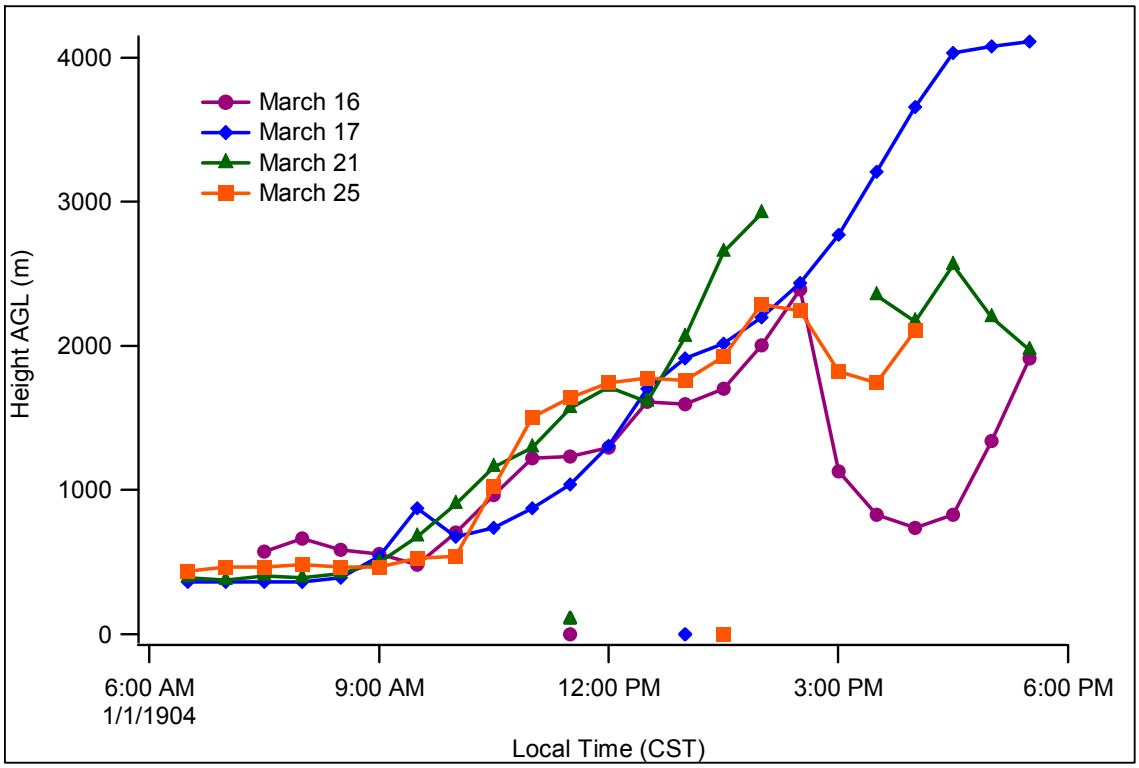

Figure 5.6. Convective boundary layer height for new particle formation event days during the MILAGRO campaign. The symbols on the x-axis represent the time that the formation event started on the specific day. The boundary layer height was subjectively determined from the 915MHz wind profiler backscatter profiles by UAH personnel.

Table 5.2 provides a summary of new particle formation events recorded by the Stanier group in 2006 regarding the time the events began, the frequency of events, the growth rates of the newly formed particles, and their composition. Also included in the table is a comparison to previous results from new particle formation observations in Mexico City, recorded by Dunn, Jimenez et al. in 2003. Additionally, the results from recent observations of new particle formation occurring in the Chinese mega-city of Beijing are included.

As shown in Table 5.2, our findings concerning new particle formation in Mexico City are consistent with previous observations. While the frequency of new particle formation events may have seasonal dependence, events occur on approximately 30% of days during the spring in Mexico City. When compared to Beijing, another mega-city with similar pollution problems, the frequency is the same at 30%. In general, for continental boundary layer observations of new particle formation, the vast majority of reported particle growth rates are in the range of 1-10 nm/hr (Kulmala and Kerminen 2008) and the growth rates observed in both Mexico City and Beijing fall within the expected range.

In Beijing, the growth of newly formed particles was attributed largely to condensation of sulfates. Sulfuric acid has long been known to contribute to the growth of newly formed particles. However, in many locations, the observed growth rates cannot be explained by condensation of sulfuric acid alone. For example, a previous study by Stolzenburg et al. modeled the contribution of H_2SO_4 to aerosol growth using all available observations at the time. While observed growth rates in some locations could be contributed to condensation of H_2SO_4, most locations experienced growth rates up to 20 times larger than could be explained by H_2SO_4 alone (Stolzenburg, McMurry 2005), supporting the idea that other species contribute to nanoparticle growth in the atmosphere. Thermal Desorption Chemical Ionization Mass Spectrometry (TDCIMS) measurements performed by J. N. Smith (in press.) during the MILAGRO campaign

suggest that in Mexico City, organic components may contribute largely to nanoparticle growth.

The timing of the events occurring in Mexico City is significantly later in the day when compared to events in Beijing. In Beijing, events typically occurred between 9:00 and 11:00 am, and some as early as 6:00 am. In Mexico City however, events typically occur in the afternoon. Our results conclude that this can be attributed to the local basin meteorology and unique boundary layer evolution (leading to rapid ventilation in the afternoon and decreased pre-existing surface area) as discussed previously in the chapter.

Table 5.2. Comparison of new particle formation events in Mexico City to events occurring in Beijing regarding frequency of events, onset of event, as well as growth and composition of newly formed particles.

	Mexico City 2003 May[1]	**Mexico City 2006 March**	**Beijing 2006 August**[3]
Frequency	3 of 10 (30%)	4 of 15 (27%)	30%
Event start time (local time)	13:00-14:45	11:30-13:30	9:00-10:00
Growth Rates	4.7-9 nm/hr	5.4-9.6 nm/hr	12.-5.6 nm/hr 0.1-11.2 nm/hr 3 yr ave.
Composition	undetermined	organics[2]	sulfate

[1]Dunn, Jimenez et al. 2004
[2]Iida, Stolzenburg et al. 2008
[3]Wiedensohler, Cheng et al. 2009

5.4 Number-based Emission Factors

Carbon dioxide is the primary carbon-containing product of fuel combustion and can provide a good estimate of the amount of fuel burned (McGaughey, Desai et al. 2004). Representative values, known as fuel-based emission factors, are useful in relating total carbon emissions (in the form of CO_2 and CO) to pollutant concentrations (particle number in this case).

In March, 2006, during the MILAGRO field campaign, observations at the T0 location could often be characterized by morning conditions with high particle mass concentrations, low mixing heights, and highly correlated particle number and carbon dioxide, indicative that particle number is controlled by primary emissions. The objectives of the data analysis presented here are to determine a number based emission factor that is representative of Mexico City. That emission factor will then be compared to others from both the United States and Europe.

Figure 5.7 shows the twenty-four hour time series of both particle number concentration (blue trace) and carbon dioxide concentration (green trace) for three different days during the campaign. At the T0 research site, the particle size distributions were measured using the DAASS II (SMPS) by the Stanier research group, and CO_2 was measured by the Eichinger group using a Licor LI-7500 CO_2 analyzer. March 11 and March 18 are used to highlight time periods during the morning hours when particle concentrations are dominated by primary emissions and CO_2 and particle number are highly correlated. March 17 is highlighted to show a time period during afternoon boundary layer ventilation when the coupling between CO_2 and number breaks down.

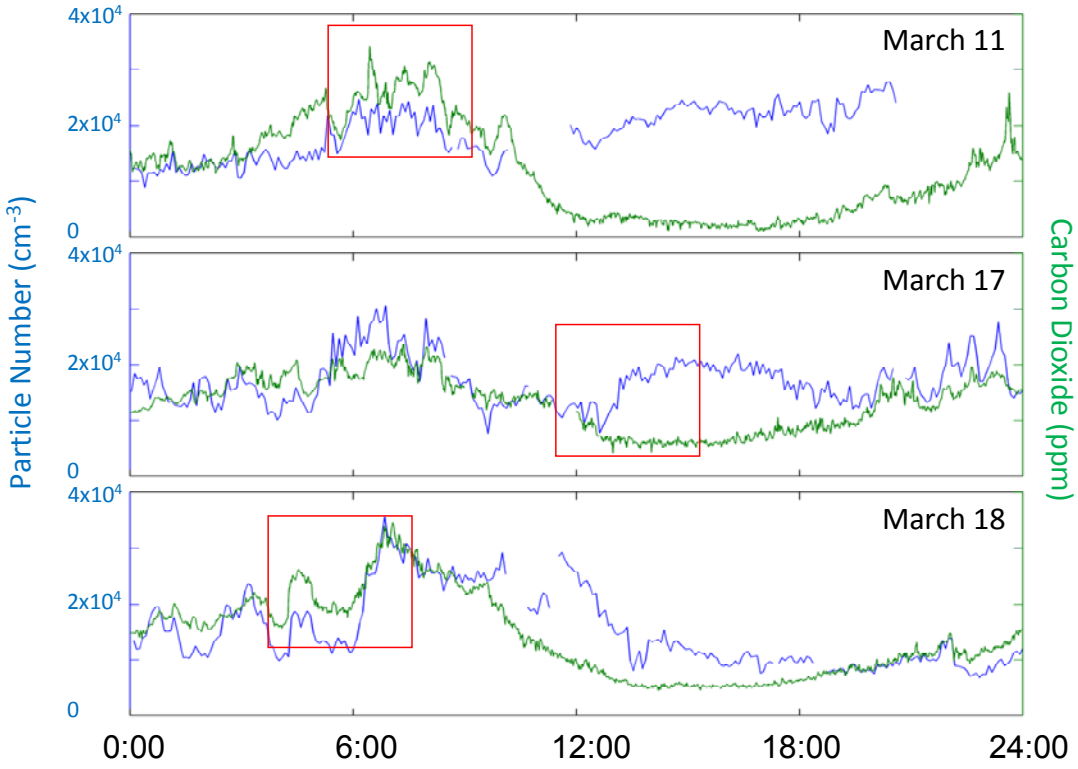

Figure 5.7. The particle number concentration and CO_2 time series for three different days during the MILAGRO campaign as measured from the T0 research location. March 11 and March 18 are highlighted for time periods when number is controlled by primary emissions (and CO_2 and number are highly correlated). March 17 is highlighted during a time period of ventilation of the boundary layer when the coupling between the two breaks down.

5.4.1. Method of Retrieving Number Based Emission Factors

The calculation of the number-based emission factors were performed with the script 'number vs. CO2', written by C. Stanier in 2009. The algorithm can be found in Appendix D, and an overview of the method is included here. While the CO_2 monitor and the SMPS were both located at T0 research site, they were separated by a distance of approximately 150 meters. The first step in the data reduction assumes that wind brings parcels of pollution with both particles and CO_2, but that the peaks may be shifted slightly in time due to the physical separation of the instruments. The next step is to process the particle number and CO_2 data in order to obtain two smoothed signals. The

CO_2 data was averaged from 10Hz to 1 minute. Then it was smoothed slightly using a second order Savitsky Golay filter with a seven minute time window. The 5 minute particle number concentrations were then interpolated to a 1 minute time basis using cubic splines. Next, random periods of time are identified that correspond with peaks. The time intervals can include multiple peaks and time windows between 5 and 90 minutes are allowed. Then, both CO_2 (green trace) and number (blue trace) are integrated during the same time periods. For each pair of integrals, one point is created. This analysis is illustrated in Figure 5.8.

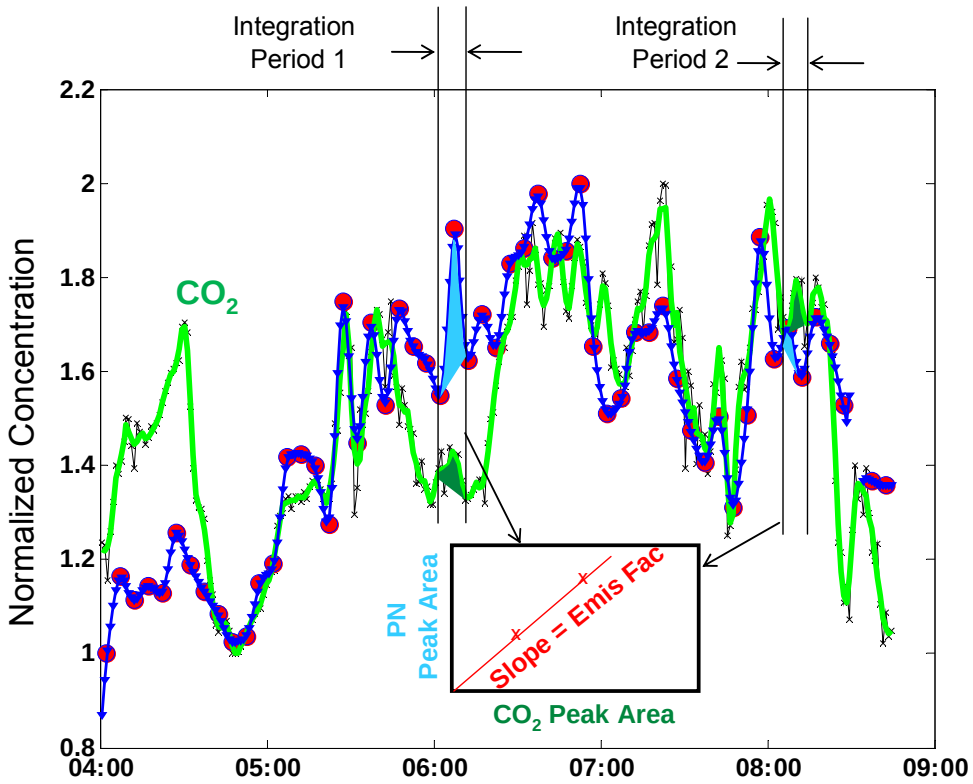

Figure 5.8. Illustration of the method used to retrieve number-based emission factors using correlation between CO_2 and particle number for Mexico City. The black 'x' symbols represent raw CO_2, while the green trace represents the smoothed CO_2 signal. Red dots represent raw SMPS values while the blue trace represents smooth particle number signal.

Figure 5.9 provides an example of what a plot of particle number peak area vs. CO_2 peak area would look like if all emission sources had the same signature for particle number relative to CO_2.

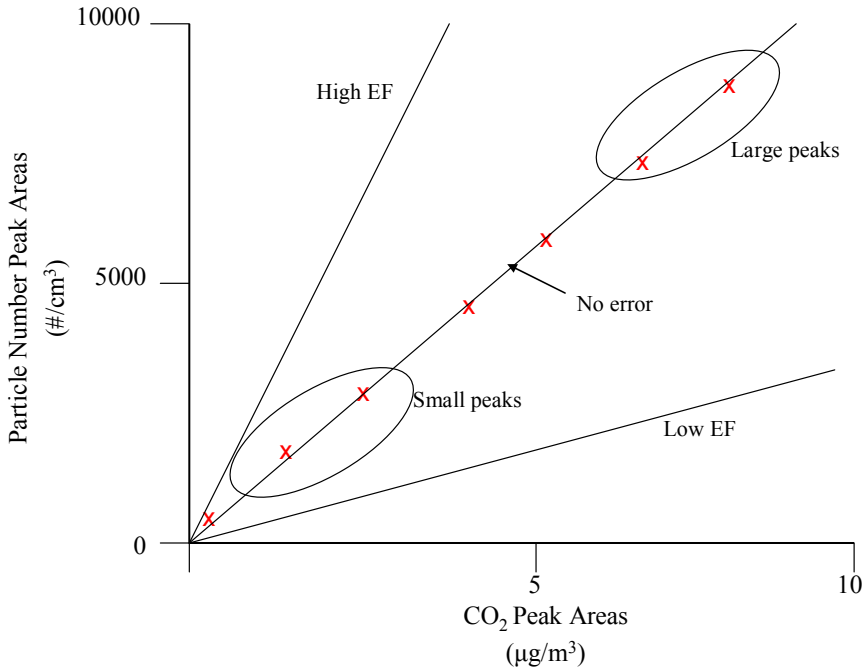

Figure 5.9. Theoretical plot of particle number peak area vs. CO_2 peak area, if all emission sources had the same signature ratio of particle number concentration to CO_2.

5.4.2. Results

The analysis method described in the previous section was applied to the SMPS size distributions and CO_2 concentrations recorded from March 10 to March 20, 2006 at the T0 research site during the MILAGRO campaign. The emission factors, represented here as the ratio of particle number concentration (#/cm^3-hr) to CO_2 (ppm-hr), were determined according to different time periods of the day, wind direction, and particle size bins. The results of the wind directional analysis are shown in Figure 5.10.

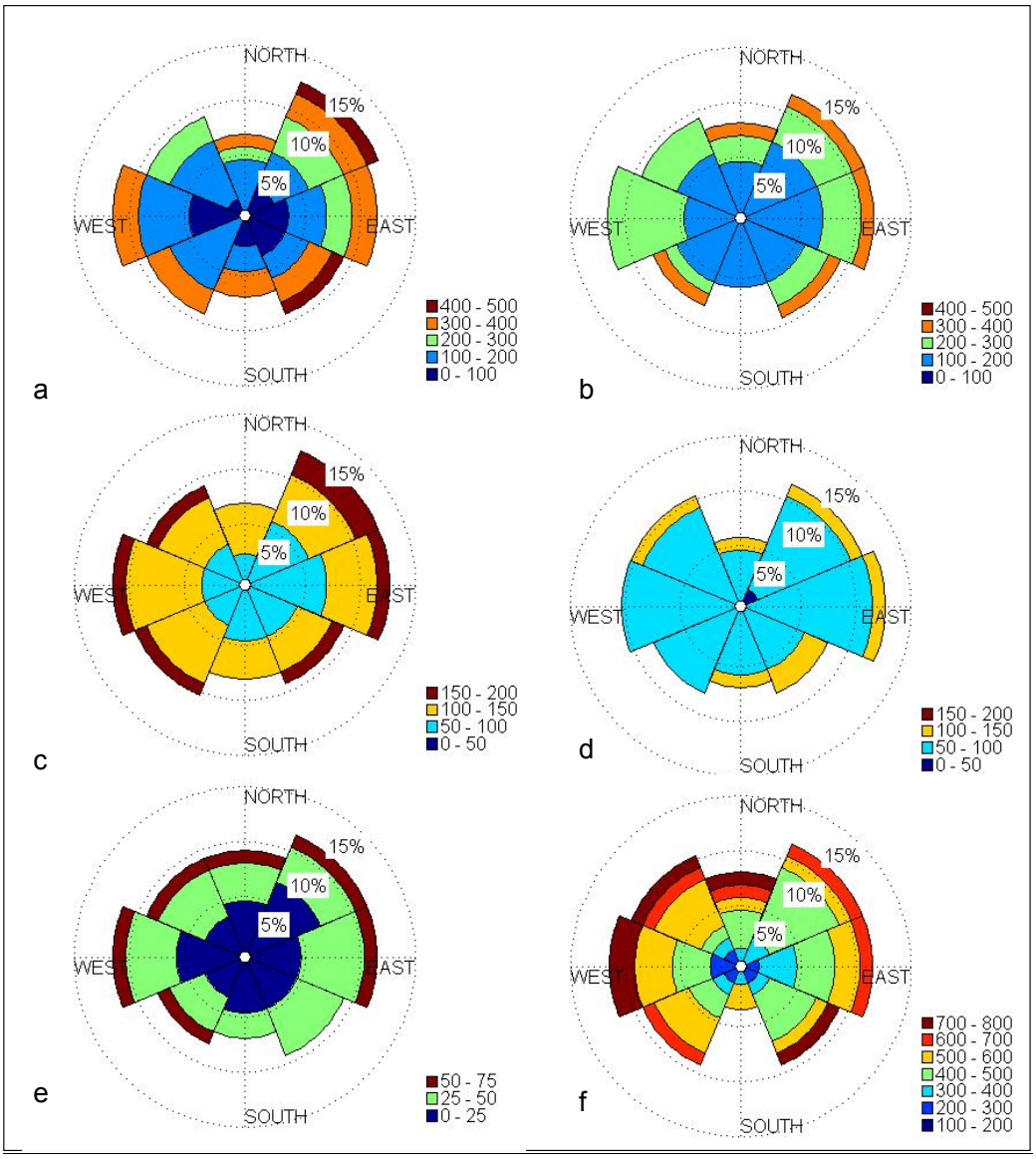

Figure 5.10. Wind directionally dependent emission factors for Mexico City for 15-20 nm (a), 20-50 nm (b), 50-100 nm (c), 100-200 nm (d), and 200-500 nm particles(e). Panel (f) represents the emission factors for particles from 15-500 nm. The color scale at the right of each wind rose corresponds to the emission factor as a ratio of particle peak area (#/cm^3-hr) to CO_2 peak area (μg/m^3-hr).

Figure 5.10 represents the directionally dependent emission factors for March 10-20. Panels (a) through (e) represent the emission factors for specific size bins of the particle size distribution (see figure caption for description) and panel (f) shows the

emission factors for particles across all size bins (from 15-500 nm). The color scales for each wind rose represent emission factors as a ratio of particle peak areas (#/cm^3-hr) to CO_2 peak areas (ppm-hr) and have been scaled for each specific size bin. While there is some minor variability in the directionally dependent emission factors, it does not appear that wind direction has a significant effect on the emission factors measured at T0, regardless of particle size.

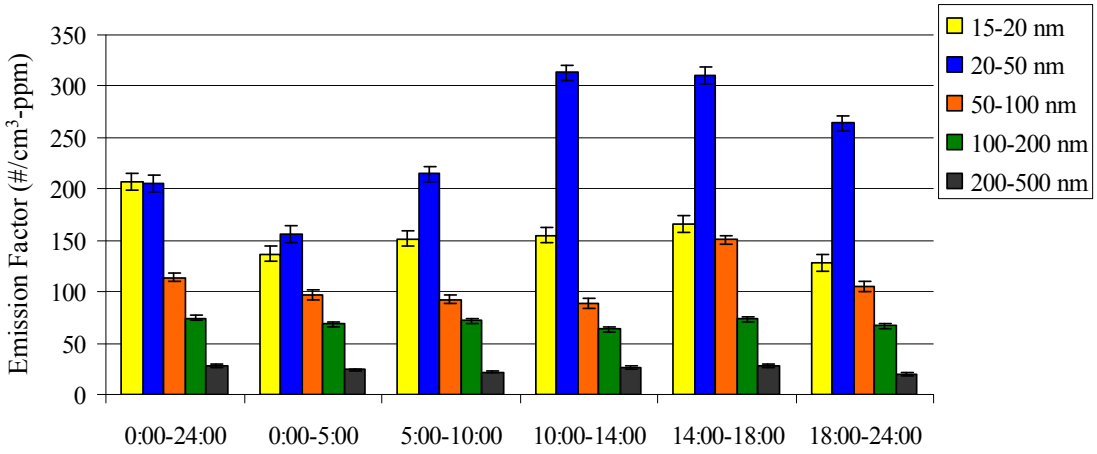

Figure 5.11. Average emission factors (March 10 to March 20) according to time of the day, separated into 5 different size bins.

Figure 5.11 shows the average diurnal pattern of the emission factor, classified by particle size. The emission factor for particles in the 100-200 nm and 200-500 nm range remain fairly consistent throughout the day. For particles of smaller sizes (15-20 nm, 20-50 nm, and 50-100 nm), the emission factor increases during the day, peaking from 14:00-18:00, and then decreasing slightly from 18:00-24:00. Emission factors during the afternoon new particle formation events were isolated to determine the effect they have on the diurnal pattern seen in Figure 5.11. During new particle formation events, number concentrations increase, while CO_2 decreases which would seemingly increase the

emission factor. However, the retrieval method works by selecting peak areas, and long term increases in background concentrations may go undetected. After plotting the emission factors for new particle formation days versus non event days, it was concluded that new particle formation does not account for the trend.

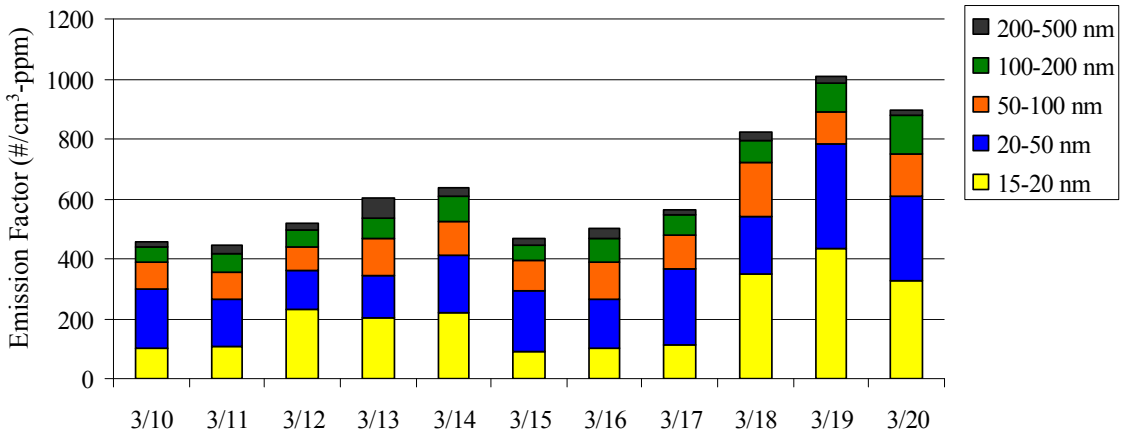

Figure 5.12. Emission factors versus day of study, segregated by particle size.

The emission factors, averaged across the eleven days that were analyzed are represented in Figure 5.12. The emissions factors, particularly in the 15-20 and the 20-50 nm size range, are variable with notable increases on the 18th, 19th, and 20th. A cold-front, often called a "Norte" passed through Mexico City between the 14th and the 15th of March. Norte events are associated with increased humidity and precipitation, which may account for the decrease in emission factor on the 15th, but cannot account for the increase on the 18th, 19th, and 20th beyond the pre-Norte levels. Possible reasons for this increase, such as correlation with major biomass burning, will be further examined.

The overall, average emission factor calculated for Mexico City is 502 #/cm^3-ppm CO_2. The next step in the analysis was to apply this average emission factor to the

Mexico City plume as it travels downwind. We are able to do this using aircraft measurements of CO_2 provided by Stephanie Vay (NASA) and particle number provided by Tony Clark (University of Hawaii) obtained aboard the NASA DC-8. Figure 5.13 represents a map of the Mexico City area, including the flight path taken by the DC-8 aircraft on March 11, 2006. Yellow pushpin icons represent the T0, T1, and T2 measurement locations. The colorscale represents CO_2 concentrations measured aboard the aircraft from 380 ppm (blue) to 400 ppm (red). The Mexico City plume can easily be identified, with the highest CO_2 concentrations just above the city center and decreasing concentrations further outside of the city as shown below.

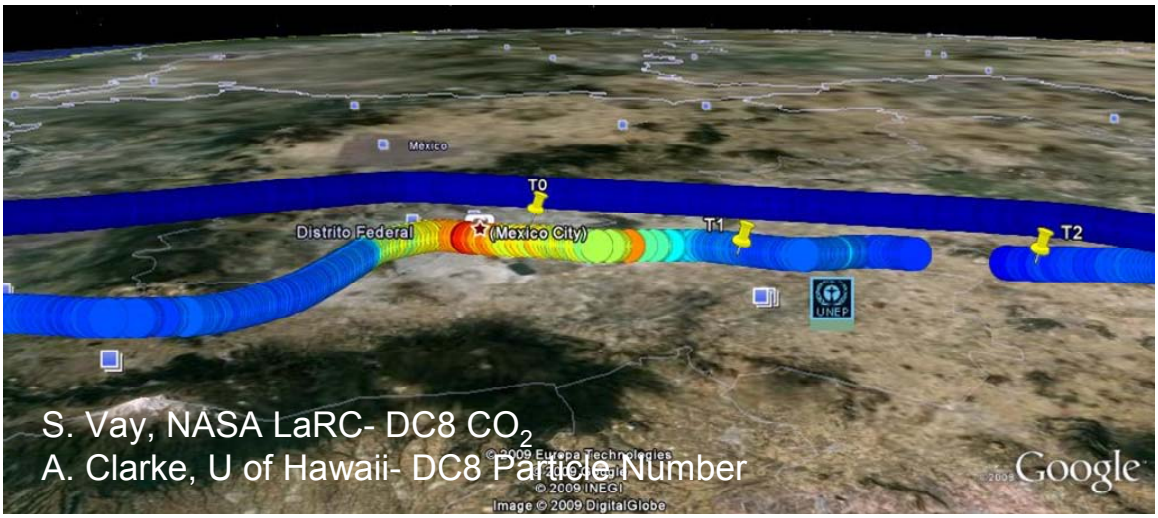

Source: Plot created using Google Earth, 2009.

Figure 5.13. March 11, 2006, DC-8 flight track plotted over map of Mexico City. Yellow icons represent the main ground-based sampling locations. The colorscale used on the flight track represents CO_2 concentrations as measured by S. Vay (NASA) ranging from 380 ppm (blue) to 400 ppm (red).

Applying the calculated average emission factor (502 #/cm^3-ppm CO_2) to the measured CO_2 concentrations aloft allows us to predict the particle number concentrations. Then, this predicted particle number concentration can be compared to

the actual particle number concentration measured aloft to determine how well the emission factor performs when applied to the plume as it travels downwind of the city. Figure 5.14 provides an example of this comparison. The Δ CO_2 concentration (red), or the increase in CO_2 above a baseline concentration, is plotted on the left y-axis versus distance from the center of the Mexico City plume. The corresponding predicted increase in particle number concentration above the baseline (Δ particle number) is calculated by multiplying Δ CO_2 by the average emission factor (502 #/cm^3-ppm) and is plotted in blue. The actual measured Δ particle number is plotted in green.

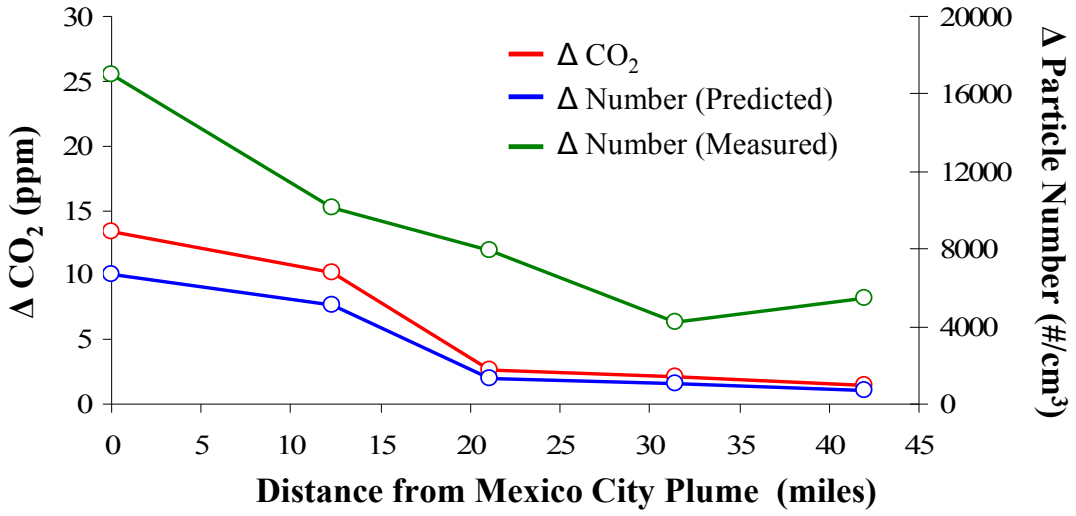

Figure 5.14. Comparison of the predicted increase in particle number above a baseline (Δ particle number, blue) associated with an increase in CO_2 (Δ CO_2) to the measured increase in particle number (green).

As shown in Figure 5.14, the measured Δ particle number is significantly higher than predicted using the emission factor determined at the ground level. This is an interesting result, suggesting that there is a source of particles aloft that comes without CO_2. An aerosol dynamics model could be employed to determine how the particle size

distribution would evolve as it travels downwind (due to coagulation, condensation, etc.), however the dynamic processing can not account for an increase in overall concentration. Therefore, new particle formation is a likely explanation for the elevated particle number concentrations and provides support for the hypothesis that particles may preferentially nucleate aloft.

5.4.3 Conclusions and Discussion

The representative emission factor, averaged across all wind directions, time of day, and particle size is 502 ((#/cm^3-hr)/ (ppm-hr)). Conversions of this emission factor can be made for comparison to previously determined emission factors in other areas. For example, by assuming a percentage of carbon in gasoline, the average emission factor can be converted to units of #/kg-fuel.

Further analysis of the method used to determine the emission factors will be performed to ensure the most representative factors. For example, using the current method, an emission factor will still be calculated for time periods when there is no actual peak in CO_2 or particle number concentration (i.e. an emission factor will be calculated from 2 noise signals). What affect does that have on the overall calculation? Our first step in answering this question will be to compare the emission factor calculated from time periods where large CO_2 and number peaks are highly correlated (during high motor vehicle traffic hours) to emission factors calculated during periods when baseline CO_2 levels are present (and large peaks are absent). After the best method for determining the number-based emission factors has been determined, the temporal variations will be examined.

The application of the emission factor to the Mexico City plume as it travels down wind will also be examined in further detail. Analysis similar to that presented in Figure 5.14, which was performed on data obtained in the "fresh" Mexico City plume, can be applied to data obtained during other DC-8 flights. The DC-8 intersected the plume at

various points in its trajectory, and it would be possible to examine the evolution of the plume, with respect to CO_2 and number, further down-wind after the plume has aged.

5.5 Summary and Conclusions

The DAASS II was deployed in Mexico City, in March 2006, as part of the MILAGRO field campaign. Size distribution measurements were made at the urban research site (T0). New particle formation events were observed on 4 of the 15 days sampled (27%), which is similar to previous observations made in 2003 by Dunn et al. (Dunn, Jimenez et al. 2004) who observed events on 30% of days sampled during periods of sudden decrease in condensational sink.

It appears that winds blowing from the northwest, which is an area that is densely populated with large SO_2 point sources, are seen more often than winds from any other direction during new particle formation events. However, longer sample time periods resulting in more than 4 event days, would be required in order to make a definitive conclusion.

It was hypothesized that new particle formation in Mexico City occurs following periods of decreased pre-existing aerosol surface area. The unique geographical setting of Mexico City creates conditions where sudden increased boundary layer growth in the early afternoon is common and leads to ventilation. The timing of the new particle formation events in Mexico City (between 11:30 and 13:30) supports the hypothesis, although more extensive analysis involving lidar and vertically resolved pollutant concentrations using aircraft data may be useful for parameterization of the contributing factors.

Number-based emission factors were determined using a method of peak identification in co-located SMPS and CO_2 measurements. There was no notable difference in the emission factor with varying wind direction which is not surprising considering the central urban location of the measurement site. A trend in diurnal

variation of the emission factors, with a maximum between 14:00 and 18:00 was noted but could not be explained by afternoon new particle formation or by standard error in the analysis method, and will be explored further. Trends in day-to-day variation of the emission factor, especially in the 15-20 and 20-50 nm size ranges require further analysis. Comparisons of the representative emission factor in Mexico City to those determined in other locations can be made using the CO_2 normalization of this work.

CHAPTER 6: SUMMARY AND RECOMMENDATIONS

The focus of this work was to advance the understanding of atmospheric new particle formation. The thesis combined instrumentation development and advanced aerosol sampling techniques with field and laboratory studies. The resultant data was then analyzed in order to parameterize new particle formation events in terms of the chemical mechanism, vertical profile, frequency, intensity, and associated meteorology.

One of the first objectives was to develop instrumentation that would allow us to supplement the traditional size distribution measurements with measurements of aerosol response to changes in temperature, relative humidity, and concentration. A Dry-Ambient Aerosol Size Spectrometer (DAASS) was constructed in order to obtain a measure of aerosol water content simultaneously with traditional size distribution measurements. The DAASS was then deployed in Mexico City as part of the MILAGRO field campaign. While the DAASS operated successfully according to its design, the measurement of aerosol water was difficult due to the environmental conditions. The indoor enclosure housing the DAASS was unexpectedly warmer than the ambient conditions, and consequently the aerosols were dried as they entered the inlet and traveled inside to the instrument. This prevented accurate measurements of particle size at ambient conditions. It is recommended for future deployments of the DAASS in field campaigns that extra precautions are taken in order to ensure that the inlets and instruments are kept at ambient temperatures. This is easily accomplished by housing the instruments out-of-doors in a protected environment. A series of fans may also be used to draw ambient air into the enclosure housing the instruments to regulate temperature. It is also recommended that characterization of the inlet losses be carried out in the field prior to data collection. As the instrument is disabled and reconfigured, minor adjustments in the instrumentation set-up such as bends in tubing and pipe fittings may alter the losses of the inlet. Characterization of the losses in the field provides a more

accurate representation of the overall losses, which is used to correct the measured sized distributions, resulting in a finalized data set. Although a few minor adjustments are recommended before future deployments, the DAASS has operated successfully and was able to provide the desired data regarding ultrafine aerosols and new particle formation in Mexico City.

A Differential Mobility Analyzer (DMA) was designed and constructed in order to provide the group with a means for Tandem-Differential Mobility Analysis (TDMA). A thermo-denuding flow cell prototype was also designed and constructed for future volatility TDMA studies. In order for the DMA system to be fully operational, further optimization is required. A high voltage meter/probe should be used to verify that the voltage output from the module to the column is accurate, as this is important to ensure the particles are accurately sized. The accuracy of the particle sizing should then be verified using engineered particles of a known size, such as polystyrene latex spheres. Optimization of the labview code controlling the sheath flow rates may also be required.

One of the objectives of the thesis was to parameterize new particle formation events in the Midwestern United States. The goal was to parameterize the frequency and intensity of the events in terms of the precursor gas concentrations (according to the ternary mechanism) and associated meteorology. We also wanted to determine the vertical and horizontal extents of the events. The first field campaign aimed at this objective occurred in Bondvillle, Illinois at the Bondville Environmental and Atmospheric Research Site (BEARS) in August, 2005. A nano-SMPS, CPC, and SO_2 monitor were deployed and supplemental data was obtained from BEARS collaborators.

It was determined that new particle formation events in Bondville occur on 25% of days, between the hours of 9:00 and 11:00 am. The analysis led to the conclusion that the events occurred under conditions of elevated SO_2 concentrations and average condensational sink. The growth of the newly formed particles was observed over several hours suggesting that the events were regional in nature, and not confined to

specific air masses. A specific area of long-range transport was not identified, as events occurred during winds from multiple directions. Two different types of new particle formation were observed in Bondville, one where new particles were detected at 5 nm and another type where new particles were not detected until 10 nm. Nothing in the measured data could provide an explanation for the difference between the two events. However, it is hypothesized that the two different types of events support the notion that there are instances where particles may nucleate aloft and mix down to the ground through turbulent mixing processes (i.e. the 10 nm particles nucleated aloft and grow before being detected).

Unfortunately, the ammonia monitor operated by the Illinois State Water Survery was not operating at the Bondville site during the 2005 campaign. Therefore, the events could not be parameterized according to the ternary mechanism. It is suspected, however, that new particle formation in the Midwest is not ammonia limited under most circumstances. The SO_2 monitor operating during the Bondville campaign was able to provide qualitative information about concentration, leading to the conclusion that new particle formation occurs during periods of increased SO_2 concentrations. A drift in the internal parameters on the SO_2 monitor led to negative baseline values over time, and therefore qualitative information about SO_2 concentrations was not recorded.

A second Midwestern field campaign was conducted in West Branch, Iowa during the summer of 2008. The objective of the study was to observe new particle formation events while simultaneously obtaining information about the vertical profile of gas and aerosol phase pollutants. Measurements were made at the base of the NOAA television tall tower, which provides vertical resolution of CO, CO_2 and meteorological parameters. A nano-SMPS, APS and lidar were deployed at ground level. Rawinsondes were launched twice daily through collaboration with Ken Davis at Penn State University. Information about boundary layer height and growth was determined using the tall tower, lidar, and rawinsondes.

New particle formation events were observed on 40% of days sampled. The events were classified into three distinct types; strong morning formation events, afternoon formation events, and intermittent events. The new particle formation events occurring in West Branch have been correlated with winds from the south, which is an area of increased SO_2 emissions. Boundary layer growth was similar on event and non-event days.

Prior to the field campaigns, multiple hypotheses were formed regarding Midwestern new particle formation, and were based on the assumption that nucleation in the Midwest occurs according to the ternary mechanism, and is not ammonia limited. One hypothesis was that nucleation is sulfuric acid limited, and as elevated plumes travel to the site, nucleation occurs aloft and the new particles are only detected when mixed down to the ground. Another hypothesis was that sulfuric acid concentrations are sufficient throughout the atmosphere for nucleation to occur, and new particle formation is inhibited by condensational sink. Perhaps situations exist where nucleation occurs homogeneously throughout the atmosphere. A third hypothesis was that although new particle formation and boundary layer evolution appear to be linked, they are only driven by the same factors and are actually independent.

As a result of the field campaigns in Bondville and West Branch, it was concluded that more than one of the proposed hypotheses regarding new particle formation in the Midwest is valid. For example, if nucleation is sulfuric acid limited, there may be situations where sulfuric acid plumes are emitted aloft and travel to the site. New particle formation may then occur in the plume aloft, and be detected at the ground only during boundary layer growth and vertical mixing. However, if this sulfuric acid limited scenario is accurate, it is possible that other situations exits where the sulfuric acid plume is advected to the site at ground level creating conditions favorable for nucleation, regardless of the boundary layer activity. Therefore, a sulfuric acid limited

scenario may or may not be linked to vertical motion and boundary layer activity, depending on the altitude of the plume.

In order to definitively complete the objective of parameterization of new particle formation, another Midwestern field campaign is required. On-site measurement of gas-phase ammonia and sulfuric acid concentrations is necessary in addition to the meteorological and radiation data. In order to observe the vertical profile of formation events, vertically resolved measurements and lidar are also required. A first generation SO_2 measurement system was deployed at the tall tower in West Branch in 2008, and was designed to take measurements at all 3 levels of the tower. Unfortunately, there were design errors in the calibration system rendering the data invalid. However, a second generation calibration system has been designed and the required parts have been obtained for its construction (see Appendix D). It is recommended that improvements to the vertically resolved SO_2 monitoring system be made, and a second campaign be conducted at the tower. Vertically resolved SO_2 measurements provide vital information for the parameterization of nucleation and the determination of the vertical profile. Ammonia measurements would be necessary in order to parameterize formation events according the ternary mechanism. Including consistent lidar data in the second deployment would add further information about the vertical profile of aerosols and condensational sink and would complete the data set.

In March 2006, the DAASS was deployed in Mexico City as part of the MILAGRO field campaign. The objective of the deployment was to determine the water content of the aerosols, as well as to characterize new particle formation events. Events were observed on 27% of days studied, and occurred following periods of sudden decrease in condensational sink. These results are consistent with previous studies conducted in Mexico City. The sampling period was not long enough in order to determine a correlation (or lack of) with a specific source region. All of the events

occurred in between the hours of 11:30 and 13:30, which is later in the day when compared to other mega-cities.

From the study, we have concluded that new particle formation in Mexico City occurs during periods of decreased condensational sink at the ground level, and that the sudden decrease in condensational sink at the ground is related to the unique boundary layer activity seen in a mountain basin. The slow morning growth of the boundary layer, followed by a sudden increase in height in the afternoon, brings cleaner air from aloft to the ground, thereby decreasing the condensational sink and allowing new particle formation to occur.

We were also able to determine size resolved number-based emission factors representative of Mexico City using the correlation between CO_2 concentration and particle number. An average value of 502 #/cm^3-ppm is reported. The emission factors were examined according to time of day, particle size, and wind direction. In the preliminary analysis, there is no notable difference in the emission factor with varying wind direction. Trends in daily and hourly variation in the emission factors will be analyzed further prior to publication. Comparisons of the representative emission factor in Mexico City to those determined in other locations can be made using the CO_2 normalization of this work.

Regarding new particle formation in Mexico City, specific questions concerning the vertical profile still remain. We have determined that rapid increases in boundary layer height, coincident with rapid decreases in pre-existing surface area precede formation events. However, it has not been determined if the particles nucleate aloft and are brought to the ground through vertical mixing, or if the vertical mixing brings the clean air down to the ground which decreases pre-existing surface area, and triggers nucleation at the ground level. Although multiple size distribution measurements were obtained at T0, particles below 10 nm were not measured. A size distribution measurement below 10 nm (down to 3nm) would allow us to determine if new particles

as small as 3nm are seen at the ground or if they are not seen until 10 nm at the ground, suggesting they may have nucleated aloft and grown before reaching the ground. Lidar data would be useful in determining aerosol concentrations aloft and should be analyzed for this objective.

Using the Mexico City emission factor, along with CO_2 measurements taken aboard the NASA DC-8 during flights over Mexico, we are able to predict aerosol number concentrations aloft. The predicted concentration can then be compared to the actual number concentration, also measured on-board the DC-8. As a result of this comparison, we have determined that particle number concentrations in the atmosphere aloft are higher than predicted by the emission factor. This result suggests a source of particles exists higher in the atmosphere and provides support for the hypothesis that nucleation may preferentially occur aloft. Further analysis of the emission factor and its evolution, as the Mexico City plumes ages and travels down-wind, will be conducted prior to publication.

APPENDIX A: BONDVILLE SUPPLEMENTAL DATA

The following figures are the 24 hour backward trajectories from Bondville, Illinois for all 6 of the days where new particle formation occurred. The figures were created using the NOAA HYSPLIT (Hybrid Single-Particle Lagrangian Integrated Trajectory) model, which is available online (http://www.ready.noaa.gov/ready/open/hysplit4.html).

The HYSPLIT trajectories show an aerial view of the path an air parcel took and a view of its movement at different altitudes. The section at the bottom of the map shows the height of the air parcel measured at these corresponding tick marks. The height of the air parcel is measured in meters above ground level (AGL).

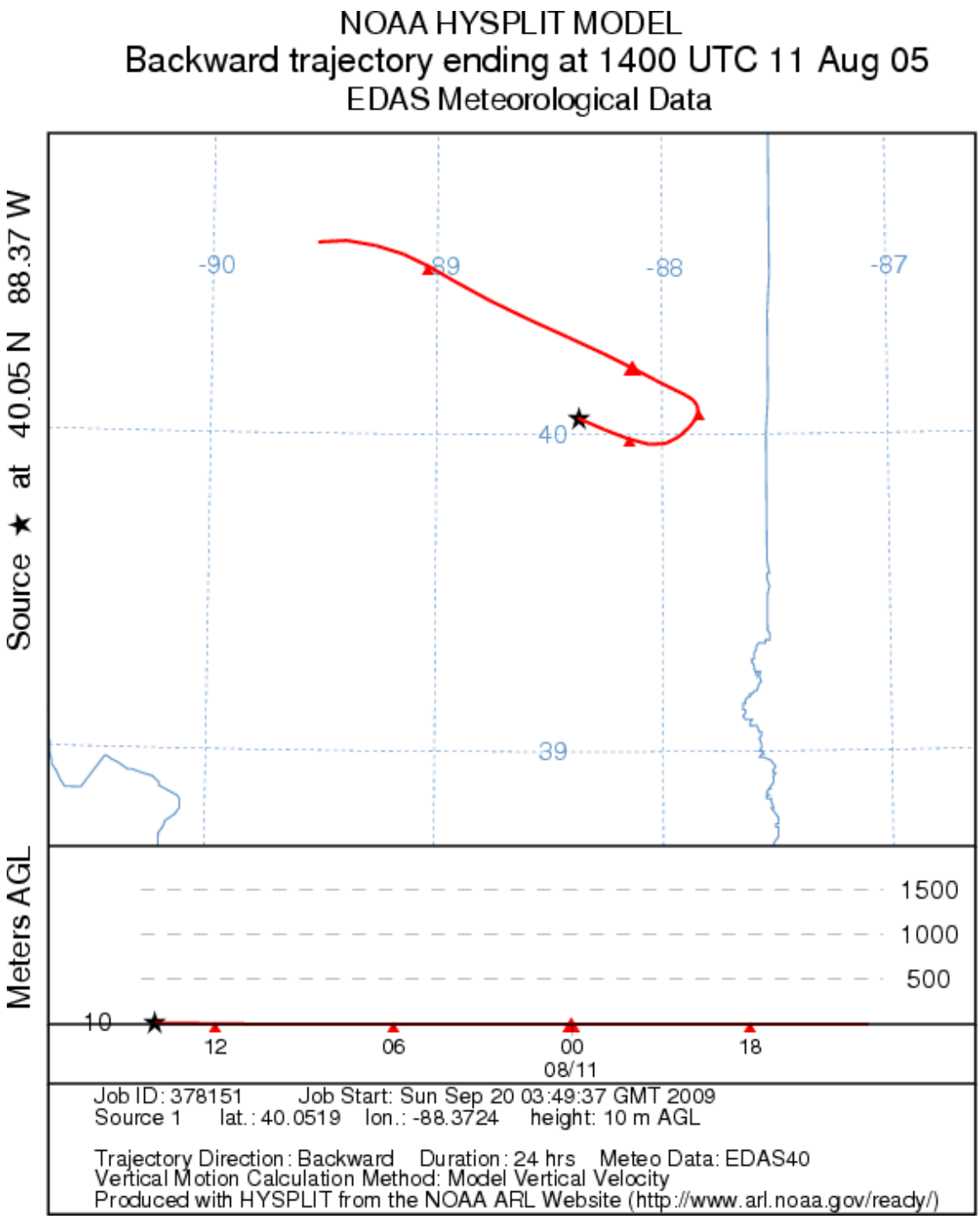

Figure A.1. Twenty-four hour back trajectory for August 11, 2005, ending in Bondville, Illinois at the onset of a new particle formation event.

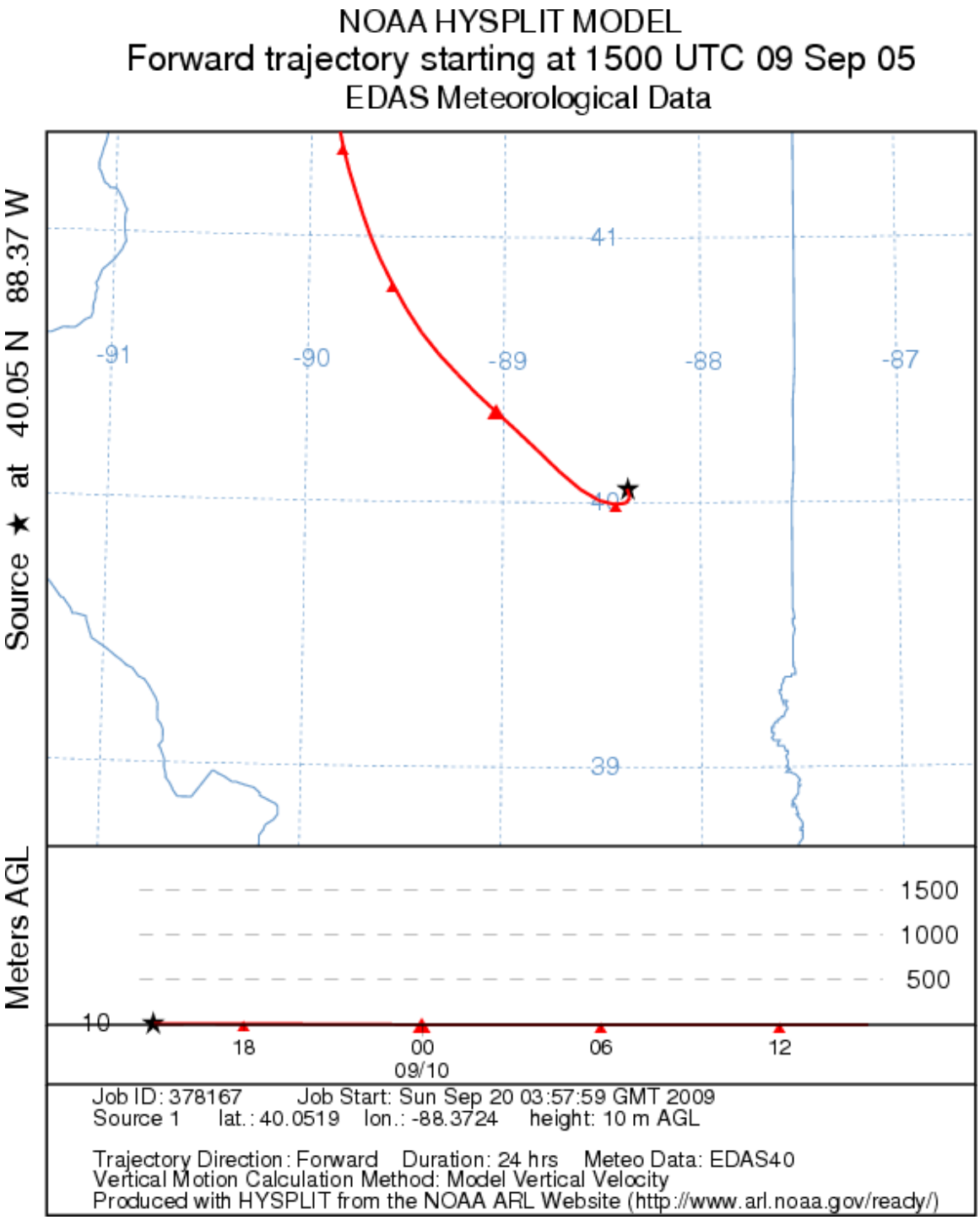

Figure A.2. Twenty-four hour back trajectory for September 9, 2005, ending in Bondville, Illinois at the onset of a new particle formation event.

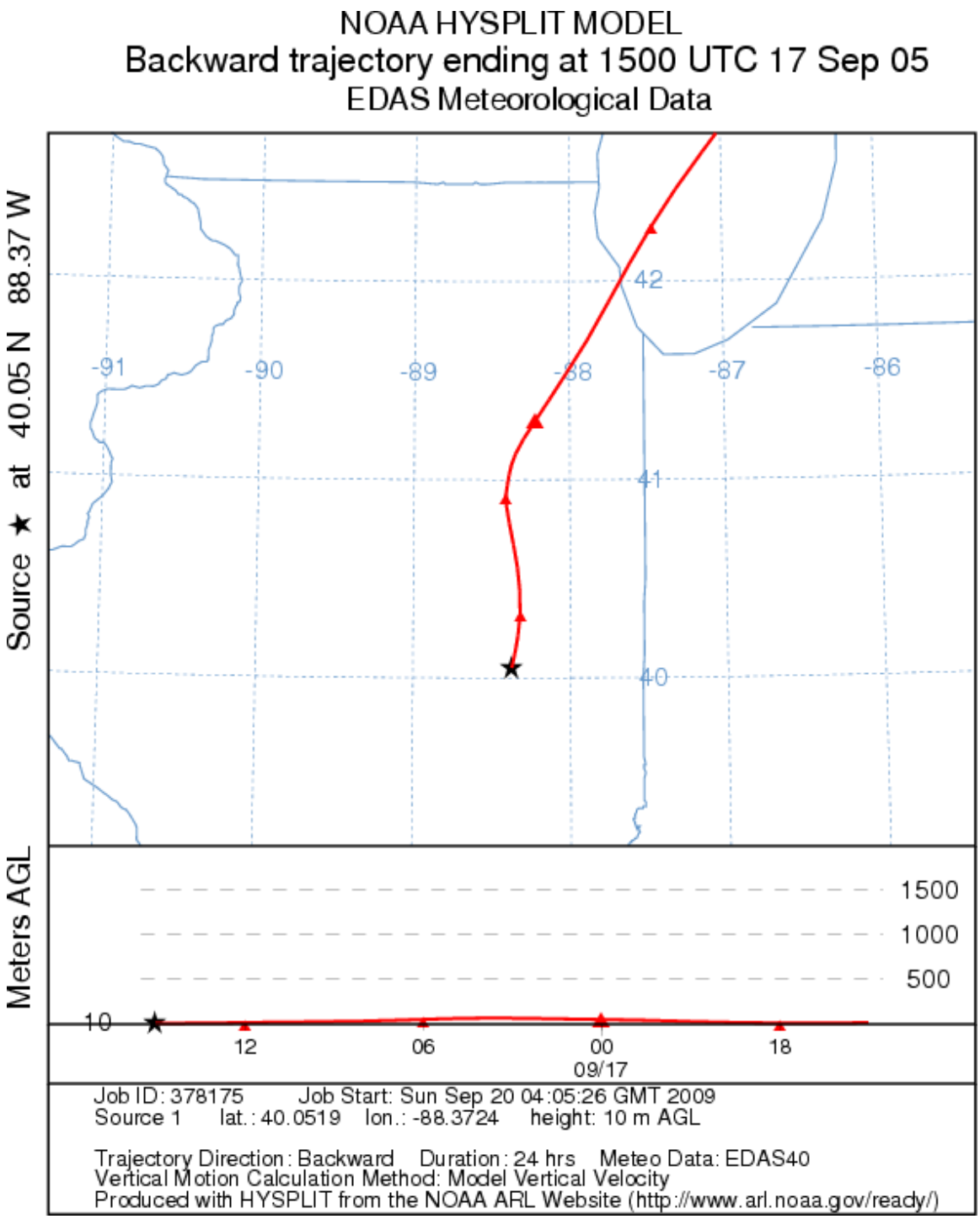

Figure A.3. Twenty-four hour back trajectory for September 17, 2005, ending in Bondville, Illinois at the onset of a new particle formation event.

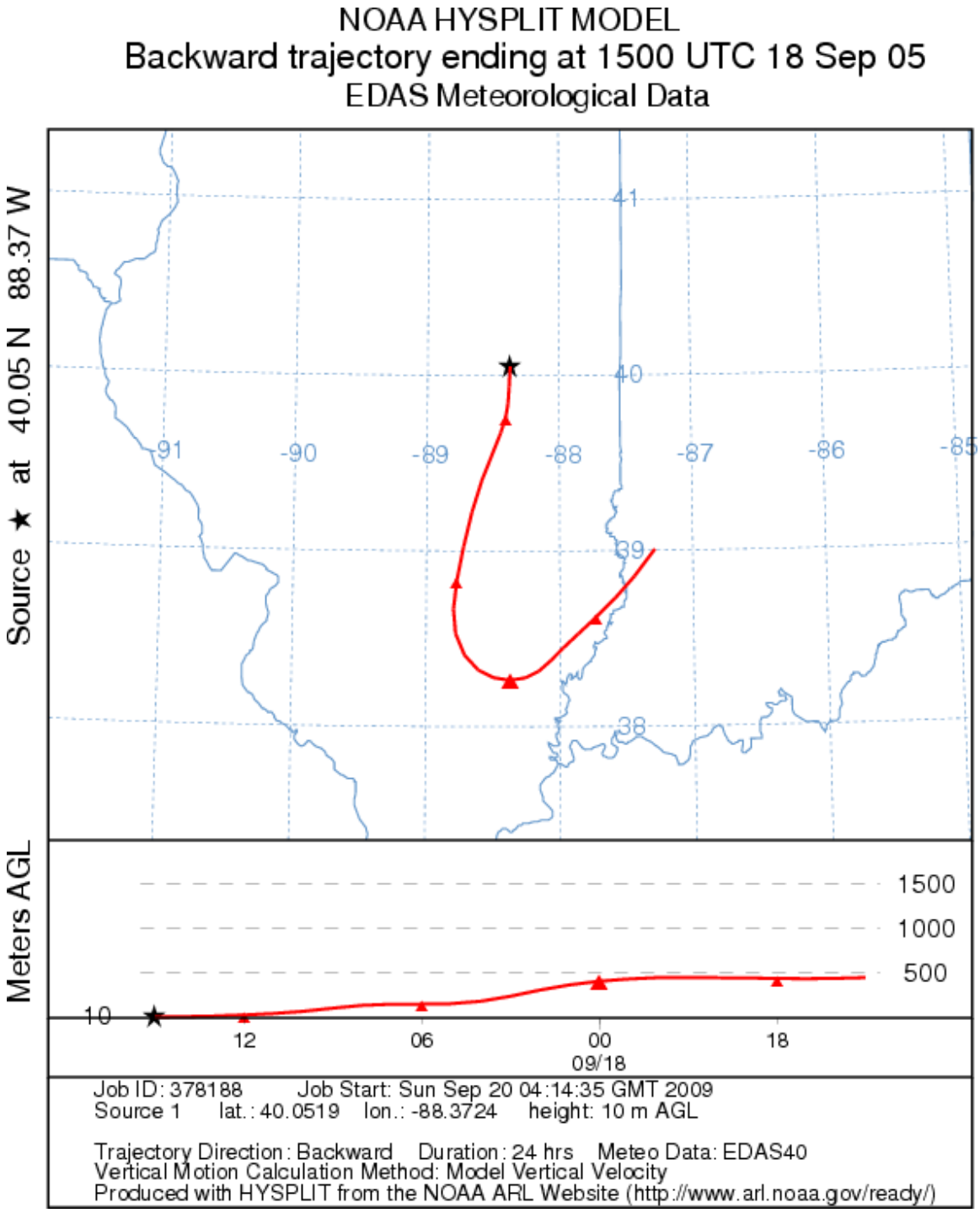

Figure A.4. Twenty-four hour back trajectory for September 18, 2005, ending in Bondville, Illinois at the onset of a new particle formation event.

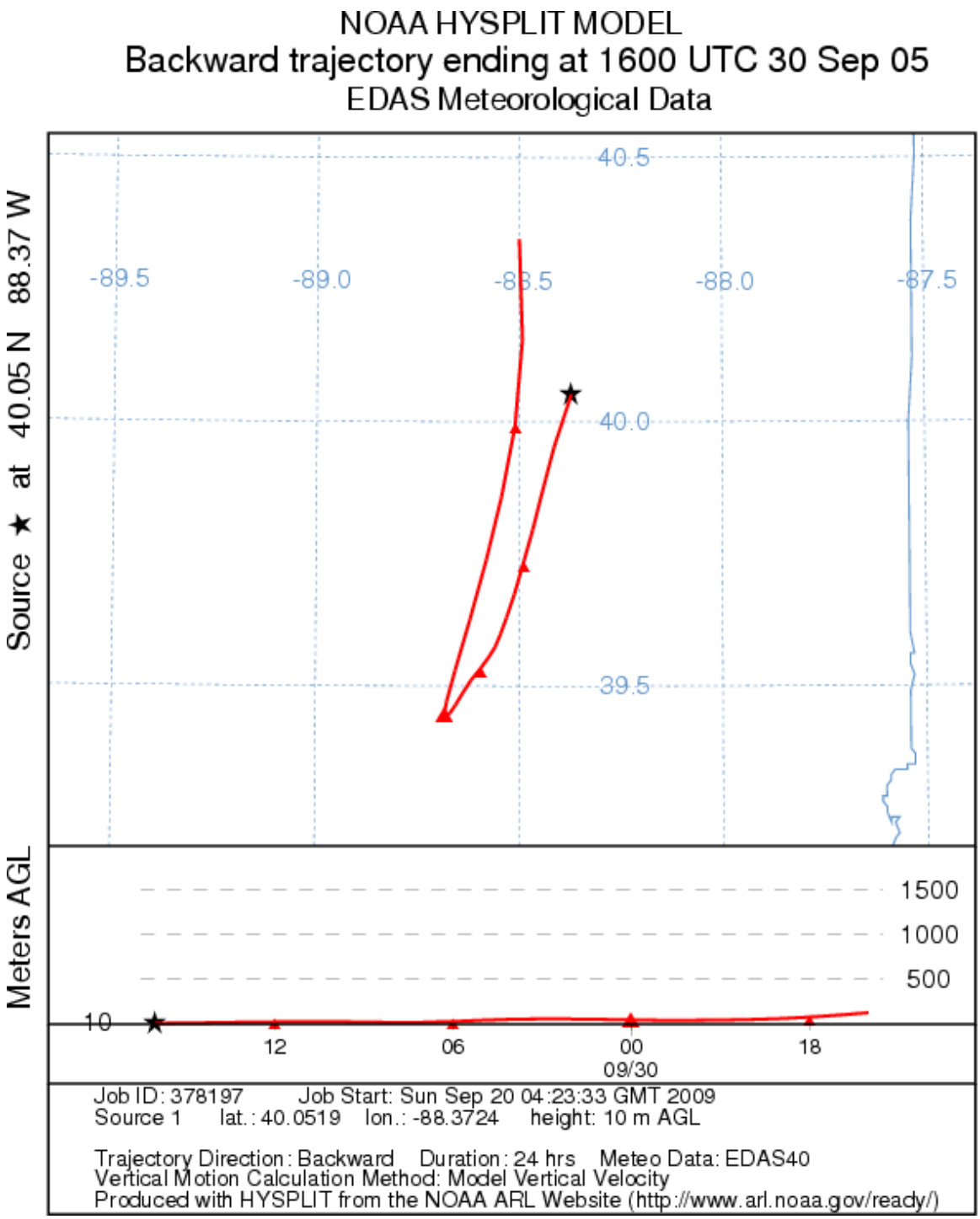

Figure A.5. Twenty-four hour back trajectory for September 30, 2005, ending in Bondville, Illinois at the onset of a new particle formation event.

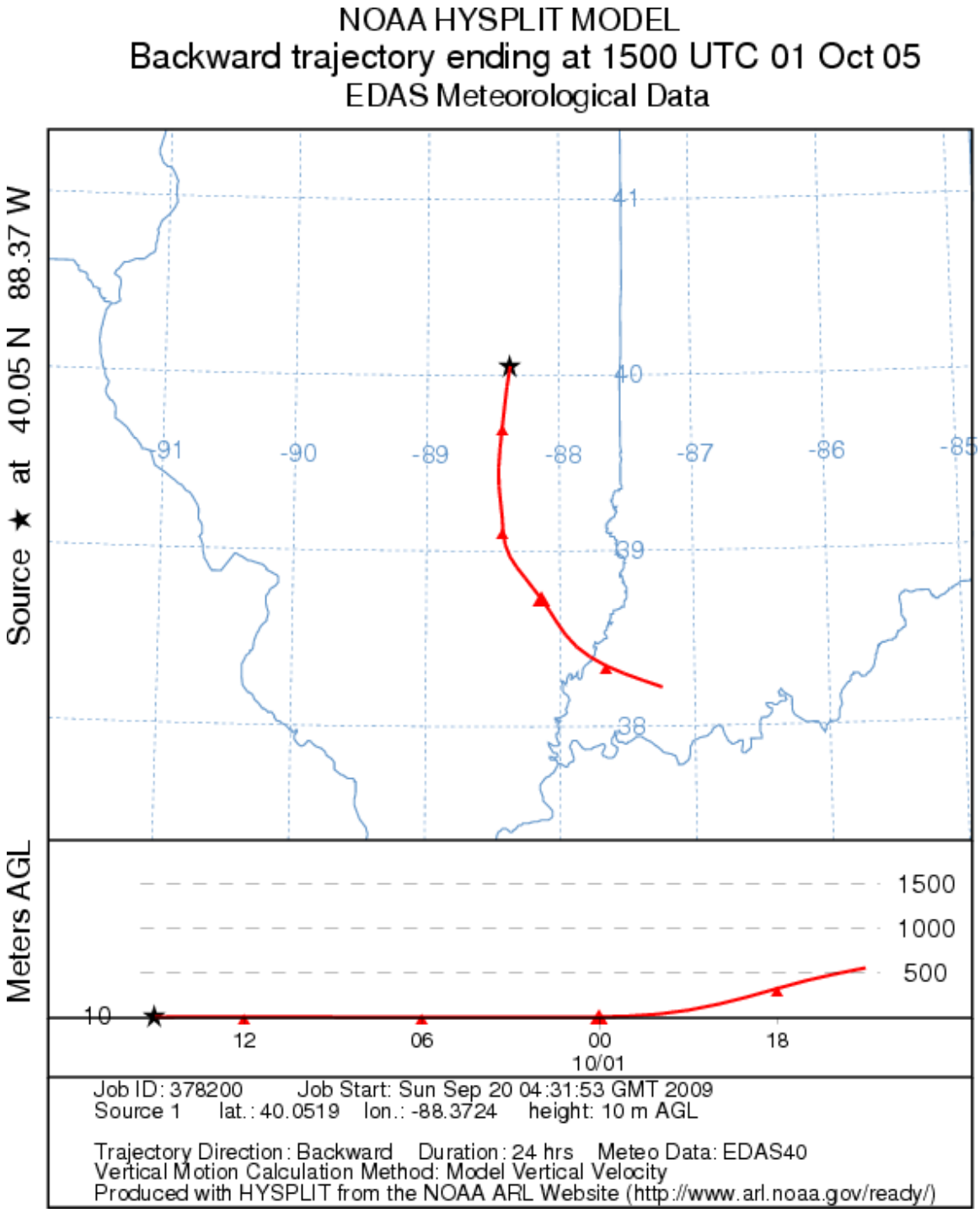

Figure A.6. Twenty-four hour back trajectory for October 1, 2005, ending in Bondville, Illinois, at the onset of a new particle formation event.

APPENDIX B: WEST BRANCH SUPPLEMENTAL DATA

B.1 Rawinsonde Data

Radiosondes were launched near the West Branch, Iowa monitoring location twice daily during the campaign, with the first launch occurring in the afternoon of June 20 and the last launch on the morning of July 6. The balloons were launched by the Ken Davis group at Penn State University at a farm nearby to avoid the tall tower. The measured variables (temperature, pressure and relative humidity) were used to calculate the potential temperature profiles and the water mixing ratios. The following plots include these estimates of potential temperature and mixing ratio versus height for each of the launches.

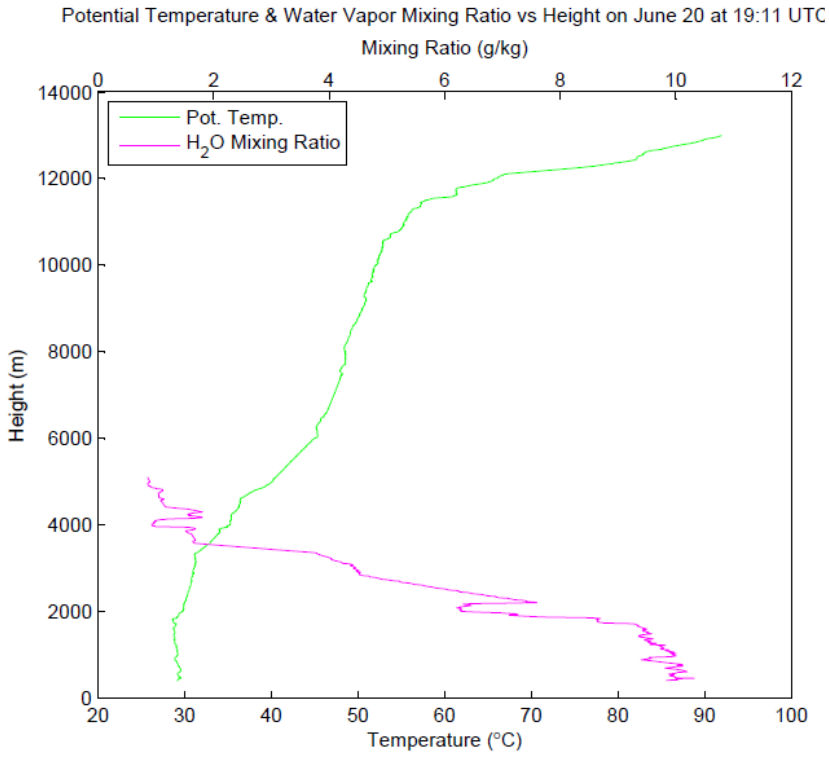

Figure B.1. Afternoon rawinsonde measurements recorded at West Branch, Iowa on June 20, 2008.

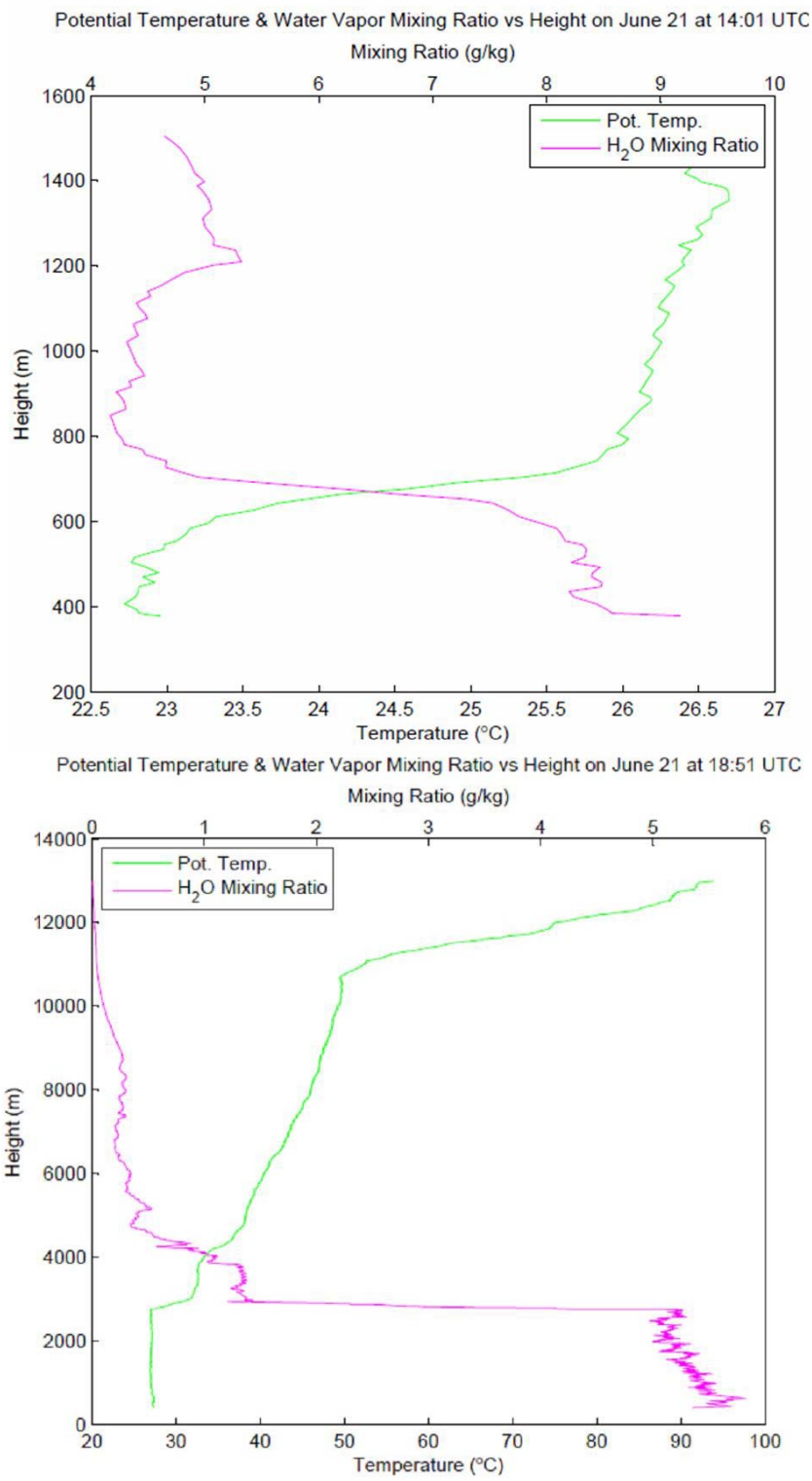

Figure B.2. Morning (top) and afternoon (bottom) rawinsonde measurements recorded at West Branch, Iowa on June 21, 2008.

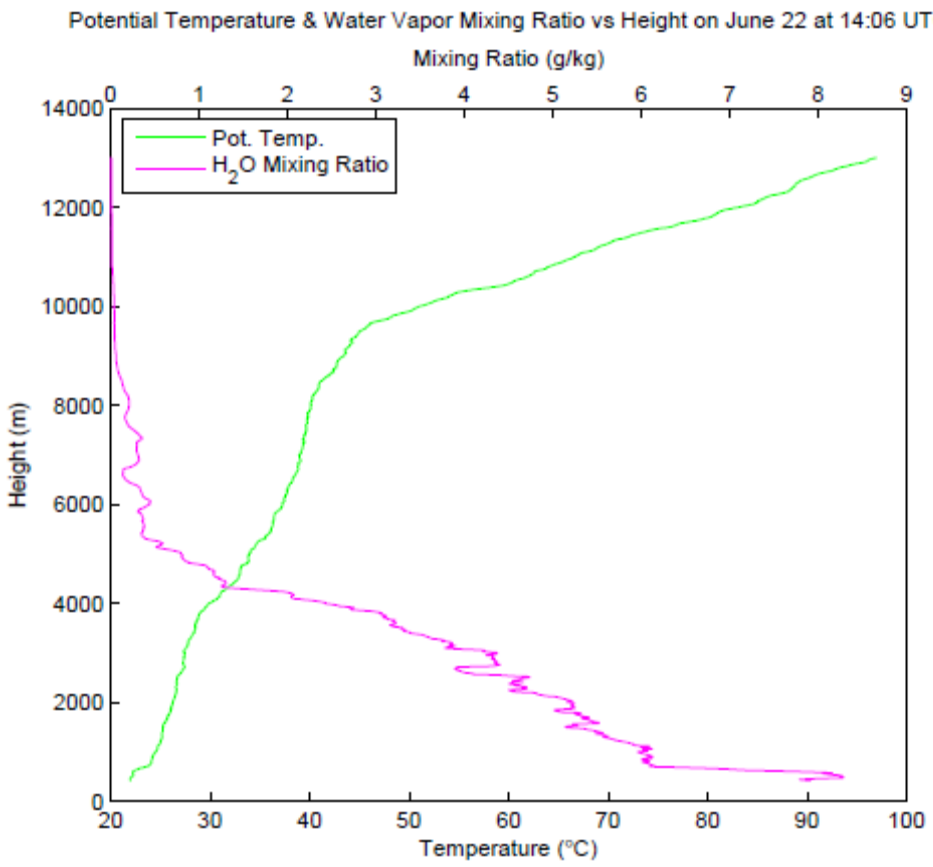

Figure B.3. Morning rawinsonde measurements collected at West Branch, Iowa on June 22, 2008.

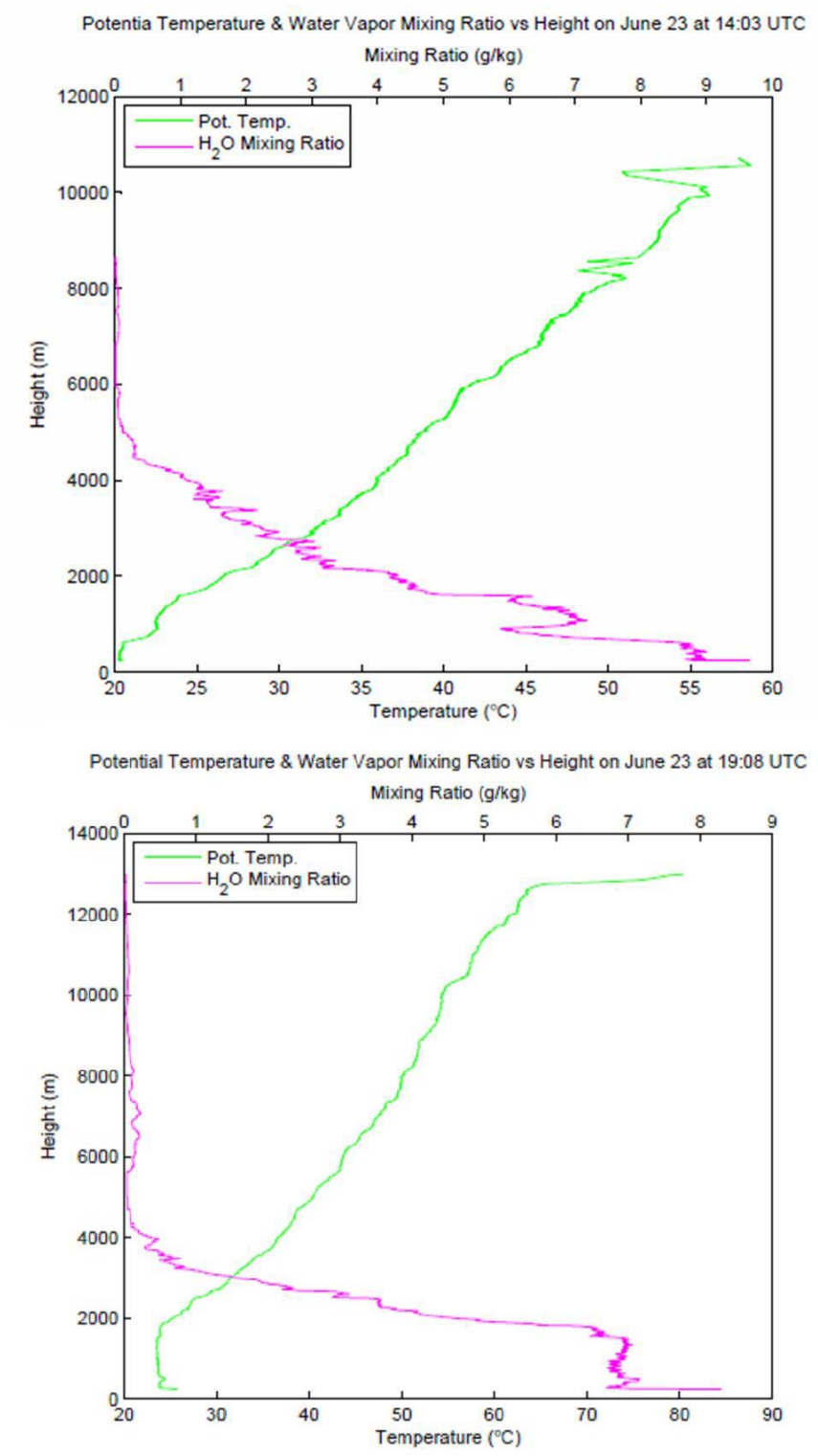

Figure B.4. Morning (top) and afternoon (bottom) rawinsonde measurements recorded at West Branch, Iowa on June 23, 2008.

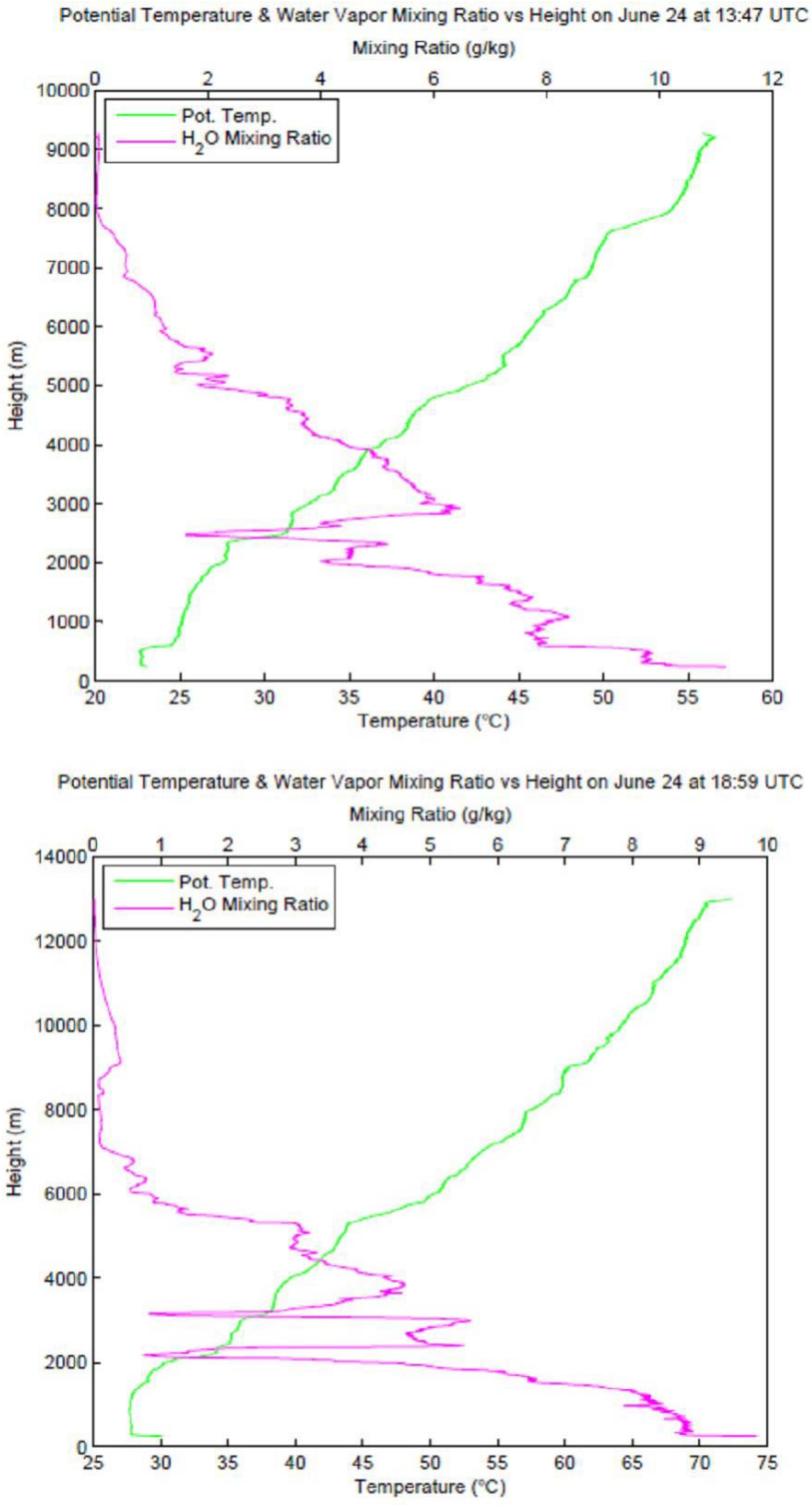

Figure B.5. Morning (top) and afternoon (bottom) rawinsonde measurements recorded at West Branch, Iowa on June 24, 2008.

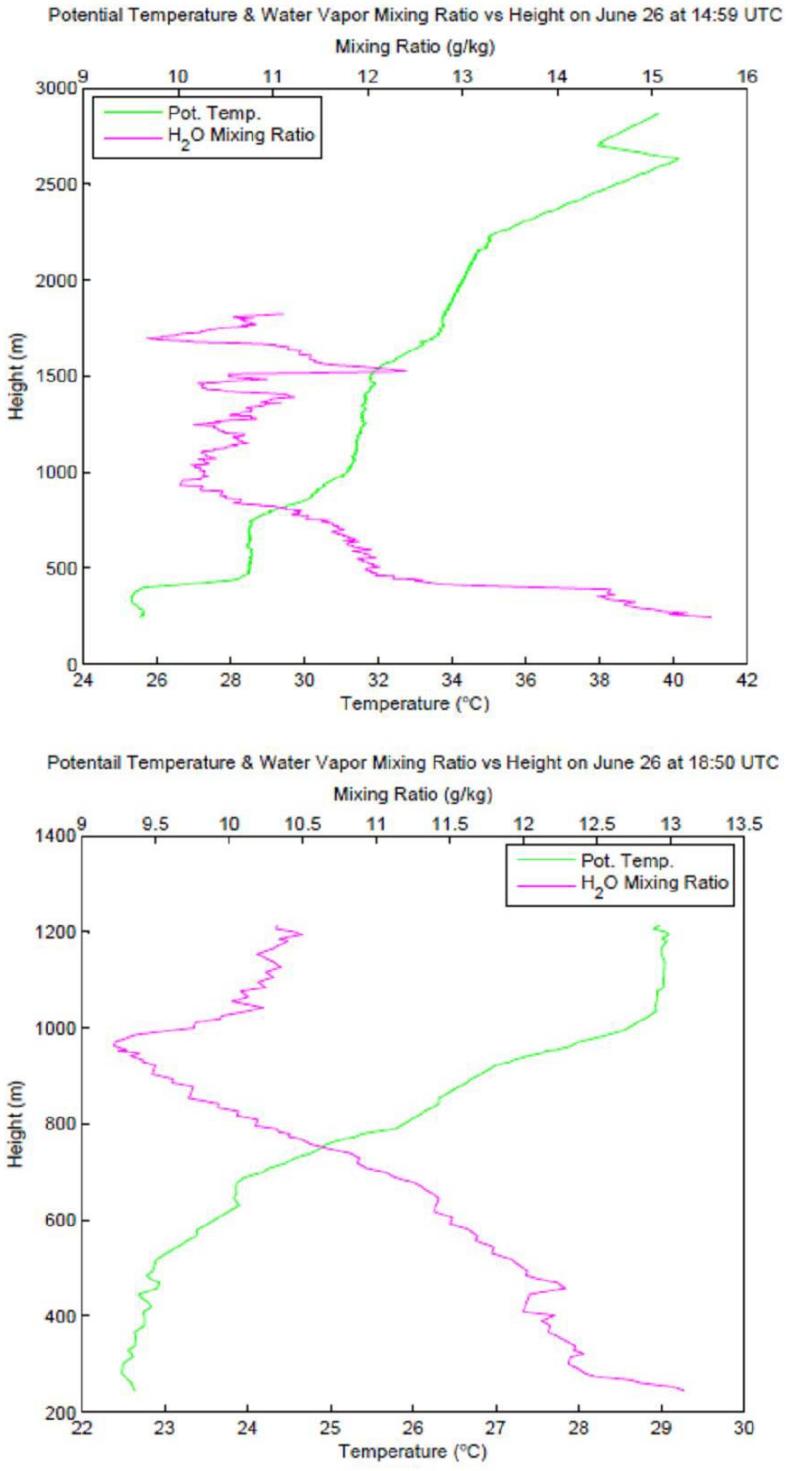

Figure B.6. Morning (top) and afternoon (bottom) rawinsonde measurements recorded at West Branch, Iowa on June 26, 2008.

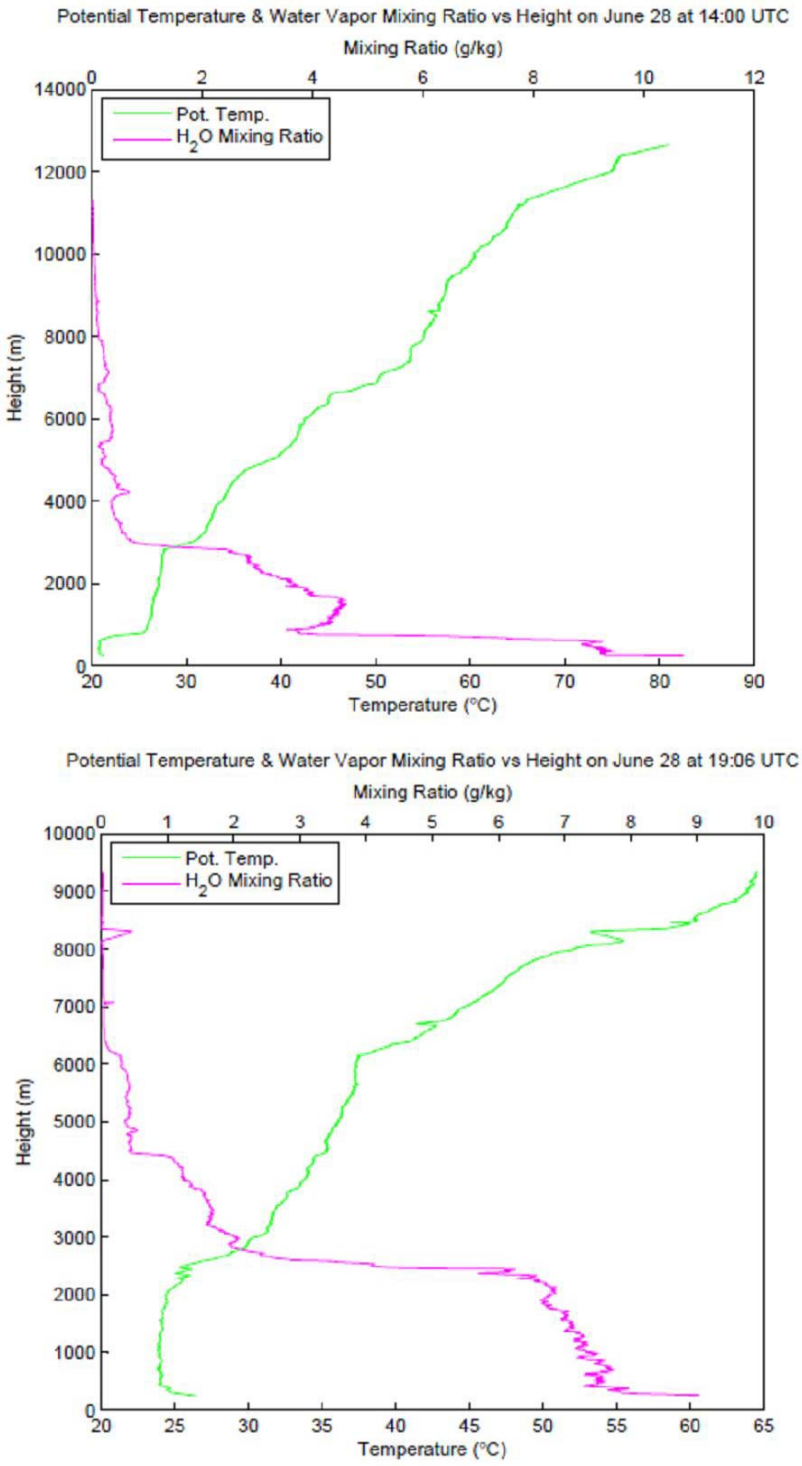

Figure B.7. Morning (top) and afternoon (bottom) rawinsonde measurements recorded at West Branch, Iowa on June 28, 2008.

B.2 Labview Controls

All of the controls for valve switching, data logging, and time averaging were custom controls created in Labview. The 'virtual instruments' or vi's are stored on the following ftp site: ftp:\\ftp.iihr.uiowa.edu. The following vi's were created during the West Branch campaign:

print_so2_valve_switch

print_zero_valve_switch

so2_reader

so2_solenoids_v2

switch_so2_valves

get4_RHT_vals

print_drydil_valve_switch

RH_reader_v3

test_time_averaging

timestamped_filename

tsi_flow_reader

vais_reader2

APPENDIX C: MEXICO CITY SUPPLEMENTAL DATA

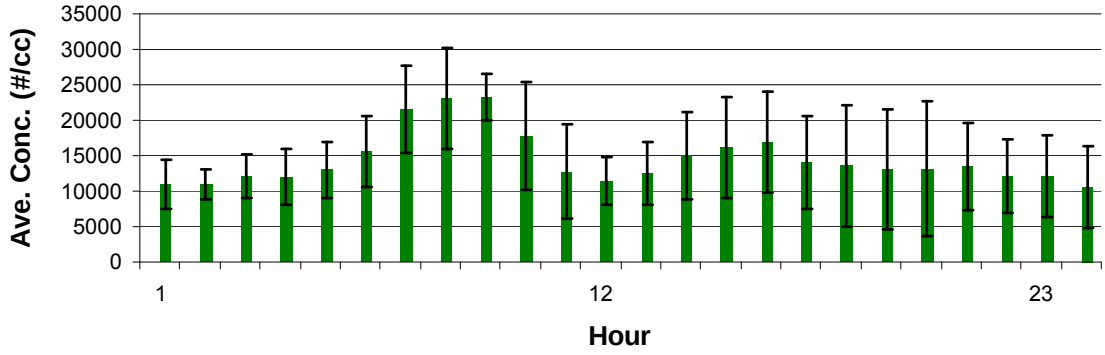

Figure C.1. Average diurnal profile of particle number concentration for non nucleation days during MILAGRO campaign. Error bars represent one standard deviation.

The following algorithm was applied for the number-based emission factor analysis using particle number concentrations and CO_2, which was described in Section 2.4 of the thesis.

Number_vs_CO2.m algorithm

1. pick calendar date for analysis
2. load CO2 data for that period (1 sample every 60 seconds)
3. load meteorological data for that period (1 sample every 100 seconds)
4. load particle number / size data (1 sample every 2 minutes, BNL data; 1 sample every 5 minutes, U of Iowa data)
5. load key settings, including
    a. randompeak.time_window_minimum_min (4 minutes)
    b. randompeak.time_window_maximum_min (90 minutes)
    c. max_timeshift_min (5 minutes)
    d. randompeak.num_peaks (500)

    In a-d the suffix min refers to the units of the variable (minutes)
6. Based on size range of interest, extract a time series of size-specific number concentration versus time
7. Enter random peak identification section of program

8. (optionally) limit time period of analysis to a subset of the day, using the variables starttime and endtime
9. Make a vector of master timestamps using the CO2 timestamps, limited to those between starttime and endtime (this variable is CO2_timestamps)
10. Interpolate the number time series to the CO2 timestamps using the function genutil_timeseries_interp_missing_data. Any data gaps in excess of 5 minutes are labeled as missing values. Any data gaps smaller than 5 minutes are filled in using interpolation or extrapolation.
11. Attempt to identify a single shift in the number timestamps that maximizes the correlation between number and CO2
12. Apply the timeshift and generate final time series for peak identification. For number and CO2, smooth using a 7^{th} order Savitzy-Golay filter. smooth_num; smooth_CO2, final_CO2times.
13. Normalize the y values of the number and CO2, such that the minimum value corresponds to 1.0 and the maximum value to 2.0.
14. Label each time (each element of final_CO2times) as within the wind direction of interest, or not (using variable good_wind_flag)
15. Enter peak identification while loop
    a. Randomly select a peak width (window_duration) between the minimum and maximum peak width values
    b. Randomly choose number or CO2 as the starting variable (50/50 chance of either)
    c. Find the number (CO2) values closest in time to the start and end periods of the random window
    d. Check that each number (CO2) value is a local minimum (e.g. the points on either side must be greater).
    e. If condition d is not met, restart the peak identification loop at step 15
    f. If condition d is met, now check that the wind was from the zone of interest for at least 75% of the time interval. If not met, return to start at step 15
    g. Determine a baseline timeseries for this period using the get_baseline subroutine. A baseline is needed in order to have a peak area. The simplest baseline is just the line between the two local minimum. This is done for both number and CO2
    h. Determine the peak areas during the time period by integrating under the data (trapezoidal integration using matlab trapz) and by integrating under the baseline
    i. Make the areas from h into a datapoint (a datapoint consists of a CO2 peak area and a number peak area).
    j. Repeat a-i until randompeak.num_peaks have been identified. Note – peaks can be identified more than once.
16. Determine an emission factor by fitting a line through all the CO2 peak areas (x data) and number peak areas (y data). Use robust regression from matlab robustfit, which is insensitive to outliers. Determine standard error from the statistics output of robustfit.

17. Record on hard disk, the emission factor, the time period of interest, the date of interest, the size bin, the standard error, and the wind direction of interest.
18. Repeat as needed for other times, dates, size bins, and wind directions.

APPENDIX D: INSTRUMENTATION

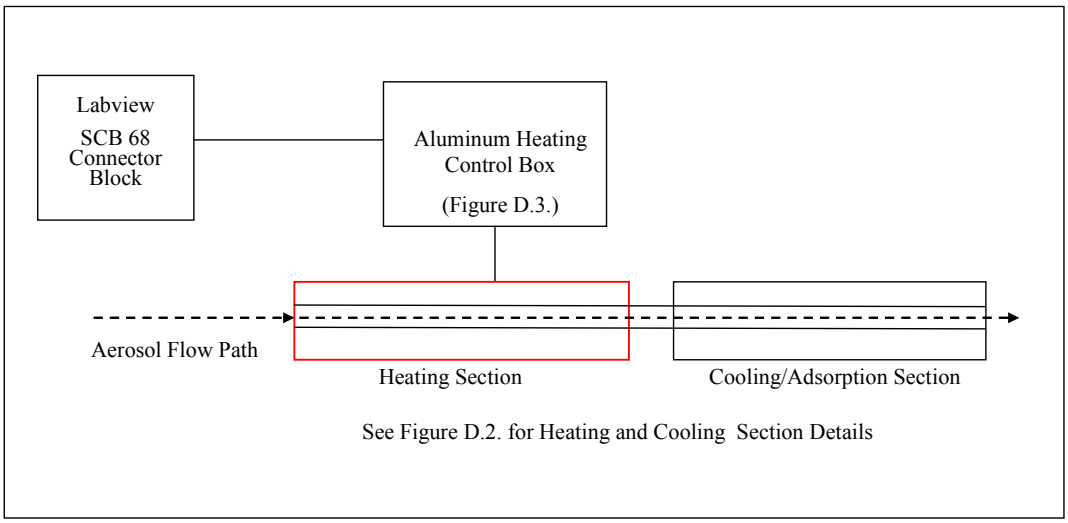

Figure D.1. Thermodenuder set-up overview.

#	Description	Vendor/Part Number
1	Coiled Heaters	Watlow 120V 500 W coiled heaters P/N 62H65A3X-1171
2	J type thermocouple	Watlow P/N Z635335
3	Adheshive J type TC	Omega SA1-J
4	Stainless Steel Perforated Tubing	Perf Tube, Inc Custom Part
5	Thermocouple Probe (1/8" OD)	Omega JMTSS-125E-6
6	Activated Carbon	Fisher Sci (6-14 Mesh)

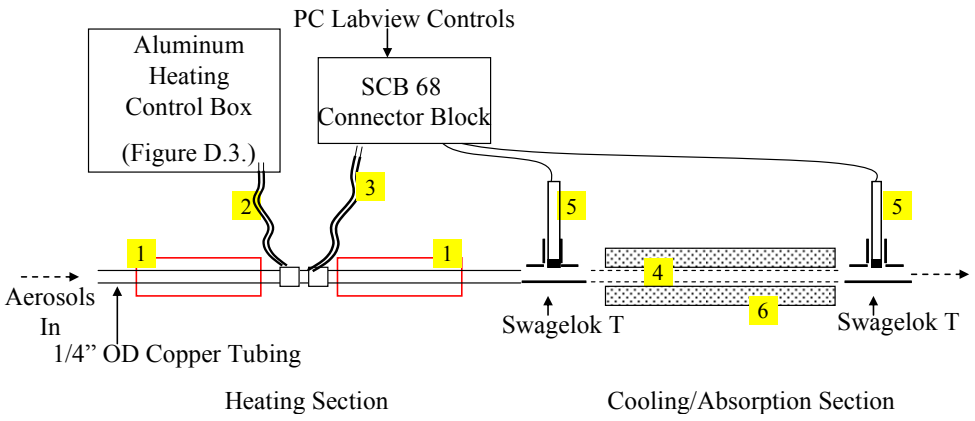

Figure D.2. Thermodenuder heating and cooling section details.

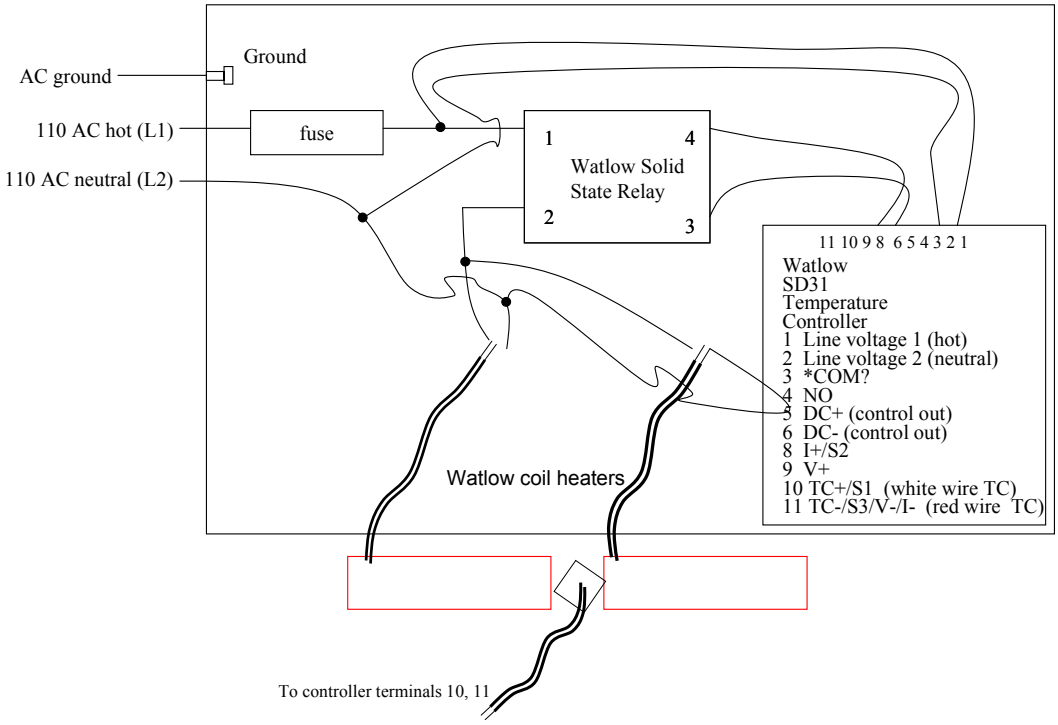

Figure D.3. Wiring diagram for aluminum thermodenuder heating control box.

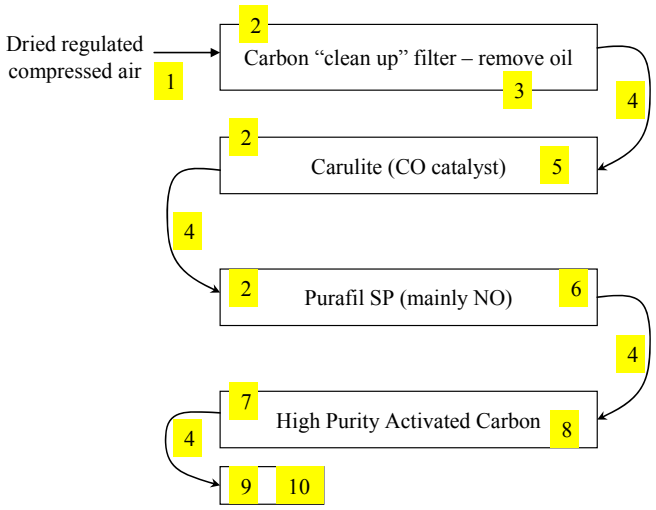

#	Description	Vendor/Part Number
1	Inlet Tubing, ¼" Poly	
2	Restek Refillable Hydrocarbon Trap	Fisher 06-711-818 1/4" swage option
3	Activated Carbon Granules	
4	FEP Teflon Tubing	Fisher
5	Carulite 300	Carus Chemical
6	Purafil SP Media	
7	Filter Holder	Discovery Science 8131
8	Activated Carbon Media	Discovery Science 8124
9	Filter Holder	Hylok Micron Inline Filter FI2-H-4T-7-316
10	7 micron stainless replacement element	Hy Lok 7-316

Figure D.4. Design and parts for the SO_2 monitor zero system.

REFERENCES

Adams, P. J. and J. H. Seinfeld (2002). Predicting global aerosol size distributions in general circulation models. *Journal of Geophysical Research-Atmospheres* 107(D19).

Alley, R. (2007). Climate Change 2007: The physical science basis [Working Group I to the Fourth Assessment Report of the Intergovernmental Panel on Climate Change], IPCC.

Banta, R. M. (1985). Late-Morning Jump in TKE in the Mixed Layer over a Mountain Basin. *Journal of the Atmospheric Sciences* 42: 407-411.

Boy, M., M. Kulmala, T. M. Ruuskanen, M. Pihlatie, A. Reissell, P. P. Aalto, P. Keronen, M. Dal Maso, H. Hellen, H. Hakola, R. Jansson, M. Hanke and F. Arnold (2005). Sulphuric acid closure and contribution to nucleation mode particle growth. *Atmospheric Chemistry and Physics* 5: 863-878.

Brock, C. A., R. A. Washenfelder, M. Trainer, T. B. Ryerson, J. C. Wilson, J. M. Reeves, L. G. Huey, J. S. Holloway, D. D. Parrish, G. Hubler and F. C. Fehsenfeld (2002). Particle growth in the plumes of coal-fired power plants. *Journal of Geophysical Research* 107: 4155.

Buzcu-Guven, B., S. G. Brown, A. Frankel, H. R. Hafner and P. T. Roberts (2007). Analysis and Apportionment of Organic Carbon and Fine Particulate Matter Sources at Multiple Sites in the Midwestern United States. *Journal of the Air & Waste Managment Association* 57: 606-619.

Clement, C. F. and I. J. Ford (1999). Gas-to-particle conversion in the atmosphere: II. Analytical models of nucleation bursts. *Atmospheric Environment* 33: 489-499.

Cocker, D. R., N. E. Whitlock, R. C. Flagan and J. H. Seinfeld (2001). Hygroscopic properties of Pasadena, California aerosol. *Aerosol Science and Technology* 35(2): 637-647.

Dal Maso, M., M. Kulmala, I. Riipinen, R. Wagner, T. Hussein, P. Aalto and K. Lehtinen (2005). Formation and growth rates of fresh atmospheric aerosols: eight years of aerosol size distribution data from SMEAR II, Hyytiala, Finland. *Boreal Environ. Res.* 10: 323.

deFoy, B., J. D. Fast, S. J. Paech, D. Phillips, J. T. Walters, R. L. Coulter, T. J. Martin, M. S. Pekour, W. J. Shaw, P. P. Kastendeuch, N. A. Marley, A. Retama and L. T. Molina (2008). Basin-scale wind transport during the MILAGRO field campaign and comparison to climatology using cluster analysis. *Atmospheric Chemistry and Physics* 8: 1209-1224.

Dunn, M. J., J. L. Jimenez, D. Baumgardner, T. Castro, P. H. McMurry and J. N. Smith (2004). Measurements of Mexico City nanoparticle size distributions: Observations of new particle formation and growth. *Geophysical Research Letters* 31(10).

Dusek, U., G. P. Frank, L. Hildebrandt, J. Curtius, J. Schneider, S. Walter, D. Chand, F. Drewnick, S. Hings, D. Jung, S. Borrmann and M. O. Andreae (2006). Size matters more than chemistry for cloud-nucleating ability of aerosol particles. *Science* 312(5778): 1375-1378.

Easter, R. C. and L. K. Peters (1994). Binary Homogenous Nucleation: Temperature and Relative Humidity Fluctuations, Nonlinearity, and Aspects of New Particle Production in the Atmosphere. *Journal of Applied Meteorology* 33: 775-784.

Fast, J. D., B. de Foy, F. A. Rosas, E. Caetano, G. Carmichael, L. Emmons, D. McKenna, M. Mena, W. Skamarock, X. Tie, R. L. Coulter, J. C. Barnard, C. Wiedinmyer and S. Madronich (2007). A meteorological overview of the MILAGRO field campaigns. *Atmospheric Chemistry and Physics* 7(9): 2233-2257.

Gaydos, T. M., C. O. Stanier and S. N. Pandis (2005). Modeling of in situ ultrafine atmospheric particle formation in the eastern United States. *Journal of Geophysical Research-Atmospheres* 110(D7).

Hinds, W. (1999). *Aerosol Technology: Properties, behavior, and measurement of airborne particles*, John Wiley & Sons, Inc.

Iida, K., M. R. Stolzenburg, P. H. McMurry and J. N. Smith (2008). Estimating nanoparticle growth rates from size-dependent charged fractions: Analysis of new particle formation events in Mexico City. *Journal of Geophysical Research-Atmospheres 113*(D5).

Jauregui, E. (1988). Local wind and air pollution interaction in the Mexico Basin. *Atmosfera* 1: 131-140.

Khlystov, A., C. O. Stanier, S. Takahama and S. N. Pandis (2005). Water content of ambient aerosol during the Pittsburgh Air Quality Study. *Journal of Geophysical Research* 110(D07S10).

Kittelson, D. B., W. F. Watts and J. P. Johnson (2004). Nanoparticle emissions on Minnesota highways. *Atmospheric Environment* 38(1): 9-19.

Korhonen, P., M. Kulmala, A. Laaksonen, Y. Viisanen, R. McGraw and J. H. Seinfeld (1999). Ternary nucleation of H2SO4, NH3, and H2O in the atmosphere. *Journal of Geophysical Research-Atmospheres* 104(D21): 26349-26353.

Kovalev, V. A. and W. E. Eichinger (2004). *Elastic Lidar: Theory, Practice, and Analysis Methods*, John Wiley & Sons, Inc.

Kuang, Z. M. and Y. L. Yung (2000). Reflectivity variations off the Peru Coast: Evidence for indirect effect of anthropogenic sulfate aerosols on clouds. *Geophysical Research Letters* 27(16): 2501-2504.

Kulmala, M. and V. M. Kerminen (2008). On the formation and growth of atmospheric nanoparticles. *Atmospheric Research* 90(2-4): 132-150.

Kulmala, M., H. Vehkamaki, T. Petaja, M. Dal Maso, A. Lauri, V. M. Kerminen, W. Birmili and P. H. McMurry (2004). Formation and growth rates of ultrafine atmospheric particles: a review of observations. *Journal of Aerosol Science* 35(2): 143-176.

Kulmala, M., L. Laakso, K. E. J. Lehtinen, I. Riipinen, M. D. Maso, T. Anttila, V.-M. Kerminen, U. Horrak, M. Vana and H. Tammet (2004). Initial steps of aerosol growth. *Atmospheric Chemistry and Physics* 4: 2553-2560.

Kulmala, M., M. Dal Maso, J. M. Makela, L. Pirjola, M. Vakeva, P. Aalto, P. Miikkulainen, K. Hameri and C. D. O'Dowd (2001). On the formation, growth and composition of nucleation mode particles. *Tellus Series B-Chemical and Physical Meteorology* 53(4): 479-490.

Kulmala, M., P. Korhonen, I. Napari, A. Karlsson, H. Berresheim and C. D. O'Dowd (2002). Aerosol formation during PARFORCE: Ternary nucleation of H2SO4, NH3, and H2O. *Journal of Geophysical Research-Atmospheres* 107(D19).

Lear, G. (2003). NADP 2003 Long-term monitoring: Supporting science and informing policy and technical committee meeting.

Lewandowski, M., M. Jaoui, J. H. Offenberg, T. E. Kleindienst, E. O. Edney, R. J. Sheesley and J. J. Schauer (2008). Primary and Secondary Contributions to Ambient PM in the Midwestern United States. *Environmental Science & Technology* 42(9): 3303-3309.

Lohmann, U. and J. Feichter (2005). Global indirect aerosol effects: a review. *Atmospheric Chemistry and Physics* 5: 715-737.

Maynard, A. D., R. J. Aitken, T. Butz, V. Colvin, K. Donaldson, G. Oberdorster, M. A. Philbert, J. Ryan, A. Seaton, V. Stone, S. S. Tinkle, L. Tran, N. J. Walker and D. B. Warheit (2006). Safe handling of nanotechnology. *Nature* 444(7117): 267-269.

McGaughey, G. R., N. R. Desai, D. T. Allen, R. L. Seila, W. A. Lonneman, M. P. Fraser, R. A. Harley, A. K. Pollak, J. M. Ivy and J. H. Price (2004). Analysis of motor vehicle emissions in a Houston tunnel during the Texas Air Quality Study 2000. *Atmospheric Environment* 38: 3363-3372.

Nilsson, E. D. and M. Kulmala (1998). The potential for atmospheric mixing processes to enhance the binary nucleation rate. *Journal of Geophysical Research-Atmospheres* 103(D1): 1381-1389.

Nilsson, E. D., U. Rannik, M. Kulmala, G. Buzorius and C. D. O'Dowd (2001). Effects of continental boundary layer evolution, convection, turbulence and entrainment, on aerosol formation. *Tellus Series B-Chemical and Physical Meteorology* 53(4): 441-461.

Oberdorster, G., E. Oberdorster and J. Oberdorster (2005). Nanotoxicology: An emerging discipline evolving from studies of ultrafine particles. *Environmental Health Perspectives* 113(7): 823-839.

Park, K., D. Dutcher, M. Emery, J. Pagels, H. Sakurai, J. Scheckman, S. Qian, M. R. Stolzenberg, X. Wang, J. Yang and P. H. McMurry (2008). Tandem Measurements of Aerosol Properties- A Review of Mobility Techniques with Extensions. *Aerosol Science and Technology* 42(10): 801-816.

Pirjola, L., A. Laaksonen, P. Aalto and M. Kulmala (1998). Sulfate aerosol formation in the Arctic boundary layer. *Journal of Geophysical Research-Atmospheres* 103(D7): 8309-8321.

Posselt, R. and U. Lohmann (2008). Influence of Giant CCN on warm rain processes in the ECHAM5 GCM. *Atmospheric Chemistry and Physics* 8: 3769-3788.

Querol, X., J. Pey, M. C. Minguillon, N. Perez, A. Alastuey, M. Viana, T. Moreno, R. M. Bernabe, S. Blanco, B. Cardenas, E. Vega, G. Sosa, S. Escalona, H. Ruiz and B. Artinano (2008). PM speciation and sources in Mexico during the MILAGRO-2006 Campaign. *Atmospheric Chemistry and Physics* 8: 111-128.

Rader, D. J. and P. H. McMurry (1986). Application of the tandem differential mobility analyzer to studies of droplet growth or evaporation. *Journal of Aerosol Science* 17(5): 771-787.

Ramanathan, V., C. Chung, D. Kim, T. Bettge, L. Buja, J. T. Kiehl, W. M. Washington, Q. Fu, D. R. Sikka and M. Wild (2005). Atmospheric brown clouds: Impacts on South Asian climate and hydrological cycle. *Proceedings of the National Academy of Sciences* 102(15).

Ramanathan, V., P. J. Crutzen, J. T. Kiehl and D. Rosenfeld (2001). Atmosphere - Aerosols, climate, and the hydrological cycle. *Science* 294(5549): 2119-2124.

Randles, C. A. and V. Ramaswamy (2008). Absorbing aerosols over Asia: A Geophysical Fluid Dynamics Laboratory general circulation model sensitivity study of model response to aerosol optical depth and aerosol absorption. *Journal of Geophysical Research-Atmospheres* 113(D21).

Rivera, C., G. Sosa, H. Wohrnschimmel, B. d. Foy, M. Johansson and B. Galle (2009). Tula industrial complex (Mexico) emissions of SO2 and NO2 during the MCMA 2006 field campaign using a mobile mini-DOAS system. *Atmospheric Chemistry and Physics* 9: 6351-6361.

Siebert, H., F. Stratmann and B. Wehner (2004). First observations of increased ultrafine particle number concentrations near the inversion of a continental planetary boundary layer and its relation to ground-based measurements. *Geophysical Research Letters* 31(9).

Stanier, C. O., A. Y. Khlystov and S. N. Pandis (2004). Nucleation events during the Pittsburgh air quality study: Description and relation to key meteorological, gas phase, and aerosol parameters. *Aerosol Science and Technology* 38: 253-264.

Stanier, C. O., A. Y. Khlystov, W. R. Chan, M. Mandiro and S. N. Pandis (2004). A Method for the In Situ Measurement of Fine Aerosol Water Content of Ambient Aerosols: The Dry-Ambient Aerosol Size Spectrometer (DAASS). *Aerosol Science and Technology* 38(12): 215-228.

Stolzenburg, M. R., P. H. McMurry, H. Sakurai, J. N. Smith, R. L. Mauldin III, F. L. Eisele, and C. F. Clement (2005). Growth rates of freshly nucleated atmospheric particles in Atlanta. *Journal of Geophysical Research* (110).

Stull, R. B. (1988). *An Introduction to Boundary Layer Meteorology*, Kluwer Academic Publishers.

Swietlicki, E., H.-C. Hansson, K. Hameri, B. Svenningsoon, A. Massling, G. McFiggans, P. H. McMurry, T. Petaja, P. Tunved, M. Gysel, D. Topping, E. Weingartner, U. Baltensperger, J. Rissler, A. Wiedensohler and M. Kulmala (2008). Hygroscopic properties of submicrometer atmospheric aerosol particles measured wth H-TDMA instruments in various environments- a review. *Tellus* 60B(432-469).

Tunved, P., H. C. Hansson, V. M. Kerminen, J. Strom, M. Dal Maso, H. Lihavainen, Y. Viisanen, P. P. Aalto, M. Komppula and M. Kulmala (2006). High natural aerosol loading over boreal forests. *Science* 312(5771): 261-263.

Weber, R. J., J. J. Marti, P. H. McMurry, F. L. Eisele, D. J. Tanner and A. Jefferson (1997). Measurements of new particle formation and ultrafine particle growth rates at a clean continental site. *Journal of Geophysical Research* 102: 4375-4385.

Weber, R. J., P. H. McMurry, L. Mauldin, D. J. Tanner, F. L. Eisele, F. J. Brechtel, S. M. Kreidenweis, G. L. Kok, R. D. Schillawski and D. Baumgardner (1998). A study of new particle formation and growth involving biogenic and trace gas species measured during ACE 1. *Journal of Geophysical Research-Atmospheres* 103(D13): 16385-16396.

Weber, R. J., P. H. McMurry, R. L. M. III, D. J. Tanner, F. L. Eisele, A. D. Clarke and V. N. Kapustin (1999). New particle formation in the remote troposphere: A comparison of observations at various sites. *Geophysical Research Letters* 26(3): 307-310.

Wiedensohler, A., Y. F. Cheng, A. Nowak, B. Wehner, P. Achtert, M. Berghof, W. Birmili, Z. J. Wu, M. Hu, T. Zhu, N. Takegawa, K. Kita, Y. Kondo, S. R. Lou, A. Hofzumahaus, F. Holland, A. Wahner, S. S. Gunthe, D. Rose, H. Su, and U. Poschl (2009). Rapid aerosol particle growth and increase of cloud condensation nucleus activity by secondary aerosol formation and condensation: A case study for regional air pollution in northeastern China. *Journal of Geophysical Research* 114.

Yu, H., Y. J. Kaufman, M. Chin, G. Feingold, L. A. Remer, T. L. Anderson, Y. Balkanski, N. Bellouin, O. Boucher, S. Christopher, P. DeCola, R. Kahn, D. Koch, N. Loeb, M. S. Reddy, M. Schulz, T. Takemura and M. Zhou (2006). A review of measurement-based assessments of the aerosol direct radiative effect and forcing. *Atmospheric Chemistry and Physics* 6: 613-666.